A hypercompact epigenetic editor based on a novel engineered Cas12f nuclease

Inaugural-Dissertation

zur

Erlangung des Doktorgrades

der Mathematisch-Naturwissenschaftlichen Fakultät

der Universität zu Köln

vorgelegt von

Sarah Rheinbay

Angenommen im Jahr 2025

Table of Contents

I. Abstract

CRISPR-associated (Cas) nucleases have become the dominant genome editing tool. However, risks associated with double-strand breaks (DSBs) have triggered the development of next generation CRISPR technologies which circumvent DSBs. This includes epigenetic editing. The well-characterized epigenetic editor (EE) *CRISPRoff* induces persistent gene silencing by targeted gene methylation and histone modifications. Numerous disease targets require *in vivo* delivery for which adeno associated viruses (AAVs) are a promising vehicle. However, the large-sized *Streptococcus pyogenes* Cas9 (SpyCas9) and the additional epigenetic effector domains exceed the AAV packaging limit. Furthermore, existing hypercompact EEs such as *OMEGAoff*, *CHARM*, and *EvoETR* face constraints in accessing DNA target sites. Specifically, the IscB-based *OMEGAoff* suffers from a suboptimal PAM profile (5'-NTAAA-3'). In contrast, both *EvoETR* and *CHARM* are challenged through complications inherent to the development of ZFN technologies, which introduce additional layers of complexity in their design and implementation. Our objective was to integrate the advantages of hypercompact EEs with the efficacy of CRISPR nucleases by substituting SpyCas9 with hypercompact nucleases from the type V-F family identified through microbial genome mining. To evaluate the novel nucleases as DNA binding platforms, we first tested 15 candidates (~450 amino acids) for CRISPR activation (CRISPRa) in HEK293T cells. As a result, we discovered that nuclease *Aeribacillus pallidus* Cas12f (ApCas12f) led to substantial reporter gene activation. The nuclease activity was further improved through protein engineering efforts, resulting in the creation of the triple mutant enhanced-ApCas12f (en-ApCas12f). We developed assays for epigenetic editing read-out utilizing *CRISPRoff* based on existing literature and observed enduring silencing of the cell surface protein *CD81* following a single hit-and-run treatment with the editor. Subsequent sequencing techniques, including amplicon sequencing and methylation sequencing, demonstrated that the promoter remained intact and exhibited high levels of CpG methylation. We assessed ApCas12f as EE by combining the enzyme with various epigenetic effector domains, achieving over >60% silencing efficiency of a reporter plasmid. Additionally, the system induced >40% promoter methylation of the locus Proprotein Convertase Subtilisin/Kexin Type 9 (*PCSK9*). These findings suggest that ApCas12f-EE holds promise as a versatile platform for precise gene regulation. Going forward, it could enable safer therapeutic approaches that are free from risks associated with DSBs. This will ultimately result in an increased number of treatment options for patients.

II. Zusammenfassung

CRISPR-assoziierte (Cas) Nukleasen haben sich zum dominierenden Werkzeug der Genomeditierung entwickelt. Die mit Doppelstrangbrüchen (DSB) verbundenen Risiken haben jedoch die Entwicklung von CRISPR-Technologien der nächsten Generation ausgelöst, die DSB umgehen. Dazu gehört die epigenetische Editierung. Der umfassend charakterisierte epigenetische Editor (EE) *CRISPRoff* induziert durch gezielte Genmethylierung und Histonmodifikationen ein permanentes *gene silencing*. Zahlreiche Krankheiten benötigen eine *In vivo* Editierung, für die Adeno-assoziierte Viren (AAV) ein vielversprechendes Vehikel sind. *Streptococcus pyogenes* Cas9 (SpyCas9) und die zusätzlichen epigenetischen Domänen überschreiten jedoch die genomische Kapazität der AAVs. Existierende hyperkompakte EE hingegen, wie *OMEGAoff, CHARM* und *EvoETR,* weisen Herausforderungen beim Zugang zur DNA-Zielsequenz auf. Insbesondere das IscB-basierte *OMEGAoff* ist durch ein suboptimales PAM-Profil (5' NTAAA-3') eingeschränkt. Im Gegensatz dazu ergeben sich sowohl für *EvoETR* als auch *CHARM* Komplikationen, die mit der Entwicklung von ZFN-Technologien verbunden sind. Unser Ziel war es, die Vorteile hyperkompakter EE mit den Charakteristiken von CRISPR-Nukleasen zu verbinden, indem wir SpyCas9 durch eine hyperkompakte Nuklease aus der Typ-V-F-Familie ersetzen, die durch mikrobielles Genom-Mining identifiziert wurden. Um die hyperkompakten Nukleasen als DNA-bindendes Protein zu evaluieren, testeten wir zunächst 15 Kandidaten (~450 Aminosäuren) auf CRISPR-Aktivierung (CRISPRa) in HEK293T-Zellen. Dabei entdeckten wir, dass die Nuklease *Aeribacillus pallidus* Cas12f (ApCas12f) eine robuste Reportergen-Aktivierung induzierte. Die Nukleaseaktivität wurde durch Protein-Engineering weiter gesteigert, was zur Entwicklung der Dreifachmutanten enhanced-ApCas12f (en-ApCas12f) führte. Wir entwickelten Assays mit *CRISPRoff* auf Basis bestehender Literatur und beobachteten ein permanentes *gene silencing* des Zelloberflächenproteins *CD81* nach transienter Expression des EE. Anschließende DNA-Sequenzanalysen, darunter Amplikon-Sequenzierung und Bisulfit-Sequenzierung zeigten, dass der Promotor intakt blieb und hohe CpG-Methylierung aufwies. Wir untersuchten ApCas12f als EE, indem wir das Enzym mit verschiedenen epigenetischen Effektordomänen fusionierten. Dabei zeigte sich *gene silencing* eines Reporterplasmids von >60%. Außerdem induzierte ApCas12f-EE eine Promotor Methylierung von >40% auf dem Lokus Proprotein Convertase Subtilisin/Kexin Typ 9 (PCSK9). Diese Ergebnisse sind Belege, dass ApCas12f-EE eine vielversprechende Plattform für eine präzise Genregulation ist. Zukünftig könnte es sicherere Therapieansätze ermöglichen, die frei von den mit DSB verbundenen Risiken sind. Dies trägt zu einer größeren Anzahl von Behandlungsmöglichkeiten für Patienten bei.

III. Abbreviations

5mC	5-methylcytosine
AAV	Adeno-associated virus
AB	Antibody
ADD	ATRX-DNMT3-DNMT3L
ALB	Albumin
ApCas12f	*Aeribacillus pallidus* Cas12f
BFP	Blue fluorescent protein
bp	Base pair
BreCas12b	*Brevibacillus reuszeri* Cas12b
CD151	Cluster of Differentiation 151
CD81	Cluster of Differentiation 81
cDNA	Complementary DNA
CDS	Coding sequence
CGI	CpG Island
CpG	Cytosine phosphate guanine
CRISPR	Clustered Regularly Interspaced Short Palindromic Repeats
crRNA	CRISPR RNA
dApCas12f	dead ApCas12f
dBreCas12f	deadBreCas12f
dCasMini	deadCasMini
DMEM	Dulbecco's Modified Eagle's Medium
DNA	Deoxyribonucleic acid
DNMT3A	DNA methyltransferase 3A
DNMT3L	DNA methyltransferase 3L
DSB	Double-strand break
dSpyCas9	Dead SpyCas9
EB	Elution buffer
EE	Epigenetic editor
ELISA	Enzyme-Linked Immunosorbent Assay
en-ApCas12f	Engineered ApCas12f
FACS	Fluorescence-activated cell sorting
FGA	Fibrinogen alpha chain
GAPDH	Glyceraldehyde-3-phosphate dehydrogenase
GFP	Green fluorescent protein
H3K9me3	Trimethylation of histone H3 at lysine 9
HDR	Homology-directed Repair
Indel	Insertion and deletion
KAP1	KRAB-associated protein 1
kb	Kilobase
LNP	Lipid nanoparticles
LNP	Lipid-based nanoparticles
min	Minute
MSA	Multiple sequence alignment
NGS	Next-generation Sequencing
NHEJ	Non-homologous end joining
NLS	Nuclear localization signal

OT	Off-target
p.t.	Post transfection
PAM	Protospacer adjacent motif
PBS	Phosphate buffered saline
PCR	Polymerase chain reaction
PCSK9	Proprotein Convertase Subtilisin/Kexin Type 9
RFP	Red fluorescent protein
R-loop	RNA-DNA hybrid structure
RNA	Ribonucleic acid
rpm	Rotations per minute
sgRNA	Single guide RNA
siRNA	Small interfering RNA
SPM	Single point mutants
SPRI	Solid-phase reversible immobilization
tracrRNA	Trans-activating RNA
TruSeq	TruSeq DNA UD Illumina Indexes
TSS	Transcription start site
VPR	VP64-p65-Rta
WT	Wild type
ZFN	Zinc finger nuclease

IV. List of Figures

1. Introduction

1.1 CRISPR technologies: mechanisms, modifications, and functional applications

Gene editing has undergone a remarkable transformation over the past few decades, starting with the development of zinc-finger nucleases (ZFN) and transcription activator-like effectors (TALEs). These engineered proteins were designed for specific DNA recognition and binding, enabling targeted modifications of the genome. However, the introduction of Clustered Regularly Interspaced Short Palindromic Repeats (CRISPR) technology has fundamentally revolutionized the field of gene editing. Unlike the protein-based recognition mechanisms as employed by ZFN and TALEs, CRISPR utilizes RNA-programmable endonucleases (Doudna & Charpentier, 2014). This approach offers the fundamental advantage of facilitating specific targeting, as the synthesis of guide RNAs (gRNAs) is relatively basic, rapid, and cost-effective. This innovation significantly simplifies the gene editing process, eliminating the need for extensive protein engineering and thereby enhancing the efficiency of precise gene insertions, deletions, and modifications (Hu et al., 2016). The transition to RNA-guided mechanisms represents a pivotal advancement in the accessibility and feasibility of gene editing technologies, opening new avenues for research and therapeutic applications.

1.1.1 From foundational discoveries to gene editing innovations

The foundational discovery of CRISPR systems can be traced back to 1993, when Francisco Mojica and his colleagues identified repetitive sequences in bacterial genomes (Mojica et al., 1993). The group speculated as well as another group that the observed sequences could be part of an adaptive immune system against bacteriophages (Mojica et al., 2005; Pourcel et al., 2005). CRISPR systems enable organisms to combat invading viruses through the cleavage of foreign genomes, often resulting in double-strand breaks (DSBs) (Bolotin et al., 2005; Garneau et al., 2010; Gasiunas et al., 2012; Marraffini & Sontheimer, 2008; Pourcel et al., 2005). Small snippets of the foreign sequence are integrated into the CRISPR locus, which enable rapid recognition of foreign genetic material in the event of a second infection with the same invader. Specifically, the CRISPR locus is transcribed into multiple gRNAs, which bind to the CRISPR nuclease. If encountering a complementary sequence, a DSB gets induced, leading to degradation of the foreign DNA, thereby neutralizing the threat posed by the invading genetic material.

The transformative potential of CRISPR technology was first realized in 2012 with the demonstration of programmable DNA cleavage by *Streptococcus pyogenes* Cas9 (SpyCas9) (Gasiunas et al., 2012; Jinek et al., 2012). Following this breakthrough, the CRISPR-Cas9 system was rapidly established in eukaryotic cells, with numerous studies confirming its efficacy and versatility (Cho et al., 2013; Cong et al., 2013; Hwang et al., 2013; Jinek et al., 2013; Mali et al., 2013). Since then, the CRISPR framework has evolved into a diverse array of gene editing tools, including base editing (Gaudelli et al., 2017; Komor et al., 2016) and prime editing (Anzalone et al., 2019), which offer enhanced precision and flexibility in genetic modifications. Additionally, the exploration of CRISPR-associated transposases represents a promising frontier in gene editing technology (Klompe et al., 2019; Strecker et al., 2019). In recent efforts, their activity in human cells was demonstrated for the first time (Tou et al., 2023).

Approximately 90% of rare diseases currently lack targeted treatments (Aartsma-Rus et al., 2021). While the prevalence of individual rare diseases is low, the cumulative number of individuals affected by various rare conditions is substantial, with approximately 30 million people in Europe suffering from rare diseases, accounting for about 6% of the population (Wakap et al., 2020). Notably, 70%-80% of rare disorders are monogenic, making them potential targets for CRISPR-based interventions. Given the immense therapeutic potential of CRISPR genome editing, controlling the outcome of DNA repair has emerged as a major area of research (Doudna, 2020). Precise repair of the mutated gene to restore the wild type sequence is essential for many diseases, such as sickle cell disease, β-thalassemia, Duchenne muscular dystrophy, and Leber's congenital amaurosis (Amoasii et al., 2017; Canver et al., 2015; Nelson et al., 2016; Tabebordbar et al., 2016). However, insertions and deletions (indels) induced through a CRISPR/Cas mediated DSB can be therapeutically beneficial for certain pathogenic mutations. This is particularly the case when the goal is to knock out a pathogenic gene and induce a loss-of-function mutation. This approach has been demonstrated *in vivo* for the first time in humans, where transthyretin amyloidosis (ATTR) was treated by knocking out the misfolded transthyretin protein using a single dose of mRNA encoding the SpyCas9 protein and a gRNA targeting *TTR* (Gillmore et al., 2021). Collectively, these advancements underscore the rapid progression of CRISPR technology and its profound implications for genetic research and biotechnology.

1.1.2 Mechanism of CRISPR immune response

The bacterial CRISPR immune response is characterized by three distinct phases: adaptation, crRNA biogenesis, and interference with the target (Figure 1A). Following the invasion of

foreign genetic material, such as that introduced by bacteriophages or plasmids, short sequences of this foreign DNA are integrated into the CRISPR repeat-spacer array as "spacers" (Amitai & Sorek, 2016). This integration is facilitated by the Cas1 and Cas2 proteins, which are essential for the adaptation process (Barrangou & Marraffini, 2014; Nuñez et al., 2014, 2015; Wei et al., 2015; Yoganand et al., 2019). This mechanism of acquiring genetic memory resembles the adaptive immune systems found in higher organisms (Barrangou et al., 2007; Makarova et al., 2006). The CRISPR array is subsequently transcribed into a long precursor CRISPR RNA (pre-crRNA), which is processed into individual crRNAs with the assistance of the RNase III enzyme. These spacers subsequently function as gRNAs during future infections (Brouns et al., 2008). The trans-activating CRISPR RNA (tracrRNA) molecules bind to these spacer transcripts, facilitating the formation of a functional guide RNA complex (Deltcheva et al., 2011). To streamline the system for gene editing, the tracrRNA and crRNA can be combined into a single guide RNA (sgRNA), thereby enhancing efficiency and simplifying the system by reducing the number of components (Figure 1B). The processed crRNA, along with the Cas protein, form a ribonucleoprotein (RNP) complex that is essential for the interference stage of the immune response. A critical aspect of CRISPR function is the presence of a protospacer adjacent motif (PAM), located on the non-target strand at the 3' end of the protospacer (Bolotin et al., 2005; Deveau et al., 2008; Horvath et al., 2008; Mojica et al., 2009). For instance, SpyCas9 recognizes and cleaves DNA three bases upstream of a 5'-NGG-3' PAM, although different Cas9 proteins from various species may recognize distinct PAM motifs (Figure 1B). The PAM serves as a safeguard to prevent the CRISPR system from attacking the host's own CRISPR locus (Gleditzsch et al., 2019). Notably, Bolotin et al., (2005) were among the first to recognize the significance of the PAM, observing that a specific nucleotide sequence consistently appeared at the end of each spacer of the target genome. The gRNA hybridizes to a 20-24 base pair protospacer on the target DNA strand, triggering a conformational change in the nuclease that is essential for its activation (Figure 1B) (Sternberg et al., 2015). This binding event results in the displacement of the single-stranded non-target strand, forming an R-loop (Gasiunas et al., 2012; Jiang et al., 2016; Szczelkun et al., 2014). Upon target recognition, the nuclease domain(s) cleave(s) the target DNA by hydrolysis of the phosphodiester backbone (Gasiunas et al., 2012). The resulting DSB activates cellular DNA repair pathways, primarily homology-directed repair (HDR) and non-homologous end joining (NHEJ) (Lieber, 2010; San Filippo et al., 2008). HDR, which necessitates a template, is restricted to the S- and G2- phases of the cell cycle in dividing cells, whereas NHEJ is typically the dominant repair pathway, often leading to indels (Hustedt & Durocher, 2016; San Filippo et al., 2008; Stark et al., 2004).

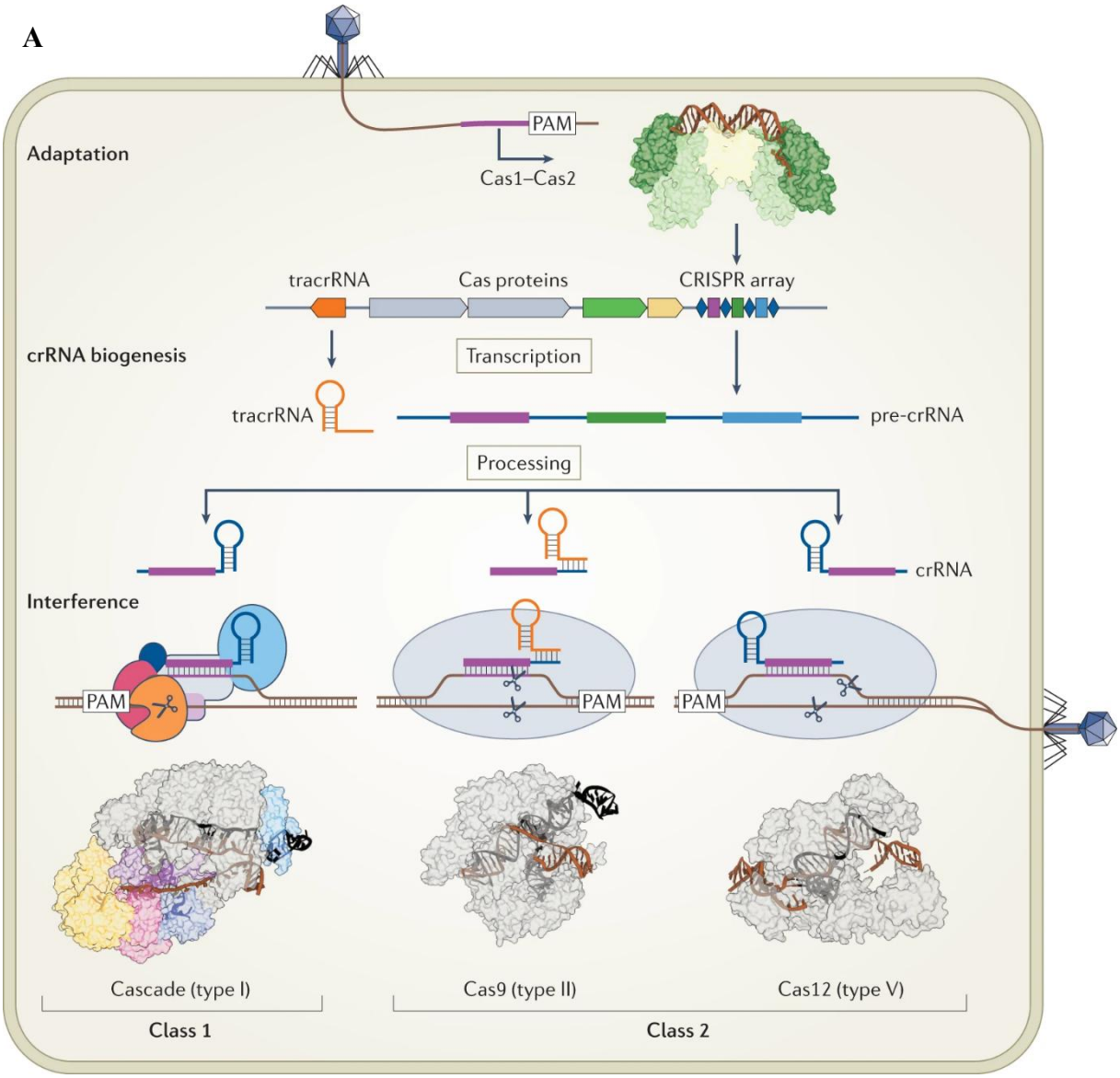

(Figure continued on next page)

B

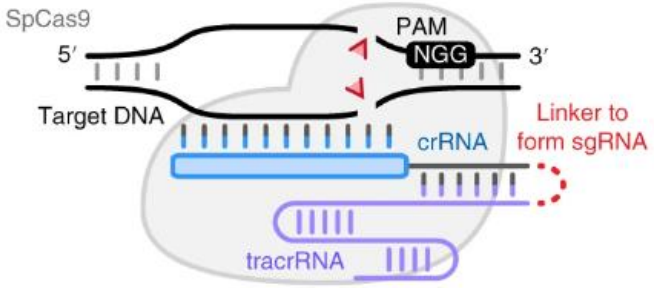

Figure 1: CRISPR immunity consists of three critical stages namely adaption, crRNA biogenesis and interference. A) The figure schematically shows an infection by bacteriophages followed by activation of CRISPR immunity. This includes the integration of foreign genetic material as short sequences into the CRISPR repeat-spacer array as "spacers (rectangles).The spacers are separated by CRISPR repeats (diamonds). This integration process is facilitated by the Cas1 and Cas2 proteins. The CRISPR array is transcribed into a long precursor CRISPR RNA (pre-crRNA), which is processed into individual crRNA with the assistance of the RNase III enzyme. The tracrRNA binds to these spacer transcripts, facilitating the formation of a functional guide RNA complex. The processed gRNAs, along with the Cas protein, forms a RNP complex essential for the interference stage of the immune response. The sgRNA within this RNP complex hybridizes to a 20-24 base pair protospacer on the target DNA strand, resulting in the displacement of the single-stranded non-target strand and forming an R-loop. Cas proteins from class I comprise multiple subunits (bottom-left), while class II comprises single effector proteins, such as Cas9 and Cas12 (bottom-right). Reprinted from *Nature Reviews Microbiology*, 20, Wang, J.Y., Pausch, P. & Doudna, J.A., Structural biology of CRISPR–Cas immunity and genome editing enzymes, 641-656, Copyright © 2022, with permission from Springer Nature. B) A critical aspect of CRISPR function is the presence of a PAM, located on the non-target strand at the 5' end of the protospacer. The RNP complex hybridizes with its sgRNA to a DNA target in case of complementary. SpyCas9 recognizes a 5'-NGG-3' PAM and induces a blunt cut three bases upstream of the PAM. The sgRNA can be formed by artificially forming a linker between the crRNA and tracrRNA. This simplifies CRISPR/Cas application in biotechnological contexts by reducing its number of components. Reprinted from *Nature Protocols*, 16, Walton, R.T., Hsu, J.Y., Joung, J.K. et al., Scalable characterization of the PAM requirements of CRISPR–Cas enzymes using HT-PAMDA, 1511-1547, Copyright © 2021, with permission from Springer Nature.

1.1.3 Discovery and classification of CRISPR nucleases

Since these early discoveries, various CRISPR systems have been identified and classified into two main categories: Class I, which relies on a multiprotein effector, and Class II, which is characterized by a single protein effector (Figure 2A) (Koonin et al., 2017). These classes can be further subdivided into specific types, based on their unique Cas protein. Class II, for instance, is divided into types II, V, and VI. This hierarchical classification underscores the diversity and complexity of CRISPR systems. The widely utilized SpyCas9 protein exemplifies the class II type II system of relying on a single effector, which greatly simplifies the application. Type V CRISPR nucleases encompass 14 subtypes, designated A through N, including the recently described type V-F family (Harrington et al., 2018; Karvelis et al., 2020; Kim et al., 2021; Koonin et al., 2017; Makarova & Koonin, 2015; Xu et al., 2021). The CRISPR locus is functionally subdivided into four principal sections, which together encompass proteins essential for adaptation, expression, interference, and signal transduction (Figure 2B) (Makarova et al., 2013, 2020; Makarova & Koonin, 2015).

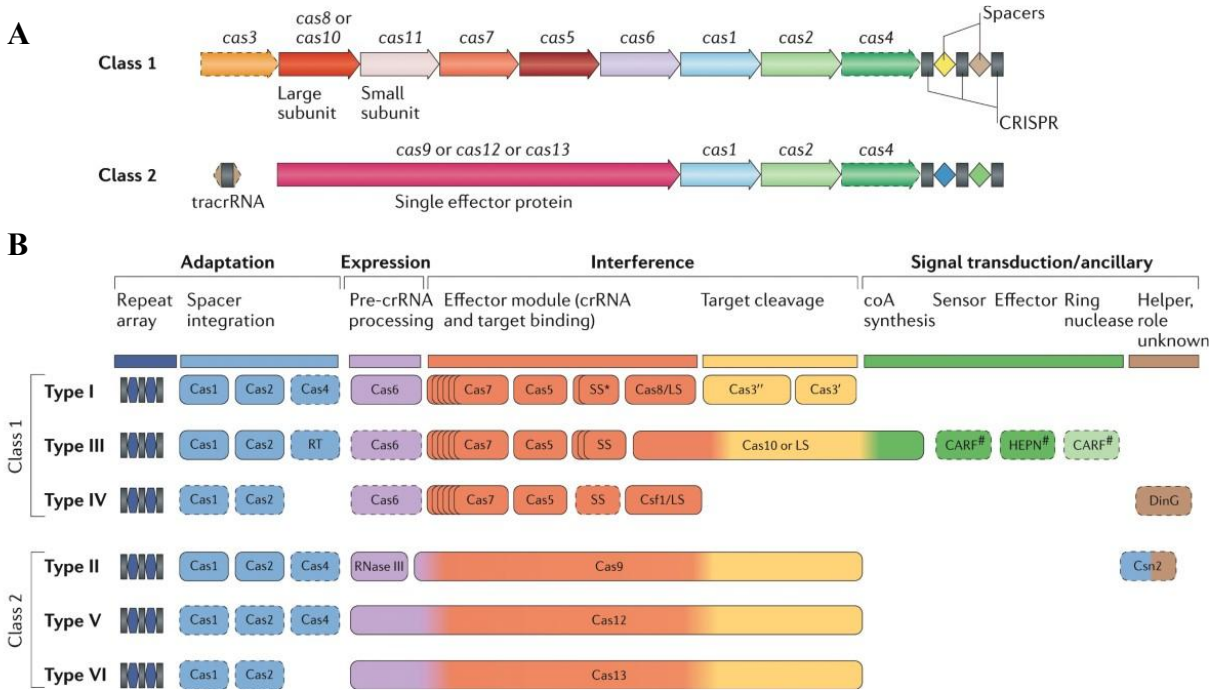

Figure 2: Classification of CRISPR/Cas systems. A) CRISPR/Cas systems can be divided into two classes, namely I and II. Class I consists of a multi domain effector protein whereas class II CRISPR-systems are characterized by a single effector protein (pink). **B)** Class I and II can be further divided into types e.g. Class I type II such as Cas9 or class II type V such as Cas12 nucleases. The CRISPR locus can be functionally divided into four main sections consisting of proteins necessary for adaption, expression, interference and signal transduction. Reprinted from *Nature Reviews Microbiology*, 18, Makarova, K.S., Wolf, Y.I., Iranzo, J. et al., Evolutionary classification of CRISPR–Cas systems: a burst of class 2 and derived variants, 67-83, Copyright © 2020, with permission from Springer Nature.

Cas12f nucleases recognize a 5' PAM and are characterized by staggered cutting, which generates sticky ends, in contrast to a 3' PAM and the blunt cuts produced by SpyCas9 (Figure 3). Additionally, they function as heterodimers and possess a single RuvC domain (Garneau et al., 2010; Wu et al., 2024). A prominent candidates from the type V-F family is represented by Cas12f from uncultured archaea (Un1Cas12f) and its engineered variant termed CasMini (529 amino acids (aa)) (Xu et al., 2021).

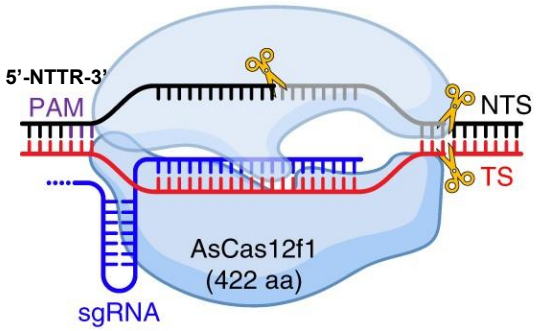

Figure 3: Schematic illustration of a type V-F nuclease. Type V nucleases such as AsCas12f recognize a 5' PAM, which is often T-rich, and induces a staggered cut. Reprinted from Nature Chemical Biology, 17, Wu, Z., Zhang, Y., Yu, H. et al., Programmed genome editing by a miniature CRISPR-Cas12f nuclease, 1132-1138, Copyright © 2021, with permission from Springer Nature.

Previous work from us and others has shown that novel CRISPR-Cas systems can be identified from microbes. Such systems include for example, CRISPR-Cas from *Acidibacillus sulfuroxidans* (AsCas12f, 422 aa) (Figure 3) and Un1Cas12f. In previous efforts by our group, a mining pipeline to discover novel enzymes with improved properties such as fidelity, targeting range, immunogenicity, size etc. has been set up. Starting from ~170k genomes, thousands of potential CRISPR systems have been identified and prioritized for further testing of DNA cutting *in vitro*. Active nucleases were selected for testing of DNA cutting *in cellulo*. This led to the identification of hypercompact nuclease *Aeribacillus pallidus* Cas12f (ApCas12f), as described in patent WO 2023/237587 A1.

1.1.4 Risks associated with DNA double-strand breaks

Genome editing through targeted DNA cleavage relies on the cell's intrinsic repair mechanisms, which encompass at least five distinct pathways: base excision repair, nucleotide excision repair, mismatch repair, microhomology-mediated end joining (MMEJ), HDR, and NHEJ. Each of these pathways is complex and can yield multiple outcomes beyond the desired edit, complicating the precision of genome editing (Yeh et al., 2019). The cellular response to DSBs includes cell cycle arrest, which persists until the break is repaired (Krenning et al., 2019). Cells are halted at specific checkpoints, and the duration of DSB repair, along with its susceptibility to errors, remains poorly understood. The accuracy of DNA rejoining is influenced by the nature of the damaging agent and the end structures formed by the DSB, which varies among different CRISPR nucleases (Bétermier et al., 2014; Lieber, 2010). DSBs activate the p53 damage response. Cell culture experiments have shown that if cells survive this response, there could be a selection bias towards those with mutated p53, which can promote oncogenic survival (Haapaniemi et al., 2018). The toxicity associated with DSBs is influenced by cutting efficiency and off-target (OT) effects, independent of chromatin context (Friskes et al., 2022). Furthermore, reports on chromosomal abnormalities resulting from CRISPR/Cas9 treatment exist. These abnormalities include inversions, chromothripsis, and translocations. However this was observed in cell culture experiments, and not in patients in clinical studies (Liu, Zhang, et al., 2021; Papathanasiou et al., 2021). For instance, there are studies which have described that in CRISPR/Cas9-treated mouse embryos, over 20% of deletions exceeded 250 base pairs (Adikusuma et al., 2018; Kosicki et al., 2018). Another study has observed that in human embryos, approximately half of the DSBs remained unrepaired, leading to the loss of chromosome arms (Zuccaro et al., 2020).

Efforts to mitigate off-target effects have focused on enhancing the specificity of gene-editing tools. However, due to the concept of incurring DSBs, even the most specific nuclease may still cause events originating from unrepaired DSBs (Leibowitz et al., 2021). Nonetheless, it is crucial to note that while these reports exist on genotoxicity observed in cell culture experiments, on-going *in vivo* studies such as *NTLA-2001* demonstrate that CRISPR/Cas9 induced DSBs are save and well tolerated by patients (Gillmore et al., 2021). The development of next-generation CRISPR technologies that circumvent DSBs includes epigenetic editing, which modifies gene expression through epigenetic marks such as DNA methylation and histone modification, rather than altering the DNA sequence itself (Amabile et al., 2016; Liu et al., 2016; Nuñez et al., 2021).

1.2 The epigenetic landscape

Epigenetics refers to the study of heritable changes in gene expression that do not involve alterations to the underlying DNA sequence. Despite every cell in an organism containing the same genetic material, there are profound differences in transcriptional activity among various cell types. These differences are primarily driven by epigenetic mechanisms determining which genes are expressed and which are silenced (Allis & Jenuwein, 2016). As reviewed by Breunig et al., (2021), the concept of epigenetics was significantly advanced by Conrad Hal Waddington et al., (1942), who introduced a compelling visual metaphor for cellular development. He depicted the totipotent zygote as a marble positioned atop a hill, symbolizing its inevitable descent down various pathways of differentiation (Figure 4). While cells can follow multiple developmental trajectories, these pathways are governed by specific gene activities that shape the cellular landscape. A defining characteristic of all cellular fates is the gradual reduction of available options, ultimately leading each cell to a terminally differentiated state, akin to a marble coming to rest in a dead-end valley. In humans, there are approximately 400 distinct cell types (Vickaryous & Hall, 2006). Waddington coined the term "epigenetics" to encompass the non-genetic processes that contribute to phenotypic expression, emphasizing the importance of these mechanisms in cellular identity.

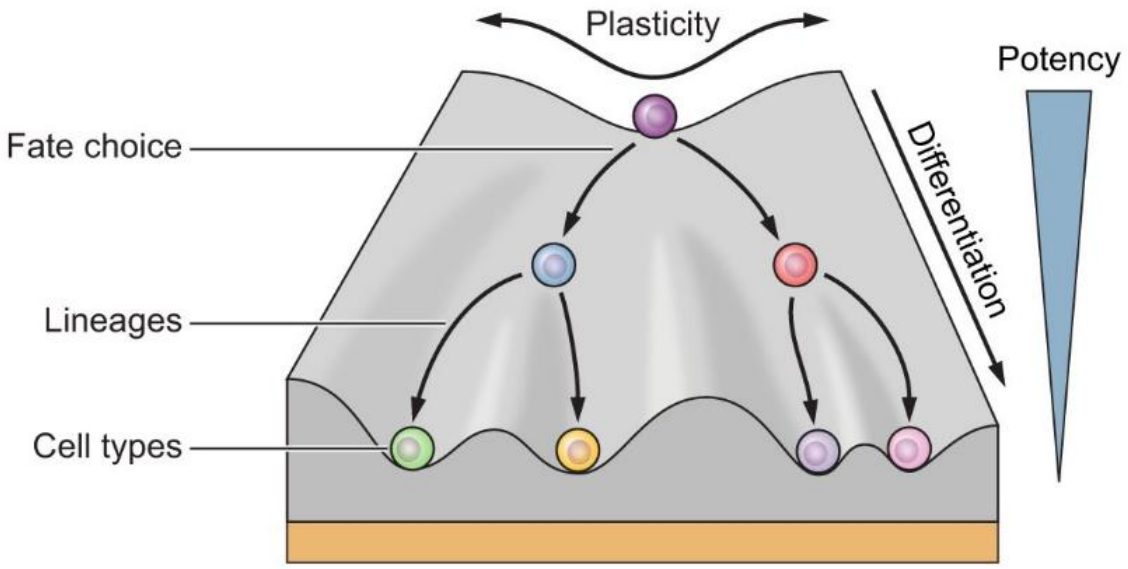

Figure 4: Visual metaphor "Waddington landscape" to describe cellular differentiation. Cell differentiation culminates in the formation of mature cell types, characterized by a gradual reduction in potency. Waddington et al., (1942) depicted cell differentiation as a marble rolling down a hill, symbolizing the inevitable descent along various pathways of differentiation. This metaphor illustrates how each cell ultimately reaches a terminally differentiated state, akin to a marble coming to rest in a dead-end valley. Reprinted from *Physiological Reviews*, 101 (1), Breunig, C., Köferle, A., Neuner, A., Wiesbeck, M., Baumann, V., & Stricker, S., CRISPR Tools for Physiology and Cell State Changes: Potential of Transcriptional Engineering and Epigenome Editing, 177-211, Copyright © 2021, with permission from Springer Nature.

Chromatin can be classified into two distinct types: euchromatin and heterochromatin. Euchromatin is characterized by a less condensed structure, allowing for active transcription and gene expression, while heterochromatin is more densely packed and typically associated with transcriptional repression and stable gene silencing. Epigenetic regulation involves multiple layers of control, beginning at the DNA level. The first epigenetic mark to be discovered was DNA methylation, as reported by Hotchkiss et al., in 1948, which is predominantly associated with gene silencing (Du et al., 2015). In embryonic stem cells, approximately 25% of DNA methylation occurs outside of cytosine-phosphate-guanine (CpG) contexts, while in differentiated cells, 98% of methylation is found within the typical context CpG (Lister et al., 2009). Approximately 75% of promoters contain CpG islands, which are dense regions of CpG dinucleotides. This prevalence indicates that these promoters are subject to regulation by DNA methylation, playing a crucial role in the control of gene expression (Edwards et al., 2017). Methylation specifically occurs at the fifth carbon of cytosine residues (Razin & Riggs, 1980). This modification inhibits the binding of transcription factors (TFs), as many TFs are unable to interact with methylated DNA (Eden & Cedar, 1994). Additionally, DNA methylation promotes the binding of repressor proteins, further contributing to transcriptional repression (Eden & Cedar, 1994; Lewis et al., 1992). A third effect of DNA

methylation is the consolidation of chromatin into heterochromatin, which inhibits access to DNA and further contributes to transcriptional repression (Newell-Price et al., 2000). De novo methylation is carried out by the DNA methyltransferases DNMT3A and DNMT3B (Okano et al., 1999). DNMT3L acts as a co-factor and interacts with DNMT3A and DNMT3B to guide this complex to DNA regions linked with unmethylated lysine 4 on histone H3 (H3K4me0) (Edwards et al., 2017) (Figure 5).

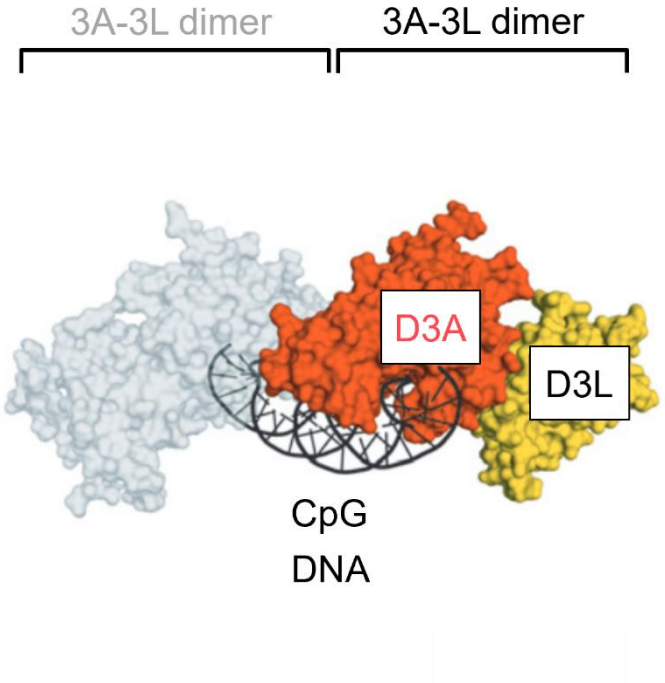

Figure 5: DNMT3A (3A) – DNMT3L (3L) dimer. The de novo methyltransferase 3A forms a dimer with its co-factor 3L. The complex targets DNA regions with unmethylated lysine 4 on histone H3 (H3K4) and introduces DNA CpG methylation. Reprinted from Cell, 184 (9), Nuñez, J. K., Chen, J., Pommier, G. C., Cogan, J. Z., Replogle, J. M., Adriaens, C., Ramadoss, G. N., Shi, Q., Hung, K. L., Samelson, A. J., Pogson, A. N., Kim, J. Y. S., Chung, A., Leonetti, M. D., Chang, H. Y., Kampmann, M., Bernstein, B. E., Hovestadt, V., Gilbert, L. A., & Weissman, J. S., Genome-wide programmable transcriptional memory by CRISPR-based epigenome editing, 2503-2519, Copyright © 2021, with permission from Elsevier.

In contrast, DNMT1 is responsible for the maintenance of DNA methylation, specifically targeting hemi methylated DNA after replication (Li et al., 1992; Okano et al., 1999). The DNMT3 family, which includes DNMT3A & B, is characterized by three distinct functional domains: the ATRX-Dnmt3-Dnmt3L (ADD) domain, the PWWP domain, and the methyltransferase (MTase) domain. MTase forms complexes with its homologs, specifically DNMT3A & B, and the catalytically inactive homolog DNMT3L (Figure 5) (Nguyen et al., 2019; Suetake et al., 2004; Xu, Liu, et al., 2020). The ADD and PWWP domains serve as readers of histone modifications, specifically recognizing H3K4me0 and histone 3 lysine 36 di-methylation (H3K36me2). These interactions are crucial for inducing a conformational change that repositions the ADD domain, thereby facilitating the binding of the MTase domain to DNA (Guo et al., 2015; Weinberg et al., 2019; Xu, Li, et al., 2020). The MTase domain utilizes S-

adenosyl methionine (SAM) as the active methyl donor, a process that is essential for the transfer of methyl groups to cytosine residues within the context of CpG dinucleotides (Lee et al., 2023). The removal of DNA methylation marks is a critical aspect of epigenetic regulation, primarily mediated by the ten-eleven translocation (TET) enzyme family (Liu, Wu, et al., 2021). This family consists of three members: TET1, TET2, and TET3, which are responsible for the active demethylation of 5-methylcytosine (5mC) through a series of oxidative reactions (Goll & Bestor, 2005).

On the next level of control, DNA is wrapped around octameric histones, specifically H2A, H2B, H3, and H4, with two copies of each histone present (Breunig et al., 2021; Roth et al., 2024) (Figure 6A). The histones are positively charged due to their high content of lysine and arginine, allowing them to interact with the negatively charged DNA. Approximately 147 base pairs of DNA are associated with each histone octamer (Breunig et al., 2021). These dynamic proteins can loosen during replication and transcription, facilitating access to the underlying DNA (Roth et al., 2024). Histone residues can undergo various chemical post-translational modifications (PTMs), which modulate the interaction between histones and DNA, thereby influencing the accessibility of transcription factors. The regulation of histone modifications involves a complex interplay of "readers," "writers," and "erasers." Readers recognize specific histone modifications, while writers, such as acetylases and methylases, add these modifications, and erasers, including deacetylases and demethylases, remove them. The dynamic exchange of these PTMs allows for the upregulation or downregulation of gene expression, with over 12 known chemical modifications occurring at more than 30 sites (Roth et al., 2024). For instance, acetylation of histone tails enhances the accessibility of transcription factors and polymerases, while methylation of histone tails often inhibits access to DNA Figure 6B). Specifically, methylation of H3K9, H3K27, or H3K20 is frequently associated with transcriptionally repressed genes (Barski et al., 2007). In contrast, methylation of H3K4, H3K36 is linked to gene activation (Barski et al., 2007; Koch et al., 2007). Notably, methylation of H3K9 has been shown to correlate with DNA methylation, indicating a complex interplay between these two epigenetic modifications that contributes to the regulation of gene expression (Du et al., 2015). At the highest level, the three-dimensional organization of the genome includes topologically associated domains (TADs), which form loops of DNA that enable the activation or repression of genes within the loop, even if those genes are located far apart in the linear genome (Roth et al., 2024).

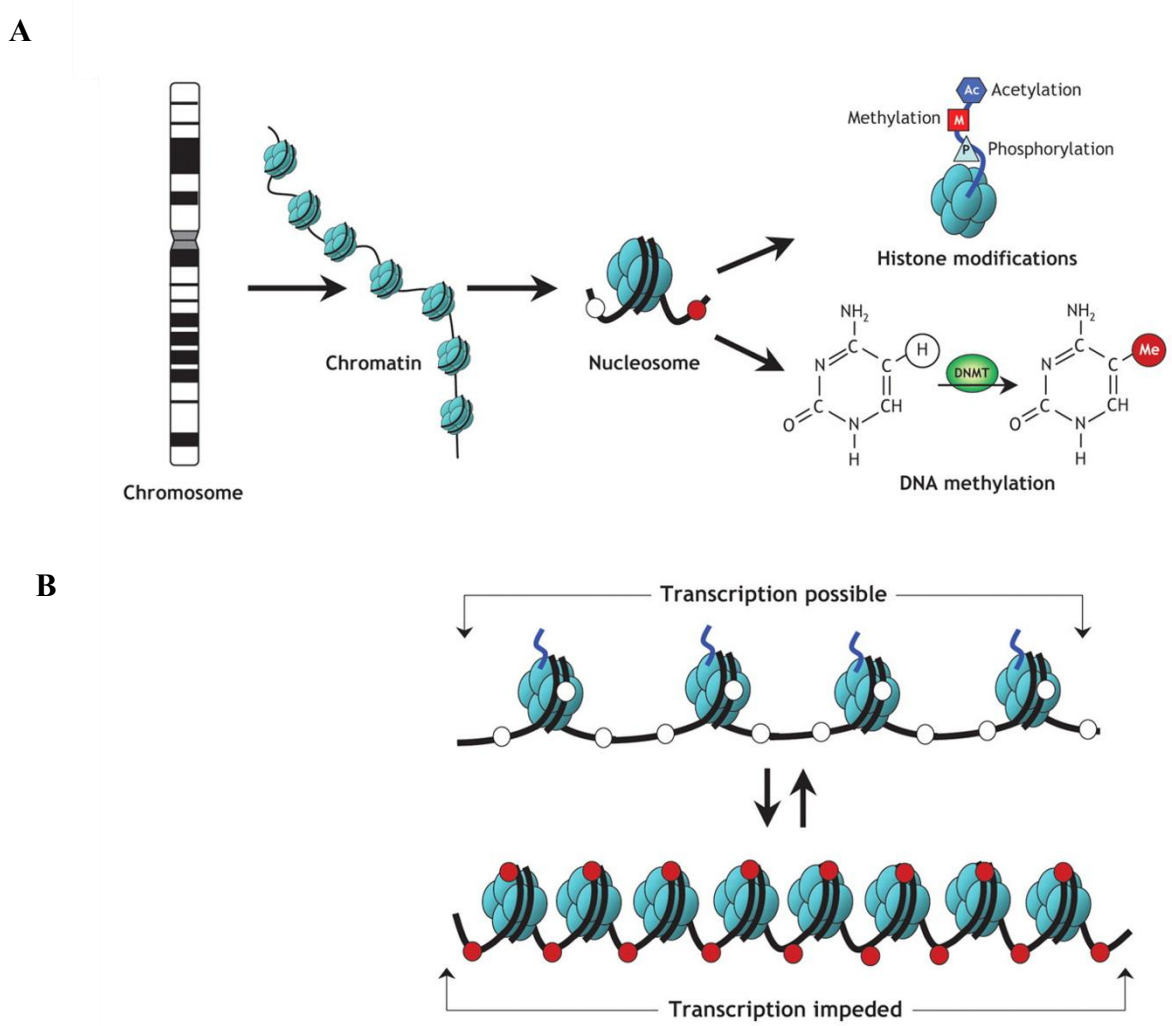

Figure 6: Chromatin organization and structure. A) Chromatin exhibits multiple levels of organization, with regulatory mechanisms influencing gene expression at each stage. At the most fundamental level, DNA can undergo methylation, which is recognized as a repressive mark for gene expression. A methyl group can be added to the fifth carbon atom of cytosine, a process conducted by DNA methyltransferases (DNMTs). At the next level, DNA is wrapped around octameric histones. These histones can undergo post-translational modifications (PTMs) such as acetylation, methylation, or phosphorylation of their tails, which can either activate or repress gene expression. The structure formed by DNA wrapped around histones forms chromatin. **B)** Loosely wrapped chromatin (euchromatin) is associated with enhanced transcription, while tightly wrapped chromatin (heterochromatin) is linked to repressed transcription. Reprinted from *CMAJ*, 174 (3), Rodenhiser, D., Mann, M., Epigenetics and human disease: translating basic biology into clinical applications, 341-348, Copyright © 2006, with permission from the Canadian Medical Association.

1.3 Epigenetic editing for gene regulation

Epigenetic editing represents a transformative approach in the field of molecular biology, enabling precise modifications of the epigenome without altering the underlying DNA sequence. The field has evolved significantly, with early efforts focusing on small molecules (SMOL) that inhibit endogenous epigenetic effectors, which suffered from specificity. By acting globally, they affect multiple targets within the epigenetic machinery. This lack of specificity can result in unintended side effects (Altucci & Rots, 2016; Bhat et al., 2021; Liao et al., 2023; Wang, Jin, et al., 2024). As the field progressed, there was a pressing need for the development of more precise treatment options, one of them is CRISPR based epigenetic editing.

1.3.1 Advances in epigenetic editing: from small molecules to CRISPR editing

Epigenetic editing harnesses the principles of targeted genome editing but focuses specifically on the dynamic and reversible nature of epigenetic marks, such as DNA methylation and histone modifications. Catalytically inactive Cas9 (deadCas9/dCas9) retains the ability to bind to specific DNA sequences but lacks nuclease activity. By utilizing dCas9 fused to epigenetic modifiers, researchers can achieve site-specific alterations in the epigenetic landscape, thereby influencing gene expression patterns and cellular phenotypes (Qi et al., 2013). The advent of epigenetic editing tools has opened new avenues for therapeutic interventions, particularly in the context of diseases characterized by aberrant epigenetic regulation or gene mutations that result in the production of pathogenic proteins. Moreover, epigenetic editing facilitates the precise fine-tuning of gene expression beyond the capabilities of traditional gene repression methods, such as gene knockouts. One of the key advantages of epigenetic editing is its reversibility; since the underlying DNA sequence remains unchanged, the modifications can be transiently applied and subsequently removed (Figure 7).

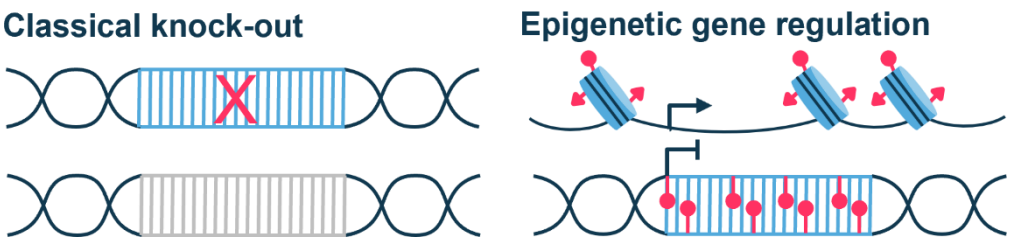

Figure 7: Comparison of classical gene editing to epigenetic editing. Classical gene editing often relies on DSBs to introduce indels, which subsequently induce frame shifts and alter the DNA sequence. In contrast, epigenetic editing targets and modulates epigenetic marks while leaving the underlying DNA sequence unchanged.

This dynamic nature of epigenetic regulation allows for a more flexible approach to gene expression modulation. For instance, DNA methylation can be removed by targeting the locus with a dCas9 fused to TET enzyme, a methylcytosine dioxygenase, which facilitates the demethylation of methylated CpGs, as demonstrated in cell lines (Amabile et al., 2016; Nuñez et al., 2021; Wu & Zhang, 2017). Recently, Trembley et al. (2025) demonstrated this phenomenon for the first time in mice. Following over 150 days of *PCSK9* silencing using CRISPRoff, methylation was subsequently removed with dCas9-TET, leading to a recovery of PCSK9 levels to 90% of baseline within just two weeks. Additionally, epigenetic editing circumvents the reliance on cellular repair pathways that are often implicated in conventional gene editing techniques, such as those that induce DSBs. The introduction of DSBs can be associated with toxicity. Circumventing this is particularly beneficial in therapeutic contexts.

Kovalev et al., (2025) have described epigenetic editing to be less prone to OT editing. However, the authors emphasized the necessity of further investigation into the potential toxicity associated with epigenetic domains. This concern arises from the possibility that the inherent non-specificity of these domains could inadvertently lead to OT editing events. In addition, the authors describe, toxic effects of the epigenetic domains may arise from high doses which are required to induce a therapeutic effect. There are currently limited reports on OT effects. Galonska et al., (2018) indicate the presence of OT methylation in cell lines. However, the authors noted that there was excessive free nuclear dCas9-DNMT3A present and did not test other epigenetic domains. The group reported that the OT methylation did not have a strong effect on gene expression, however pointing out that these dynamics may differ in systems where cells are still undergoing development. Notably, the observed OT methylation was found to be independent of the presence of sgRNAs, which hints towards OT due to unspecific binding of DNMT3A.

1.3.2 Architectural advances in epigenetic editing technologies

The architecture of epigenetic editors (EEs) has evolved significantly over the past years, starting off with the development of CRISPR interference (CRISPRi). As discussed in the review by Breuning et al. (2021), initial efforts at epigenetic silencing using CRISPRi were not stable however and only lasted as long as the editor was expressed (Figure 8A). Furthermore, these early applications often induced only moderate gene silencing (Bintu et al., 2016; Galonska et al., 2018; Huang et al., 2017; Lei et al., 2017; McDonald et al., 2016; Pflueger et al., 2018; Saunderson et al., 2017; Stepper et al., 2017; Vojta et al., 2016; Wang et al., 2018). Despite these limitations, CRISPRi, primarily utilizing dCas9 fused to Krüppel-associated box

(KRAB), proved useful in many applications. However, it was ultimately deemed insufficient for achieving the desired hit-and-run editing necessary for effective *in vivo* therapies. The advancement of epigenetic editing technologies has seen remarkable progress by Amabile et al., (2016), which demonstrated heritably silencing through assembly of the KRAB domain and the DNA methyltransferases DNMT3A and DNMT3L, collectively referred to as the "KAL" combination. Nuñez et al., (2021) further advanced the system by integrating the KAL combination into a single fusion protein known as CRISPRoff (Figure 8A and B).

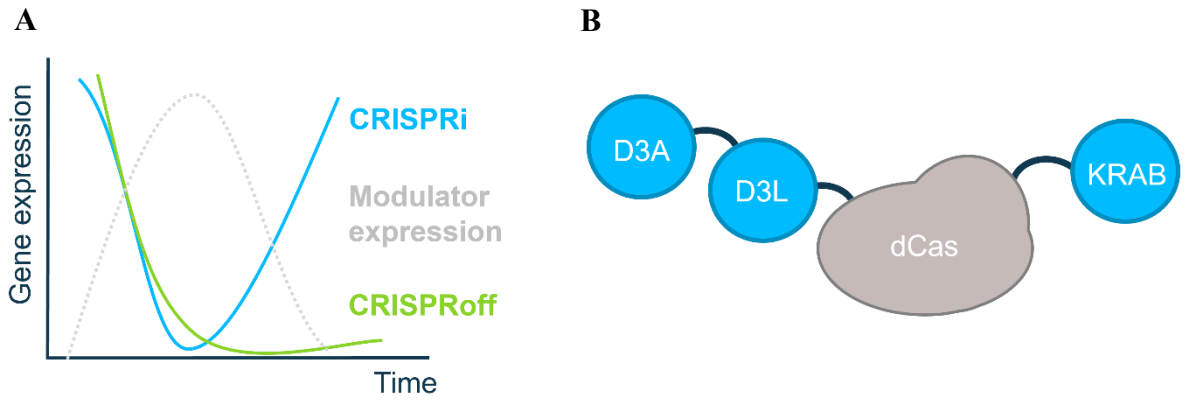

Figure 8: Epigenetic editing with CRISPRoff induces long-term gene silencing. A) Comparison of long-term and transient gene silencing mediated by CRISPRoff (indicated in green) and CRISPRi (indicated in blue), respectively. A distinct difference is that CRISPRi only induces gene repression as long as the modulator is expressed (modulator expression indicated in grey). In contrast to that, a single hit-and-run expression of CRISPRoff is sufficient to induce long-term gene repression, even after the editor is degraded. **B)** The CRISPRoff architecure comprises a catalytically inactive nuclease that mediates DNA binding to a gene of interest. The nuclease and fused with three epigenetic modifiers. These consist of the DNMT3A, DNMT3L and the KRAB domain.

The KRAB domain recruits the corepressor KAP1 (KRAB-associated protein 1) and the histone methyltransferase SETDB1, which together initiate the trimethylation of histone H3 at lysine 9 (H3K9me3). This specific histone modification serves as a binding site for heterochromatin protein 1 (HP1), which plays a crucial role in the establishment and maintenance of heterochromatin. Concurrently, DNA methyltransferases DNMT3A and DNMT3L methylate cytosine residues within CpG dinucleotides in the DNA, further reinforcing the repressive chromatin state (Figure 9) (Schönberg et al., 2023). The combined actions of H3K9me3 and DNA methylation create a robust repressive landscape and has shown promise in inducing long-term gene silencing. This innovative construct enables robust silencing that persists throughout the differentiation of induced pluripotent stem cells (iPSCs) into neurons, demonstrating its effectiveness during cellular transitions. The efficacy of CRISPRoff has been validated in various model organisms, including mice and non-human primates (NHPs) (Cappelluti et al., 2024; Tremblay et al., 2025).

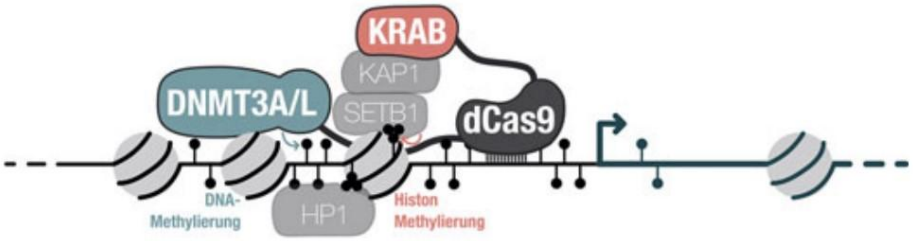

Figure 9: Mechanism of epigenetic repression mediated by DNMT3A, DNMT3L and KRAB. The widely used epigenetic domains DNMT3A, DNMT3L, and KRAB orchestrates a complex interplay of various modulators that collectively establish a repressive chromatin state. The KRAB domain recruits the corepressor KRAB-associated protein 1 (KAP1) and the histone methyltransferase SETDB1, which initiates the trimethylation of histone H3 at lysine 9 (H3K9me3). H3K9me3 functions as a binding site for heterochromatin protein 1 (HP1), which is essential for the induction and maintenance of heterochromatin formation. Furthermore, the combined actions of the DNMT3A and DNMT3L domains facilitate epigenetic modifications at the DNA level by adding methyl groups to CpG dinucleotides. Reprinted from *BIOspektrum*, 29 (1), Schönberg, P. Y., Ding, L. & Buchholz, F., Genom-Editierung ohne die DNA-Sequenz zu verändern—Geht das?, 46-48, Creative Commons CC BY License, 2023..

In addition to Cas9, there exists a diverse array of nucleases from various classes and types that can be utilized for gene editing applications. One notable example is Cas12a (also known as Cpf1), which has emerged as a widely used nuclease due to its unique properties. Type V nucleases, such as Cas12f, are particularly appealing because of their compact size, which facilitates efficient delivery. However, the number of reports concerning the application of Cas12(f) nucleases in CRISPRi or CRISPRoff contexts remains limited. Additionally, there are few studies exploring CRISPRoff with alternative nucleases. Notably, Un1Cas12f and CasX (Cas12e) have demonstrated efficacy in CRISPRi applications (Han et al., 2023; Wang, et al., 2024). Previous reports of CRISPRoff tested with alternative nucleases namely *Staphylococcus aureus* Cas9 (SauCas9) or *Lachnospiraceae bacterium* Cas12a (LbCas12a) demonstrated that they were active although efficiency was reduced by 50%-80%. On top of that, they are similarly restricted due to their large size as SpyCas9 (Nuñez et al., 2021). CRISPRoff with CasPhi (Cas12j2) mediated methylation in plants (Liu et al., 2022). In efforts to engineer a hypercompact epigenetic editors (EE) with enhanced OsCas12f1 (enOsCas12f1), long lasting silencing of the artificial reporter gene *GAPDH-Snrpn* was not shown. Silencing was transient and reactivated 10 days post transfection (p.t.). However, this was also the case for the positive control dSpyCas9CRISPRoff, indicating a potential error in the assay (Kong et al., 2023). Consequently, the actual efficacy of CRISPRoff with en-dOsCas12f may be masked by these inconsistencies. Most recently, further simplified and hypercompact epigenetic editing systems compared to CRISPRoff have been developed. This includes, Obligate Mobile Element Guided Activity OFF (OMEGAoff), coupled histone tail for autoinhibition release of methyltransferase (CHARM) and evolved engineered transcriptional repressor (EvoETR) (Cappelluti et al., 2024; Kannan et al., 2025; Neumann et al., 2024). The latter comprises a CRISPRoff system based

on ZFN instead of SpyCas9, thereby greatly reducing the overall size of the construct. Similarly, OMEGAoff represents a CRISPRoff system based on Nova IscB (engineered IscB) which is considered the ancestor of SpyCas9. It possesses a 5'-NTAAA-3' PAM that restricts its ability to access numerous target sites, particularly in promoter regions which are high in guanine and cytosine content. The CHARM systems consist of DNMT3L, the noncatalytic domain of the DNMT3A-DNMT3L dimer, coupled to an activator consisting of histone H3 tail. Thereby this system recruits endogenously expressed DNMT3A and activates it with histone H3 tail. As the system is based on a ZFN, the system is small enough to fit into an adeno-associated virus (AAV), a delivery vehicle suitable for *in vivo* therapies. When comparing CHARM to the CRISPRoff system, the authors reported similar efficiency on the targets *CD81, CD55* and *CD151*. The system has shown to be effective *in vivo* in mice to silence prion protein (PrP) (Neumann et al., 2024). Both systems, CHARM and EvoETR, are based on a ZFNs. A central advantage of ZFNs is their lower immunogenicity, attributable to the absence of bacterial epitopes, in contrast to CRISPR nucleases derived from bacterial origins (Paschon et al., 2019). However, ZFN with protein-based DNA recognition require an individual ZFN-EE for each additional target site. This will again increase the cargo size and complicate the process by requiring the use of multiple AAVs. Although, the group reported complete silencing of their target of interest with a single binding site - this may be target specific. The engineering process of ZFN consists of assembling multiple zinc finger domains into functional constructs which presents challenges in terms of modularity and compatibility. Each zinc finger domain binds to a specific triad of base pairs in the DNA. In contrast, the targeting of CRISPR nucleases is less complex by solely modifying the short spacer sequence of the sgRNA molecule. This also allows to target multiple sites by adding additional sgRNAs. Consequently, CRISPR technology simplifies the development with fewer design-related complications compared to ZFNs.

1.4 Aim of the thesis

Numerous disease targets require *in vivo* delivery of EEs to distinct tissues for which AAVs are considered a suitable delivery vehicle due to low immunogenicity and availability of multiple AAV serotypes with diverse tissue tropisms. First-generation CRISPR tools pose a significant challenge due to the size typically ranging from 1,000 to 1,500 aa, such as SpyCas9 and SauCas9. This challenge increases for second-generation tools, such as those used for epigenetic editing, which require additional functional domains. The well-characterized EE CRISPRoff based on the large SpyCas9 together with the epigenetic editing domains exceed the AAV packaging limit of ~4.5 kb by far. Recent innovations in the gene editing field have led to the development of the EE systems OMEGAoff, CHARM and EvoETR, which exhibit remarkable efficacy and have demonstrated substantial activity in both murine models and NHPs. However, while IscB-based OMEGAoff suffers from a suboptimal PAM profile (5'-NTAAA-3'), EvoETR and CHARM face challenges due to their dependence on ZFNs. Specifically, these systems necessitate the engineering of bespoken ZFNs that are tailored for a distinct DNA sequence. This requires considerable protein engineering and optimization steps, which can be time-consuming and resource-intensive. We hypothesized that a hypercompact EE could be engineered based on a Cas12f nuclease. To explore this concept, we accessed potential Cas12f nucleases that were identified through a bacterial-genome mining pipeline for CRISPR nucleases, described in section 1.1.3. Nucleases which had previously demonstrated DNA cleavage *in vitro* were selected for evaluation as DNA binding plattforms in mammalian cells. Next, our objective was to integrate the nuclease with epigenetic effector domains to enable permanent gene silencing through epigenetic modifications without the need for DSBs. Ultimately, this work seeks to contribute to the toolbox of hypercompact EE by providing a refined tool suitable for *in vivo* delivery along with the benefits of a CRISPR-based systems.

2. Material and Methods

2.1 Material

2.1.1 Mammalian cell culture media and supplements

12-well tissue culture plates (#150628)	Thermo Scientific, USA
24-well tissue culture plates (#142475)	Thermo Scientific, USA
96-well tissue culture plates (#655182)	Greiner, Austria
96-well-plate	COSTAR®; 96 Well Flat Bottom
Accutase	Merck, Germany
Culture media for HEK293T and HeLa cells	DMEM (10566016, Thermo Fisher Scientific, USA) + 10% Fetal calf (bovine) serum (FCS) + 1% penicillin-strepomycin (Life Technologies, USA)
Cell culture microplate, chimney well, flat bottom	Greiner, Austria
DPBS	Life Technologies, USA
LipoD293	SignaGen, USA
Penicillin-Streptomycin	Life Technologies, USA
Trypsin	Life Technologies, USA

2.1.2 Cells

HEK293T	Ref. CRL-3216 (ATCC), USA
HeLa	Ref. CCL-2 (ATCC), USA
MultiShot™ FlexPlate TOP10 Competent Cells	Invitrogen, USA

2.1.3 Live-cell antibody staining

APC anti-human CD81 (TAPA-1) Antibody	SigmaAldrich, USA
APC anti-human CD151 (PETA-3) Antibody	SigmaAldrich, USA
APC anti-human CD29 Antibody	SigmaAldrich, USA
Bovine Serum Albumin (A9647)	SigmaAldrich, USA

2.1.4 Next generation sequencing library preparation

Betaine (61962)	SigmaAldrich, USA
Blunt/TA Ligase Master Mix	New England Biolabs, USA
CloneAmp Hifi PCR Premix (PR8360437)	Takara, Japan
CpG Methyltransferase (M.SssI)	Thermo Fisher Scientific, USA
EpiTect Fast DNA Bisulfite Kit (50)	Qiagen, Netherlands
EpiTect Fast LyseAll Bisulfite Kit (200)	Qiagen, Netherlands
Lysis buffer	1:800 Proteinase K, 10 mM TRIS, pH 7.0 0.05% SDS
OneTaq Hot Start Quick-Load 2X Master Mix	New England Biolabs, USA
Q5-HF Master mix	New England Biolabs, USA
Qubit dsDNA HS Kit	Thermo Fisher Scientific, USA
TruSeq DNA UD Indexes v2	Illumina, USA
Ultra II End Prep Enzyme Mix	New England Biolabs, USA
Ultra II EP Buffer	New England Biolabs, USA

2.1.5 Next generation sequencing primers

ALB, fwd primer	GGGTGTGTTTCGTCGAGATG
ALB, rev primer	GTGCGCAAAAGAAAATTACAGTCA

CD81 amplicon 1, fwd primer	CAAGTTGGGGGTAGGTGCAG
CD81 amplicon 1, rev primer	CGGAGGCCTGGCAGGATG
CD81 amplicon 27, fwd primer	ACCACTGTGGCATCAACTCC
CD81 amplicon 27, rev primer	CGGAGGCCTGGCAGGATG
CD81, fwd primer (Nuñez et al., 2021) (bisulfite sequencing)	AAGTTGTGGGGTTATTTGTGGGTTTAGGAG
CD81, rev primer (Nuñez et al., 2021) (bisulfite sequencing)	CCCAACACCACCCACCCATCACCACCACA
CD81, fwd primer 4_2 (bisulfite sequencing)	GGAGGGTTGTATTAAGTGTATTAAGTATTTG
CD81, rev primer 4_2 (bisulfite sequencing)	CTCCTAAAACCCACAAATAACCCCACAACTT
DYNC2LI1, fwd primer	GAGATGTAAAAGGATTCCTGAAAATTATATTT
DYNC2LI1, rev primer	CTCTCTCCAAAAATACTCTCAATAACCTTTCC
FGA, fwd primer	TTCGTTTGCTTTTTCTTCTGTC
FGA, rev primer	GGCAAGAATTATTTGCCATCC
H2B, fwd primer	TCCTTGTAAAAGAAGTTGTAACTGTAAATTTTAGT
H2B, rev primer	TAATAACACCCCCAAATAACTTATTAAACTCTT
MAPT, fwd primer	ATAAAGATTTAATTATAGGAGGTGGAGAAAG

MAPT, rev primer	AAACCTTCTCCTCCAACCACTAAT
PCSK9, fwd primer (Whittaker et al., 2023) (bisulfite sequencing)	GTTTGTTTTTTAGTTTAGTTAGGATTTG
PCSK9, rev primer (Whittaker et al., 2023) (Bisulfite sequencing)	AACCTTCTAAAATATAAATACTTAACRC

2.1.6 sgRNAs

Target	**Protospacer**
Albumin	
ApCas12f sgRNA	TGTAAGACTTCACAAATACA
CD81	
ApCas12f sgRNA-a	GAGAGCGAGCGCGCAACGG
ApCas12f sgRNA-b	CCGCGCATCCTGCCAGGCC
ApCas12f sgRNA-c	CCAACTTGGCGCGTTTCGG
ApCas12f sgRNA-1	CGGCGCCCTATAAGTACTGC
ApCas12f sgRNA-2	TATAAGTACTGCGGAGCGAG
ApCas12f sgRNA-3	ATAAGTACTGCGGAGCGAGG
ApCas12f sgRNA-4	GGCCAGAGAGCGAGCGCGCA
ApCas12f sgRNA-5	GCCAGAGAGCGAGCGCGCAA
ApCas12f sgRNA-6	GAGAGCGAGCGCGCAACGGC
ApCas12f sgRNA-7	CAGTACTTATAGGGCGCCGC
ApCas12f sgRNA-8	CGCTCCGCAGTACTTATAGG
ApCas12f sgRNA-9	GGCGCGCGCCTCGCTCCGCA
ApCas12f sgRNA-10	TTGCGCGCTCGCTCTCTGGC
ApCas12f sgRNA-11	CCGTTGCGCGCTCGCTCTCT
ApCas12f sgRNA-12	TCGCCGCCGTTGCGCGCTCG
ApCas12f sgRNA-13	CCGTCGCCGCCGTTGCGCGC
SpyCas9 sgRNA-a	CGGAGAGCGAGCGCGCAACGG
SpyCas9 sgRNA-b	CGGGCCTGGCAGGATGCGCGG
SpyCas9 sgRNA-c	CGCCGAAACGCGCCAAGTTGG
CD151	
SpyCas9 CD151 sgRNA-a	CGCCGGACTCGGACGCGTGGT
SpyCas9 CD151 sgRNA-b	CGTGTCCAGGGACAATGAGCA
SpyCas9CD151 sgRNA-c	CGGACAATGAGCAGGGTGTCC

ITGB1	
SpyCas9 ITGB1 sgRNA-a	CGAGAGGAATGCGTTTCCGGA
SpyCas9 ITGB1 sgRNA-b	CGCCGGGCCGGGCTGACGCGG
SpyCas9 ITGB1 sgRNA-c	CGAGAGGCCCAGCGGGAGTCG

FGA	
ApCas12f sgRNA	ATAAAGCCTTGGTGCATTAT

PCSK9	
SpyCas9 sgRNA-41	ACCGGGAGGAGTGAGCCAGGCAGT
SpyCas9 sgRNA-49	ACCGATCGTCCGATGGGGCTCTGG
ApCas12f sgRNA-1	CTCCCGCCTCTCACCCTGCG
ApCas12f sgRNA-2	CCTCTCCCGCCTCTCACCCT
ApCas12f sgRNA-3	AGGGGCTCCTCCTCTCCCGC
ApCas12f sgRNA-4	TAGGGGCTCCTCCTCTCCCG
ApCas12f sgRNA-5	GCGCCCTAGGGGCTCCTCCT
ApCas12f sgRNA-6	AACTGGGCTGGAAGGCAGGC
ApCas12f sgRNA-7	AATCCTAACTGGGCTGGAAG
ApCas12f sgRNA-8	AAATCCTAACTGGGCTGGAA
ApCas12f sgRNA-9	AACAGCGTCAGATTACGCGC
ApCas12f sgRNA-10	CAAACAGCGTCAGATTACGC
ApCas12f sgRNA-11	CCCCAAACAGCGTCAGATTA
ApCas12f sgRNA-12	TCCCCAAACAGCGTCAGATT
ApCas12f sgRNA-13	CGCCCTCCCCAAACAGCGTC
ApCas12f sgRNA-14	GACTGGAGGATCAGGTTTCG
ApCas12f sgRNA-15	CGGACTGGAGGATCAGGTTT
ApCas12f sgRNA-16	CCGGACTGGAGGATCAGGTT
ApCas12f sgRNA-17	ATCTGATTAAACATTAACGG
ApCas12f sgRNA-18	TCGGACGATCCTATCTGATT
ApCas12f sgRNA-19	ATCGGACGATCCTATCTGAT
ApCas12f sgRNA-20	CATCGGACGATCCTATCTGA
ApCas12f sgRNA-21	GAGCCCCATCGGACGATCCT
ApCas12f sgRNA-22	CCAGAGCCCCATCGGACGAT
ApCas12f sgRNA-23	GGGGCGCGCAGATCACGCCA
ApCas12f sgRNA-24	TCTAGGGTGTGGGTGCTTGA
ApCas12f sgRNA-25	CGACGTCGCTGCGGAAACCT
ApCas12f sgRNA-26	TGAGCGCCTCGACGTCGCTG
ApCas12f sgRNA-27	GCAACCATGAGCGCCTCGAC
ApCas12f sgRNA-28	GCCTGCAACCATGAGCGCCT
ApCas12f sgRNA-29	TGAACTGAACGGCGGCGCCC
ApCas12f sgRNA-30	CCAGGCTCAGACCCTGAACT
ApCas12f sgRNA-31	GGCTCACTCCTCCAGGCTCA
ApCas12f sgRNA-32	GTCTCACTGCCTGGCTCACT
ApCas12f sgRNA-33	GAGCCAGTCTCACTGCCTGG
ApCas12f sgRNA-34	GCCCGAGCCAGTCTCACTGC

ApCas12f sgRNA-35	GCCCGCCCGAGCCAGTCTCA
ApCas12f sgRNA-36	GGCCCGCCCGAGCCAGTCTC
ApCas12f sgRNA-37	CTGCTGCAACGACGCGTCCC
ApCas12f sgRNA-38	GGCTGGGAGCTGGGAGCCGC
ApCas12f sgRNA-39	TGCGGTGGGGAGGACTGTGC
ApCas12f sgRNA-40	TGAGCCTTGCGGTGGGGAGG
ApCas12f sgRNA-41	GCGGCGCCTTGAGCCTTGCG
ApCas12f sgRNA-42	CGCCGGCGGCGCCTTGAGCC
ApCas12f sgRNA-43	TGCGCGGTCCACGCCGGCGG
ApCas12f sgRNA-44	ACGCAGGGTGAGAGGCGGGA
ApCas12f sgRNA-45	CGCAGGGTGAGAGGCGGGAG
ApCas12f sgRNA-46	CTAGGGCGCCGGCCTGCCTT
ApCas12f sgRNA-47	TAGGGCGCCGGCCTGCCTTC
ApCas12f sgRNA-48	AGGGCGCCGGCCTGCCTTCC
ApCas12f sgRNA-49	GCCTGCCTTCCAGCCCAGTT
ApCas12f sgRNA-50	GCCTTCCAGCCCAGTTAGGA
ApCas12f sgRNA-51	TCCAGCCCAGTTAGGATTTG
ApCas12f sgRNA-52	GCCCAGTTAGGATTTGGGAG
ApCas12f sgRNA-53	AGTTAGGATTTGGGAGTTTT
ApCas12f sgRNA-54	GTTAGGATTTGGGAGTTTTT
ApCas12f sgRNA-55	TCTGCGCGTAATCTGACGCT
ApCas12f sgRNA-56	CTGCGCGTAATCTGACGCTG
ApCas12f sgRNA-57	AAACCTGATCCTCCAGTCCG
ApCas12f sgRNA-58	GATCCTCCAGTCCGGGGGTT
ApCas12f sgRNA-59	CCAGTCCGGGGGTTCCGTTA
ApCas12f sgRNA-60	GTCCGGGGGTTCCGTTAATG
ApCas12f sgRNA-61	GGGGTTCCGTTAATGTTTAA
ApCas12f sgRNA-62	TTAATGTTTAATCAGATAGG
ApCas12f sgRNA-63	ATGGGGCTCTGGTGGCGTGA
ApCas12f sgRNA-64	CAGGCGTCAAGCACCCACAC
ApCas12f sgRNA-65	AGGCGTCAAGCACCCACACC
ApCas12f sgRNA-66	GGCGTCAAGCACCCACACCC
ApCas12f sgRNA-67	ACACCCTAGAAGGTTTCCGC
ApCas12f sgRNA-68	CACCCTAGAAGGTTTCCGCA
ApCas12f sgRNA-69	TAGAAGGTTTCCGCAGCGAC
ApCas12f sgRNA-70	AGAAGGTTTCCGCAGCGACG
ApCas12f sgRNA-71	CAGCGACGTCGAGGCGCTCA
ApCas12f sgRNA-72	CCGTTCAGTTCAGGGTCTGA
ApCas12f sgRNA-73	TTCAGTTCAGGGTCTGAGCC
ApCas12f sgRNA-74	GGAGGAGTGAGCCAGGCAGT
ApCas12f sgRNA-75	GGCAGTGAGACTGGCTCGGG
ApCas12f sgRNA-76	GGACGCGTCGTTGCAGCAGC
ApCas12f sgRNA-77	AGCTCCCAGCCAGGATTCCG
ApCas12f sgRNA-78	AGCCAGGATTCCGCGCGCCC
ApCas12f sgRNA-79	GGATTCCGCGCGCCCCTTCA
ApCas12f sgRNA-80	CGCGCCCCTTCACGCGCCCT
ApCas12f sgRNA-81	CTTCACGCGCCCTGCTCCTG

ApCas12f sgRNA-82	TTCACGCGCCCTGCTCCTGA
ApCas12f sgRNA-83	GCTCCTGAACTTCAGCTCCT
ApCas12f sgRNA-84	GAACTTCAGCTCCTGCACAG
ApCas12f sgRNA-85	GCACAGTCCTCCCCACCGCA
ApCas12f sgRNA-86	CCCCACCGCAAGGCTCAAGG
ApCas12f sgRNA-87	CACCGCAAGGCTCAAGGCGC
ApCas12f sgRNA-88	ACCGCAAGGCTCAAGGCGCC
ApCas12f sgRNA-89	CAAGGCTCAAGGCGCCGCCG
ApCas12f sgRNA-90	CCGGCGTGGACCGCGCACGG

Snrpn	
CasMini sgRNA-1	CGGCAAAAATGTGCGCATGT
CasMini sgRNA-2	CCTGGGACGCATGCGTAGGG
CasMini sgRNA-3	CGGCAAGACTAGCGCAGAGA
SpyCas9 sgRNA (Liu et al., 2016)	ACCGACAAACCTGAGCCATTG
SpyCas9 sgRNA (Nuñez et al., 2021)	ACCGCTCCTCAGAACCAAGCGTC
BreCas12b sgRNA-1	CGGCAAAAATGTGCGCATGT
BreCas12b sgRNA-2	CCTGGGACGCATGCGTAGGG
BreCas12b sgRNA-3	CGGCAAGACTAGCGCAGAGA

TRE3G	
Same protospacer for all tested nucleases (Xu et al., 2021)	CTCCCTATCAGTGATAGAGAACG

2.1.7 Laboratory equipment

BD FACSCanto II	BD, USA
BD FACSMelody	BD, USA
CyBio FeliX Liquid Handler	Analytik Jena, Germany
Infinite M1000 pro	Tecan, Switzerland
iQue PLUS VYB	Sartorius, Germany
Nextseq 2000	Illumina, USA

2.1.8 Software

Pre-processing of NGS files:	
Fastp	Chen et al., 2018
Fastq-join	Erik Aronesty, 2013
Ultraplex	Wilkins et al., 2021
Bismark bisulfite mapper	Krueger & Andrews, 2011
CRISPResso	Pinello et al., 2016
Geneious Prime version 2025.1 created by Biomatters	http://www.geneious.com/

2.2 Methods

2.2.1 Cloning of CRISPRa-, CRISPRoff-, sgRNA- and repoter plasmids

For the cloning of the CRISPR activation (CRISPRa) constructs, a synthesis plasmid containing the tripartite activator VP64-p65-RTA (VPR), as described by Xu et al. (2021), was ordered from Twist Bioscience (USA). It was subsequently cloned into a plasmid backbone termed pBLR1217 containing a CAG promoter, a pUC origin of replication, ampicillin resistance and TagRFP utilizing *NotI* and *Eco*RI restriction enzymes. We combined the VPR cassette n-terminally with a lacZ gene to enable a substitution of lacZ with a nuclease of interest via Golden Gate cloning using *Bsa*I (Engler & Marillonnet, 2014).

The catalytically inactive Cas12f variants were engineered by aligning the nuclease sequences to Un1Cas12f1 (PDB: 7C7L) using Geneious Prime (version 2025.1) and introducing a mutation into the first and second cutting motif of the RuvC domain. The amino acid sequences were back-translated circumventing type II restriction sites, specifically *Bpi*I and *Bsa*I. The nuclease sequences were ordered as gBlocks from Integrated DNA Technologies (IDT, USA) and subsequently cloned into the CRISPRa acceptor vector using *Bsa*I via Golden Gate cloning. The final CRISPRa plasmid is illustrated in Figure 10 and the full plasmid sequence is provided in the Appendix.

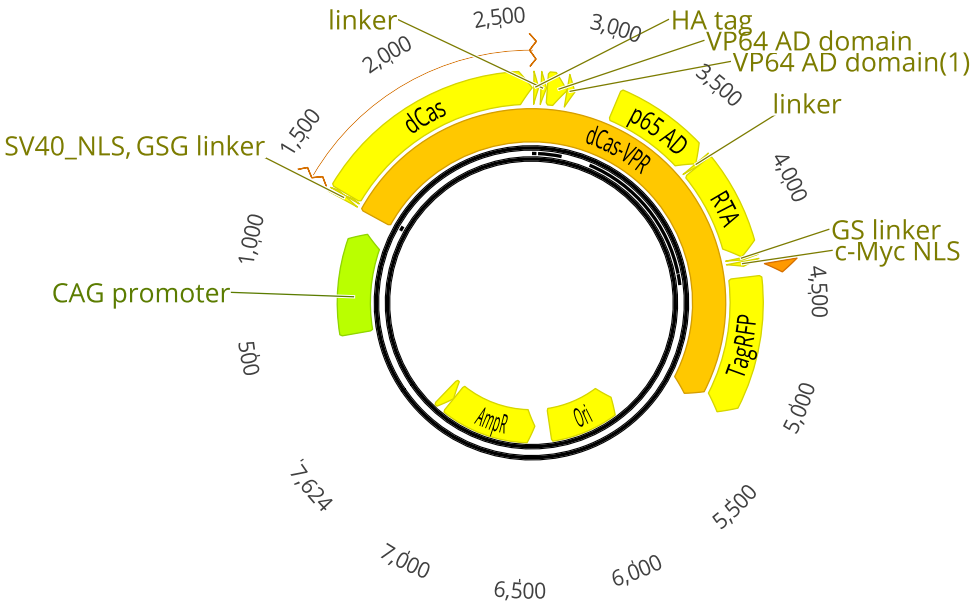

Figure 10: Plasmid map of CRISPRa constructwhich is based on the fusion of dCas with the tripartite activator VPR.

Analogously, the CRISPRoff sequence consisting of DNMT3A-DNMT3L-XTEN80-lacZ-HA-2xNLS-BFP-KRAB (CRISPRoff, as described by Nuñez et al., (2021)) was ordered from Twist Bioscience as synthesis plasmid. We integrated a lacZ cassette for subsequent substitution with a nuclease of interest. This construct was integrated into our plasmid backbone pBLR1217, using *Not*I and *Xho*I restriction enzymes, creating the CRISPRoff acceptor backbone termed pBLR2017 (Figure 11). The use of *Xho*I facilitated the exclusion of TagRFP in the backbone pBLR1217, as the ordered gene cassette incorporated TagBFP. Nucleases of interest were cloned into the CRISPRoff acceptor vector via Golden Gate cloning using *Bsa*I. The full plasmid sequence is provided in the Appendix.

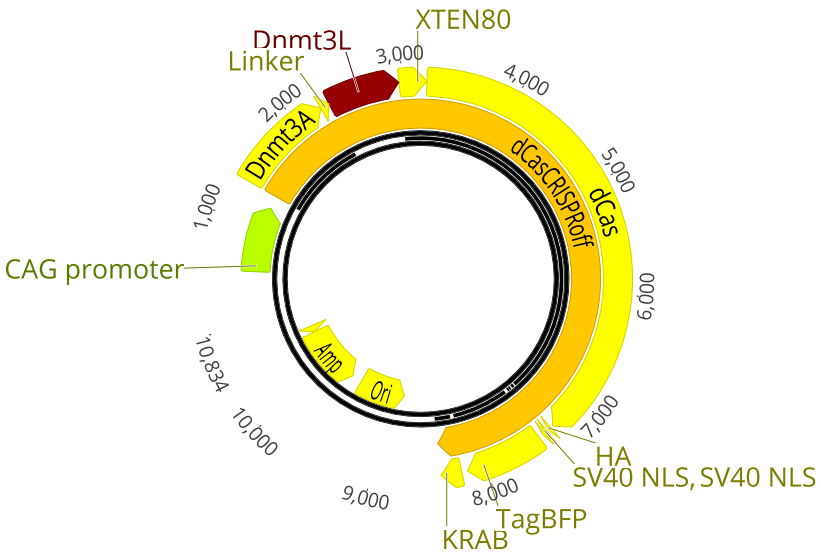

Figure 11: Plasmid map of CRISPRoff. This includes fusion of dCas with the epigenetic domains DNMT3A, DNMT3L and KRAB.

Gene fragments encoding the alternative EE architectures and CRISPRi architectures were ordered from GeneArt (Germany) as synthetic plasmids. The gene fragments encoding alternative EE1-EE4, and CRISPRi variants EE12-EE17 were subcloned by GeneArt through restriction digestions by *Xho*I and *Not*I into our backbone plasmid pBLR1217. In contrast, EE5-EE11 were cloned by digesting the CRISPRoff acceptor backbone pBLR2017 with *Bam*HI to extract the N-terminal linker XTEN80 (see Figure 11). Constructs encoding EE5-EE11 were ordered from GeneArt as synthetic plasmids and subcloned via *Bbs*I into *Bam*HI predigested pBLR2017.

We cloned U6-driven sgRNAs, with the respective sgRNA scaffolds (tracrRNA + crRNA) for each nuclease integrated into a sgRNA acceptor vector. The sgRNA scaffolds were ordered as gBlocks from IDT. We inserted a lacZ cassette as spacer, allowing for the subsequent substitution of lacZ with a spacer matching the target of interest (Figure 12). The spacers were cloned into the sgRNA backbone either through *Bsa*I or *Esp3*I. Of note, in case of Cas12f nucleases, the spacer was placed at the 5' end of the sgRNA scaffold.

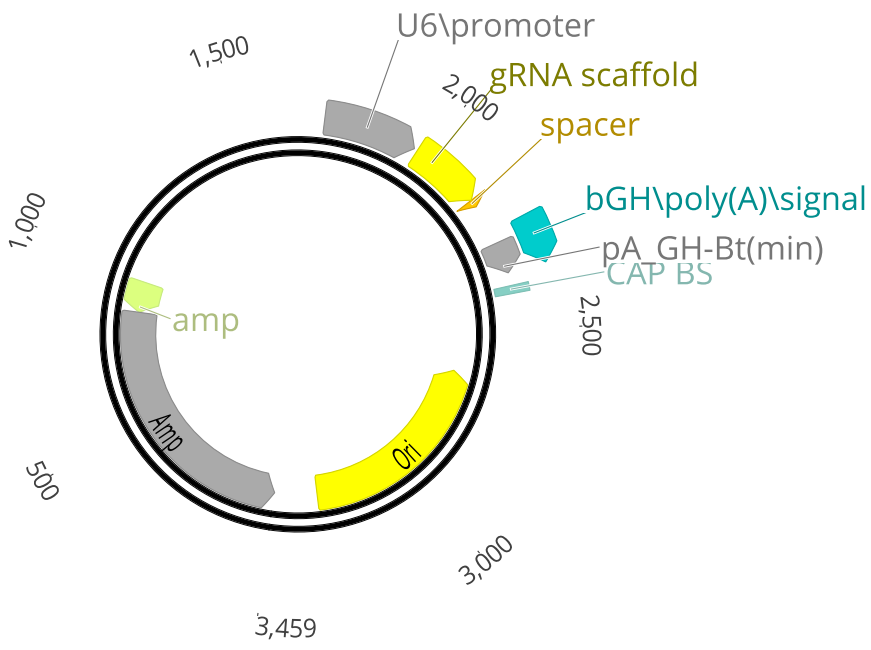

Figure 12: Plasmid map of sgRNA expression plasmid. The sgRNA plasmids contain a U6 promoter driving the expression of the sgRNA scaffold fused to the spacer for target recognition.

We cloned a reporter plasmid harboring a reporter cassette as described by Xu et al. (2021). This consisted of the *TRE3G*-minimalCMV promoter construct fused to GFP. The *TRE3G* promoter was adapted for each nuclease in accordance with their PAM preferences. Additionally, we integrated a second reporter gene, NanoLuc® (Nluc), upstream of GFP,

connected via a P2A sequence (Figure 13A) (England et al., 2016). Similarly to that, we cloned a reporter plasmid harboring the methylation-sensitive promoter *GAPDH-Snrpn* upstream of a Nluc-P2A-GFP reporter cassette (Figure 13B).

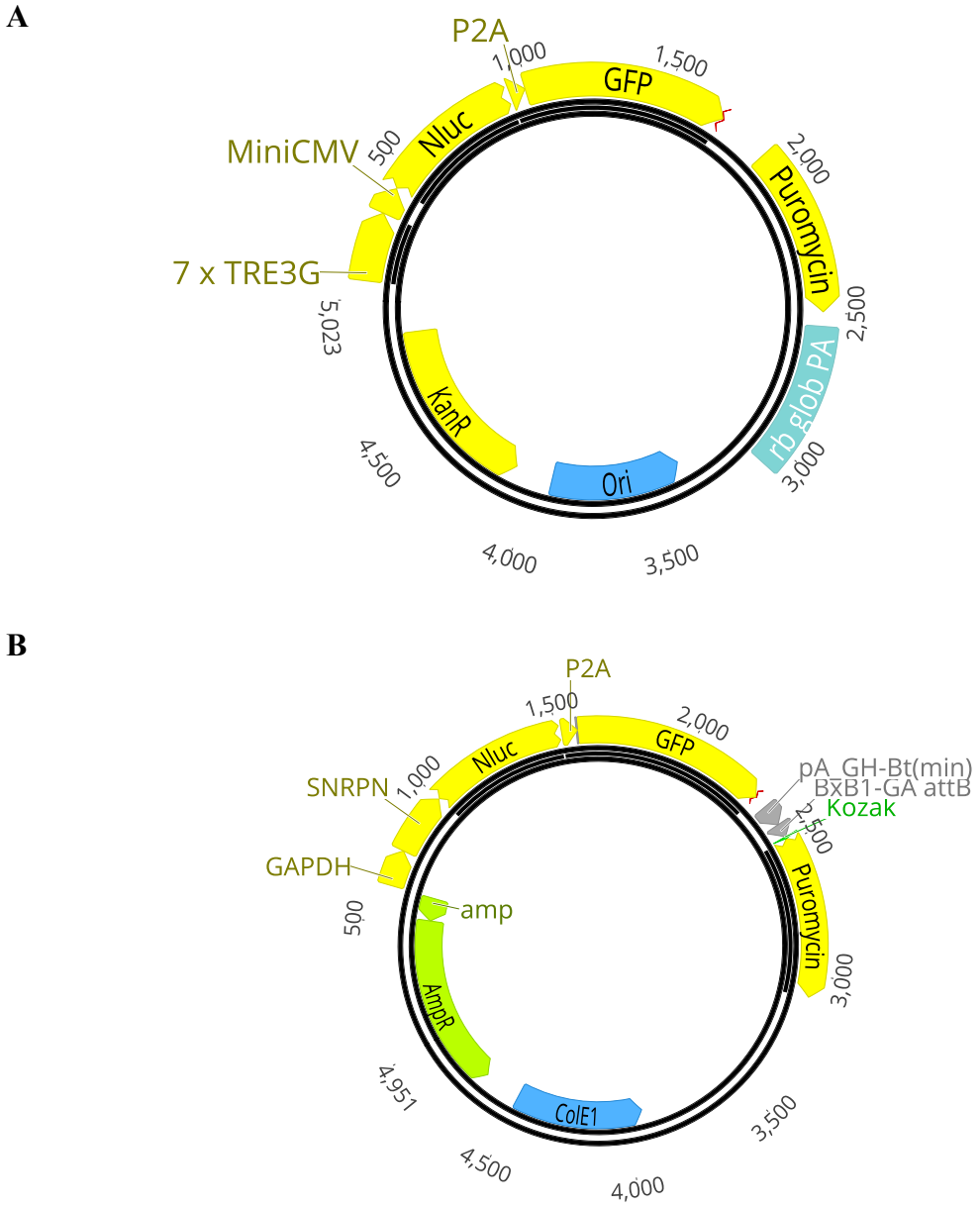

Figure 13: Plasmid map of reporter plasmids. A) Reporter plasmid harboring a promoter with seven *TRE3G* repeats enabling seven sgRNA binding sites with a single sgRNA. The promoter also includes a minimal CMV promoter. The promoter is fused to a Nluc-P2A-GFP reporter gene cassette. **B)** Fusion of the methylation-sensitive and constitutively active promoter *GAPDH-Snrpn* with the Nluc-P2A-GFP reporter gene cassette.

2.2.2 Cloning of ApCas12f *PCSK9* sgRNAs

Cloning of *PCSK9* sgRNAs was conducted as previously described but utilizing a 96-well format. Following Golden Gate cloning, an additional *Bsa*I digest was performed for 1 hour at

37°C to eliminate undigested backbone. 2 µl of the Golden Gate reaction were subsequently mixed with Top10 *E. coli* for transformation. Transformation of the Top10 cells was carried out via heat shock: the cells were incubated on ice for 20 minutes at 4°C, subjected to a 1-minute heat shock at 42°C, and then returned to ice for 5 minutes at 4°C. Afterward, the cells were subjected to recovery for 1 hour at 37°C in LB media. Following recovery, the cells were incubated for 24 hours at 37°C at 250 rpm in LB media supplemented with ampicillin. Plasmid DNA was purified using the Promega Wizard MagneSil Tfx™ System on the Analytik Jena CyBio FeliX Liquid Handler. The step of purification was kindly carried out by our colleague Sabine Jach.

2.2.3 Assessment of nucleases in transactivation assay

To assess the RNA-guided DNA binding activity of novel nucleases, a transactivation assay in HEK293T cells was adapted from Xu et al., 2021. The assay is based on a triple plasmid transfection of a dCas-VPR plasmid, sgRNA plasmid and reporter plasmid. HEK293T cells (ATCC® CRL-3216™) were cultured in DMEM containing 10% FBS and 1% Pen/Strep at 37°C in 5% CO_2 under humidified conditions. Cells were cultured in T75 flasks and were split every 2-3 days. 3-5 hours prior to transfection, cells were seeded at a density of 35.000 cells per well to reach 70%-80% confluency in a coated 96-well-plate (COSTAR®; 96 Well Flat Bottom). Cells were transfected with 140 ng dCas-VPR plasmid, 60 ng sgRNA plasmid and 25 ng target/reporter gene plasmid using LipoD293™ In Vitro DNA Transfection Reagent (SignaGen) according to the manufacturer's instructions. One day post transfection (p.t.), cells were harvested for downstream analysis of reporter gene activation. Cells were removed from the incubator, washed with PBS and incubated in 30 µL trypsin at 37°C for 10 minutes to detach cells. The cell suspension were transferred into a 96-well cell culture microplate (chimney well, Greiner bio-one, PS,F-Bottom (REF 655083)) to measure GFP reporter gene activation using an iQue FACS machine followed by Nluc luminescence read-out on an Infinite M1000 pro (Tecan) using Nano-Glo® Dual-Luciferase® Reporter Assay System Kit (Promega). In short, cells were removed from the incubator, cell culture media was reduced to 25 µL and supplemented with 25 µL ONE-Glo™ reagent to lyse cells for 10 min at 500 rpm at room temperature. 25 µL NanoDLR™ Stop & Glo® reagent was added followed by NanoLuc® luminescence read-out. Over a time course of 30 min, reporter gene expression was measured every 90 sec with 1 sec integration time. Binding activity was calculated as fold change compared to the non-targeting sgRNA control (NT ctrl).

2.2.4 Site-directed mutagenesis

Point-mutations were introduced into WT ApCas12f through ligation during amplification (LDA) cloning. This involved primers carrying the desired mutations, listed in Table 3. These primers were designed to carry a 5' phosphate group, facilitating the ligation process. Full amplification of the WT plasmid was performed, resulting in the accumulation of non-methylated PCR products. Following amplification, digestion with *DpnI* was conducted; this enzyme specifically digests methylated plasmids, while leaving the non-methylated PCR products intact. The resulting PCR products were then transformed into *E. coli*, allowing the bacteria to generate complementary strands of the plasmid. Plasmid DNA was purified using the Promega Wizard MagneSil Tfx™ System on the Analytik Jena CyBio FeliX Liquid Handler. Cloning was kindly carried out by the colleagues Dr. Andreas Neerincx and Corinna Saalwächter and subsequent purification were carried out by Konrad Odendahl.

2.2.5 Gene silencing assessment on reporter plasmids

To investigate the gene silencing capabilities of various cutting-deficient nucleases within the CRISPRoff framework, these nucleases were cloned into a CRISPRoff backbone. Reporter plasmids were subsequently constructed, incorporating either a minimal *GAPDH-Snrpn* (promoter) + Nluc-P2A-GFP (reporter gene) or a longer variant of the *GAPDH-Snrpn* (promoter) + Nluc-P2A-GFP (Stelzer et al., 2015) as described in section 2.2.1. These promoter constructs are constitutively active and are characterized by their ability to generate robust reporter gene signals, which can be effectively silenced through methylation processes (Nuñez et al., 2021). 24 hours prior to transfection, cells were seeded at a density of 18,000 cells per well in a coated 96-well plate (COSTAR®; 96 Well Flat Bottom) to achieve 70%-80% confluency. On the day of transfection, media was replaced with 100 µl fresh media containing FCS and Pen/Strep. Cells were transfected with 140 ng of dCas-CRISPRoff plasmid, 60 ng of sgRNA plasmid, and 25 ng of reporter gene plasmid using LipoD293™ In Vitro DNA Transfection Reagent. The assessment of reporter gene silencing was conducted at 72- and 96-hours post-transfection, as previously described. The assay was adapted from Nuñez et al., (2021).

To elucidate the silencing efficacy of novel epigenetic architectures, we undertook the cloning of cutting-deficient nucleases into a variety of EE constructs, as described in section 2.2.1. These constructs were designed to incorporate diverse architectural arrangements of epigenetic effector domains, thereby enabling a comprehensive evaluation of their functional capabilities. We evaluated the silencing efficiency by targeting a constitutively active reporter gene. While

experimental conditions were unchanged, a pivotal modification in our experimental design was the exchange of the reporter plasmid from the *GAPDH-Snrpn* system with the reporter plasmid *TRE3G-minimalCMV* utilized in our transactivation assay. In the latter one, we leveraged the basal expression of the reporter gene driven by a minimal cytomegalovirus (CMV) promoter. In our experiments we noted that this system provides a robust signal for the effective testing of different architectural designs of EE.

2.2.6 Cell line generation and silencing assessment

We generated reporter cell lines by stably integrating the long or minimal *GAPDH-Snrpn* reporter cassettes into the AAVS1 safe harbor locus of a HEK293T cell line. A HEK293T landing pad cell line was employed, utilizing a recombinase-mediated approach. The transgene was coupled to a puromycin resistance gene. 2 days post-transfection, the cells were cultured in media supplemented with puromycin (1 µg/mL) to enrich those with integrated reporter constructs. The cell lines were seeded one day prior to transfection in a 96-well plate and transfected with 140 ng effector plasmid and 60 ng sgRNA. 3, 4 and 7 days p.t. cells were analyzed for Nluc expression.

2.2.7 Immunofluorescence staining

HEK293T cells (ATCC® CRL-3216™) were cultured in DMEM containing 10% FBS and 1% Pen/Strep at 37°C in 5% CO2 under humidified conditions. 24 hours prior to transfection, HEK293T cells were seeded at a density of 1.8 x 10^5 cells per well to reach 70%-80% confluency in a poly-D-lysine treated 96-well plate. Cells were transfected with plasmids encoding the effector (140 ng) and single- or pools of sgRNAs (60 ng) targeting either the promoter of cell surface protein integrin beta 1 (*ITGB1*), Cluster of differentiation (*CD81*) or Cluster of differentiation (*CD151*). The cells were passaged every 2 to 3 days to monitor the durability of gene silencing. For harvesting, cells were incubated in 30 µL trypsin at 37°C for 10 minutes to facilitate detachment. Subsequently, between 3-10 × 10^4 cells were transferred into a fresh 96-well plate. Notably, 3 days p.t., no more than 50% of a confluent well was harvested to ensure the recovery of a sufficient cell number for subsequent analyses of the transfected and stressed cells. Following harvesting, the cells were washed twice with phosphate-buffered saline (PBS) containing 1% bovine serum albumin (BSA) and incubated for 45 min in the dark in 95 µL of PBS supplemented with 1% BSA and 5 µL antibody. After two additional washing steps, the cells were resuspended in 100 µL of PBS and live cell staining was analyzed using a BD FACSCanto II flow cytometer.

2.2.8 Transfection and cell sorting of HEK293T cells for epigenetic editing analysis

HEK293T cells (ATCC® CRL-3216™) were cultured in DMEM containing 10% FBS and 1% Pen/Strep at 37°C in 5% CO2 under humidified conditions. 24 hours prior to transfection, HEK293T cells were seeded at a density of 2.1 x 10^5 cells per well to reach 70%-80% confluency in a poly-D-lysine treated 24-well plate (Corning; 96 Well Flat Bottom). Cells were transfected with 700 ng effector plasmid and 300 ng sgRNA plasmid using LipoD293™ In Vitro DNA Transfection Reagent (SignaGen) according to the manufacturer's instructions. Of note, twice as much of DMEM + LipoD was used to increase transfection efficiency (2 x 50 µl DMEM + 3 µl LipoD). 2 days p.t., cells were sorted using the BD FACSMelody. Cells were carefully detached by incubation for 10 min at 37°C in 300 µl accutase. To increase cell viability, cells were maintained at 37°C during the sorting process. 6 x 10^5 cells were sorted out and plated into a 96-well plate. Culture media was composed of 50%-75% conditioned media to facilitate cell recovery after sorting. Cells were cultured by splitting every 2-3 days. Gene silencing was monitored at different time points by immunofluorescence staining as described in section 2.2.7.

2.2.9 DNA cleavage analysis through NGS

HEK293T cells (ATCC® CRL-3216™) were cultured in DMEM containing 10% FBS and 1% Pen/Strep at 37°C in 5% CO2 under humidified conditions. HEK293T cells were seeded one day prior to transfection in a 96-well plate and transfected with 140 ng effector plasmid and 60 ng sgRNA. 3 days p.t. cells were harvested and subjected to flow-cytometry analysis of BFP or GFP expression as indicator of transfection efficiency. Next, cells were transferred into a fresh PCR plated and pelleted for 5 min at 500 × g. The supernatant was discarded, and the cells were lysed in 60 µl lysis buffer (10mM Tris, pH 7.0 and 0.05% SDS supplemented with 1:800 proteinase K) for 1 hour at 37°C, followed by incubation for 30 min at 80°C to deactivate proteinase K. Editing outcomes were analyzed by next generation sequencing (NGS). For NGS library preparation, the target sequences were amplified from 3 µl cell lysates (template) using 2.5 µl barcoded primers (10 µM stock) and Q5-High-Fidelity polymerase master mix following the cycling program as stated below.

PCR steps	Temperature [°C]	Time [min]	Number of cycles
Initial denaturation	98	00:30	
Denaturation	98	00:10	34x
Annealing	66	00:30	
Elongation	72	00:15	
Final extension	72	02:00	

PCR samples were pooled and purified by mixing with Solid Phase Reversible Immobilization (SPRI) beads in equal amounts. During incubation for 5-10 min at room temperature, the amplicons were bound to the beads. The beads were washed twice with 80% ethanol. To remove residual ethanol which can interfere with elution from the beads, beads were carefully centrifuged and incubated at 37°C for up to 5 min. The library was eluted from the beads utilizing 80-100 µl elution buffer (EB) (10mM Tris, pH 8). For Illumina Adapter Ligation, amplicons were end-repaired and dA-tailed using the NEBNext® Ultra™ II End Repair/dA-Tailing Module. In brief, 2 µg of purified PCR library were mixed with 6 µl NEBNext Ultra II End Prep Enzyme Mix and 14 µl NEBNext Ultra II End Prep Reaction Buffer. The volume was raised to 100 µl with nuclease-free H_2O. The end repair was conducted in a thermocycler for 30 min at 20°C followed by 10 min at 65°C. The reaction was cleaned-up with SPRI beads and eluted into only 32 µl. 30 µl of end-prepped DNA was mixed with 32 µl blunt/TA Ligase Master Mix and 3 µL TruSeq DNA UD Illumina Indexes. The reaction was incubated for 20-60 min at RT. After adapter ligation, the volume was raised to 100 µl with EB. 80 µl of SPRI beads were added and the samples were cleaned-up as described above. The library was eluted in 52 µl EB and 50 µl were transferred to a new Eppendorf tube. The concentrations of the libraries were measured using the Qubit™ dsDNA HS Assay Kit on a Qubit fluorometer following the manufacturers' instructions. For successful cluster generation on the Illumina flow cell, the library was diluted to a concentration of 450 pM to avoid over- or underloading of the flow cell. The library was loaded onto a NextSeq 1000 P2 600 Reagent Cartridge in paired-end mode to achieve a read length of 300 bp from each side.

The resulting raw FastQ-files were processed on a Linux-based system. Adapter sequences, primers, poly-A tails and other forms of unwanted sequences were removed from sequencing reads by applying the tool "fastp" (Chen et al., 2018). Specifically, the settings *-q 30 -l 110 -i*, which enabled the filtering of low-quality reads with a quality score threshold of Q30,

indicating an error rate of less than 1 in 1000 bases. The setting *-l 110* ensured that only reads with a minimum length of 110 bases were retained for further evaluation. The trimmed forward and reverse FastQ-files were joined using the command-line tool “fastq-join” (Aronesty, 2013). The files were demultiplexed using a python script, developed by our colleague Dr. Florian Richter, based on the sample-specific barcodes. Following this preprocessing, we employed CRISPResso, a specialized software tool designed for the analysis of CRISPR editing outcomes (Pinello et al., 2016). CRISPResso facilitates the alignment of sequencing reads to a reference sequence, enabling the identification and quantification of editing events, including insertions, deletions, and substitutions.

For target *CD81*, adjustments to the protocol were implemented to address challenges associated with its high GC content. While the overall procedure adhered to the previously described steps, specific modifications were necessary to optimize the amplification process. Initially, lysed cells underwent genomic DNA (gDNA) preparation, from which 50 ng of gDNA was utilized as input for PCR. In contrast to our standard PCR protocol, we observed that increasing the primer concentrations to 3-fold enhanced PCR output. Additionally, we incorporated CloneAmp Hifi PCR Premix supplemented with betaine, to further enhance the amplification of GC-rich sequences. The PCR conditions were followed as described below:

PCR steps	**Temperature [°C]**	**Time [min.]**	**Number of cycles**
Initial denaturation	98	00:30	
Denaturation	98	00:10	34x
Annealing	62.9 (primers #1) 61.9 (primers #2)	00:05	
Elongation	72	00:07	
Final extension	72	02:00	

To further mitigate the risk of generating non-specific amplification products, the PCR was conducted with careful handling on ice and immediate purification after PCR completion as the polymerase was prone to producing numerous unspecific bands. Besides these adaptions in NGS library preparation, further adjustments were taken in the bioinformatic analysis. This includes demultiplexing in single-end mode using the tool “ultraplex” (Wilkins et al., 2021). The reads were subsequently joined using "fastq-join," as it was observed that a significant number of reads were lost if joining occurred prior to demultiplexing.

2.2.10 Bisulfite-sequencing

DNA methylation patterns were analyzed by targeted bisulfite sequencing coupled to NGS. Genomic DNA was extracted and treated with sodium bisulfite using the EpiTect Fast DNA Bisulfite Kit (Qiagen) according to the manufacturer's instructions. The initial primer pair tested for *CD81* was derived from Nuñez et al. (2021). To optimize the amplicon, we generated novel primer pairs using the MethPrimer tool (Li & Dahiya, 2002) or designed them manually. A summary of the primer pairs is provided in Table 1. The optimal annealing temperature was determined to be 61°C for the *CD81* amplicon 4_1 and 50°C for *PCSK9*. The bisulfite-converted DNA was then amplified using OneTaq Hot Start polymerase, with 100 ng of template and 1 µL of barcoded primers (100 µM stock) as per the manufacturer's guidelines.

PCR steps	Temperature [°C]	Time [min.]	Number of cycles
Initial denaturation	94	00:30	
Denaturation	94	00:30	40x
Annealing	61 (*CD81* primer 4_1) 50 (*PCSK9* primer)	00:05	
Elongation	68	00:30	
Final extension	72	02:00	

Subsequently, the resulting amplicons were subjected to NGS library preparation as previously described. Adapter sequences, primers, poly-A tails and other forms of unwanted sequences were removed from the sequencing reads by applying the tool “fastp” as previously described (Chen et al., 2018). The resulting raw fastq-files were demultiplexed in single-end mode based on sample-specific barcodes using the tool “ultraplex” (Wilkins et al., 2021). Following demultiplexing, the methylation status of the targeted genomic regions was determined using the Bismark bisulfite mapper (v0.22.3) (Krueger & Andrews, 2011). The reads were mapped to the respective reference genome and the percentage of methylated CpG sites was calculated. The specific settings included the parameter *--non_directional* meaning that the mapper does not take into account on which strand the original methylation marks were on. Besides that, the parameter *score_min L,0,-1.5* allowed for relaxed alignment, accommodating approximately 10 mismatches in non-CG contexts. This adjustment was particularly important for the *CD81* target which due to its high GC-rich content suffered from sequencing errors. Otherwise, it would have been underrepresented as reads due to the default settings that do not permit mismatches.

Table 1: CD81 bisulfite-sequencing primer. ***A. temp.: annealing temperature*****.**

Amplicon	**Orientation**	**Sequence**	**A. temp. [°C]**
Amplicon 1 (Nuñez et al., 2021)	fwd	AAGTTGTGGGGTTATTTGTGGGTTTAGGAG	61 & 55.2
Amplicon 1 (Nuñez et al., 2021)	rev	CCCAACACCACCCACCCATCACCACCACA	
Amplicon 2	fwd	TTAAGTGTATTAAGTATTTGTTTTT	53
Amplicon 2	rev	AAAACCCACAAATAACCCCACAACT	
Amplicon 3	fwd	TTTTTTAGAAGGGTTTTGGAGGTTT	61
Amplicon 3	rev	CATCAATCACTTCCCAACAACAAAA	
Amplicon 4_1	fwd	TTATGGGAGTGGAGGGTTGTATTAAGTG	61
Amplicon 4_2	fwd	GGAGGGTTGTATTAAGTGTATTAAGTATTTG	61
Amplicon 4	rev	CTCCTAAAACCCACAAATAACCCCACAACTT	
Amplicon 5	fwd	CCCCTCCATAAACCCCRCCCCRACCAACTCA	61
Amplicon 5	rev	GTGTATTTGGGTTTTGAGGTTTTGGYGAAA	

2.2.11 In-vitro methylation

To establish bisulfite sequencing, we conducted *in vitro* methylation of genomic DNA from HEK293T cells using a CpG Methyltransferase as described by the manufacturer's instructions (M.SssI). In order to determine varying degrees of methylation, a temporal gradient of *in vitro* methylation was performed. The methylated DNA was subsequently subjected to bisulfite conversion using the EpiTect Fast DNA Bisulfite Kit (Qiagen), as described by the manufacturer's instructions. The regions of interest were amplified with barcoded primers and subjected to multiplexed NGS analysis. Methylation levels and patterns were analyzed using the Bismark bisulfite mapper (Krueger & Andrews, 2011).

3. Results

3.1 Establishing assays for epigenetic editing readout

To engineer and evaluate hypercompact EEs, it was essential to establish suitable assays for assessing epigenetic silencing. For this purpose, we employed the state-of-the-art EE CRISPRoff, which has known activity, to test and validate our assays. We started by establishing an assay based on the methodology described by Nuñez et al., (2021). Following this, we conducted DNA methylation analysis using bisulfite sequencing. Taken together, these efforts laid the foundation for all subsequent engineering steps and enabled us to evaluate the efficacy of the engineered EEs.

3.1.1 Optimizations of CRISPRoff assays lead to permanent silencing of *CD81*

As described by Nuñez et al. (2021), HEK293T cells were transfected with plasmids encoding CRISPRoff alongside pools or individual sgRNAs, targeting *CD81*, *CD151*, and *ITGB1*, which encode for cell surface proteins. Protein silencing was monitored over time through live cell antibody staining, followed by flow-cytometry analysis (Figure 14A).

Cells treated with the CRISPRoff system in conjunction with a pool of sgRNA-a and -b targeting *CD81* exhibited approximately 70% reduction of *CD81*-positive cells 2 days p.t.. When tested individually, the sgRNA-a and sgRNA-b induced 20% and 50% gene silencing. Similarly, there was 60%-70% reduction of *CD151* with a pool of three sgRNAs (a+b+c), as well as through the application of individual sgRNAs (a-c). However, it is noteworthy that this silencing effect was not sustained over time; by 10 days p.t., protein levels had recovered to nearly baseline levels for both *CD81* and *CD151* as depicted in Figure 14B. For CD81, there were 5%-10% silenced cells after treatment with sgRNA-a and the gRNA pool (a+b). For samples treated with sgRNA-b, there were 20% of silenced cells detected. Across all tested sgRNA targeting CD151, silencing maintained only for 5%-10% of cells. Due to the high background noise associated with ITGB1, this target was excluded from further investigations. We tested both CRISPR interference (CRISPRi) and small hairpin RNA (shRNA) as transient controls along CRISPRoff for comparison. We observed 70% and 40% silencing of *CD81* at 2 days p.t. by CRISPRi and shRNA, respectively. However, by 10 days p.t., *CD81* expression levels returned to wild type (WT) levels. Overall, our findings indicated a discrepancy in CRISPRoff silencing efficiency relative to 80% *CD81* reduction even 21 days p.t. as by Nuñez et al. (2021), underscoring the necessity for assay optimization to increase durability of epigenetic editing. Consequently, we selected *CD81* as the primary target for subsequent assay

optimizations, aiming to refine our approach and enable effective screening for functional constructs.

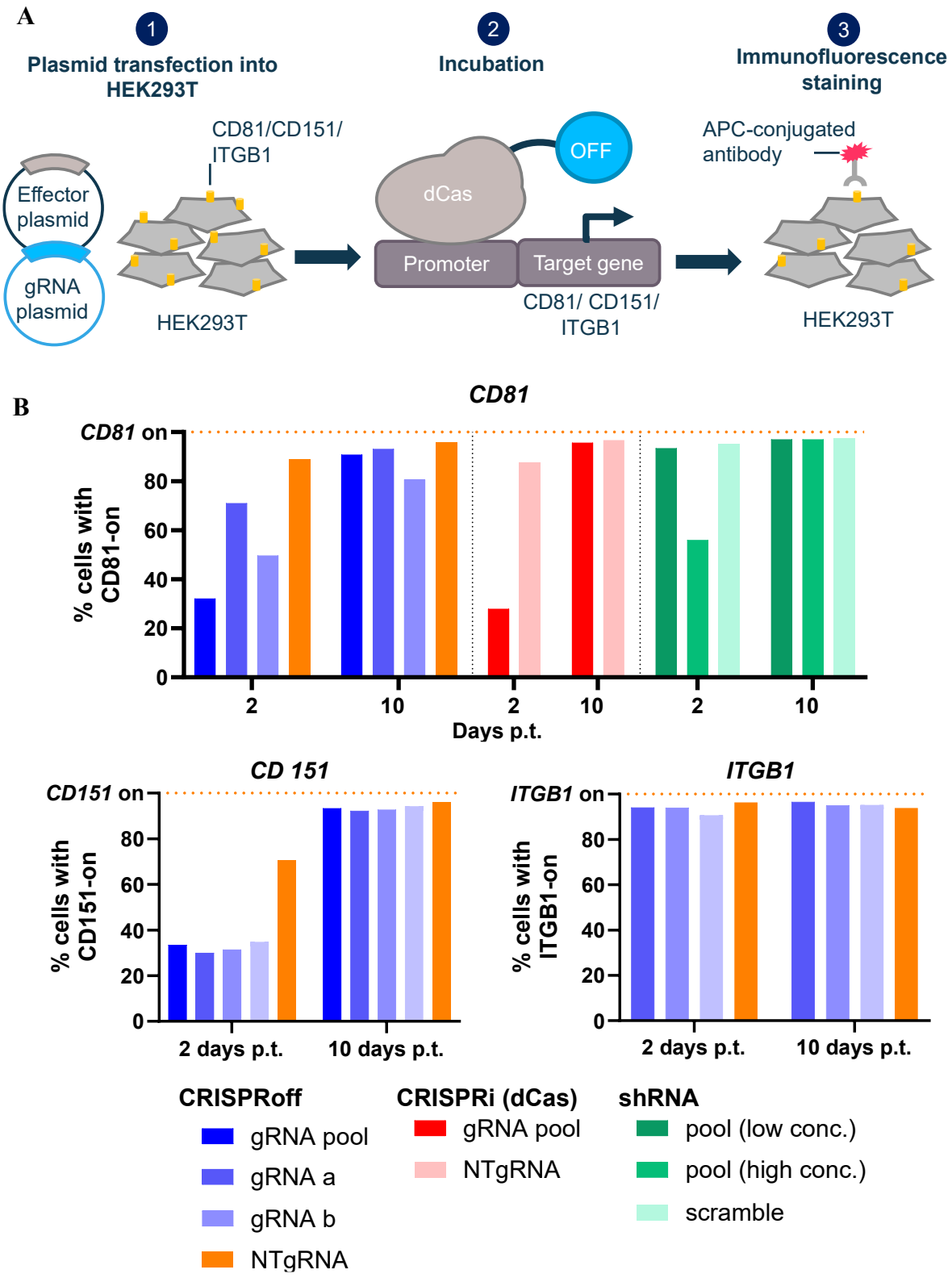

Figure 14: Weak but detectable silencing of *CD81*, *CD151* & *ITGB1* with CRISPRoff. A) HEK293T cells were transfected with plasmids encoding different gene silencing modalities. Silencing was monitored 2 and 10 days p.t. by live cell staining with allophycocyanin- (APC) conjugated antibodies followed by flow-cytometry analysis. **B)** Quantification of CD81-, CD151- and ITGB1-positive cells. Analysis of silencing efficiency mediated with individual and pools of sgRNA(s). Comparison of CRISPRoff silencing to CRISPRi and shRNA (OriGene, USA) (n = 1).

We evaluated several protocol adjustments, many of which did not enhance the durability of gene silencing. However, we achieved a substantial enhancement in the durability of CD81 gene silencing through two principal improvements in our experimental protocol. A critical adjustment involved a sorting step for transfected cells, based on a BFP tag associated with CRISPRoff, at 2 days p.t., which effectively enriched the population for those cells harboring the CRISPR editor. Specifically, unsorted samples demonstrated at 2 days p.t. 70% *CD81* silenced cells, however at 10 days p.t., *CD81* silencing was detectable for only 10% of the cell population. . Conversely, the cell sorted samples demonstrated approximately 26% residual *CD81* silencing even at 21 days p.t., after initial silencing at 5 days p.t. was similar to the unsorted samples, around 78% (Figure 15 A/B).

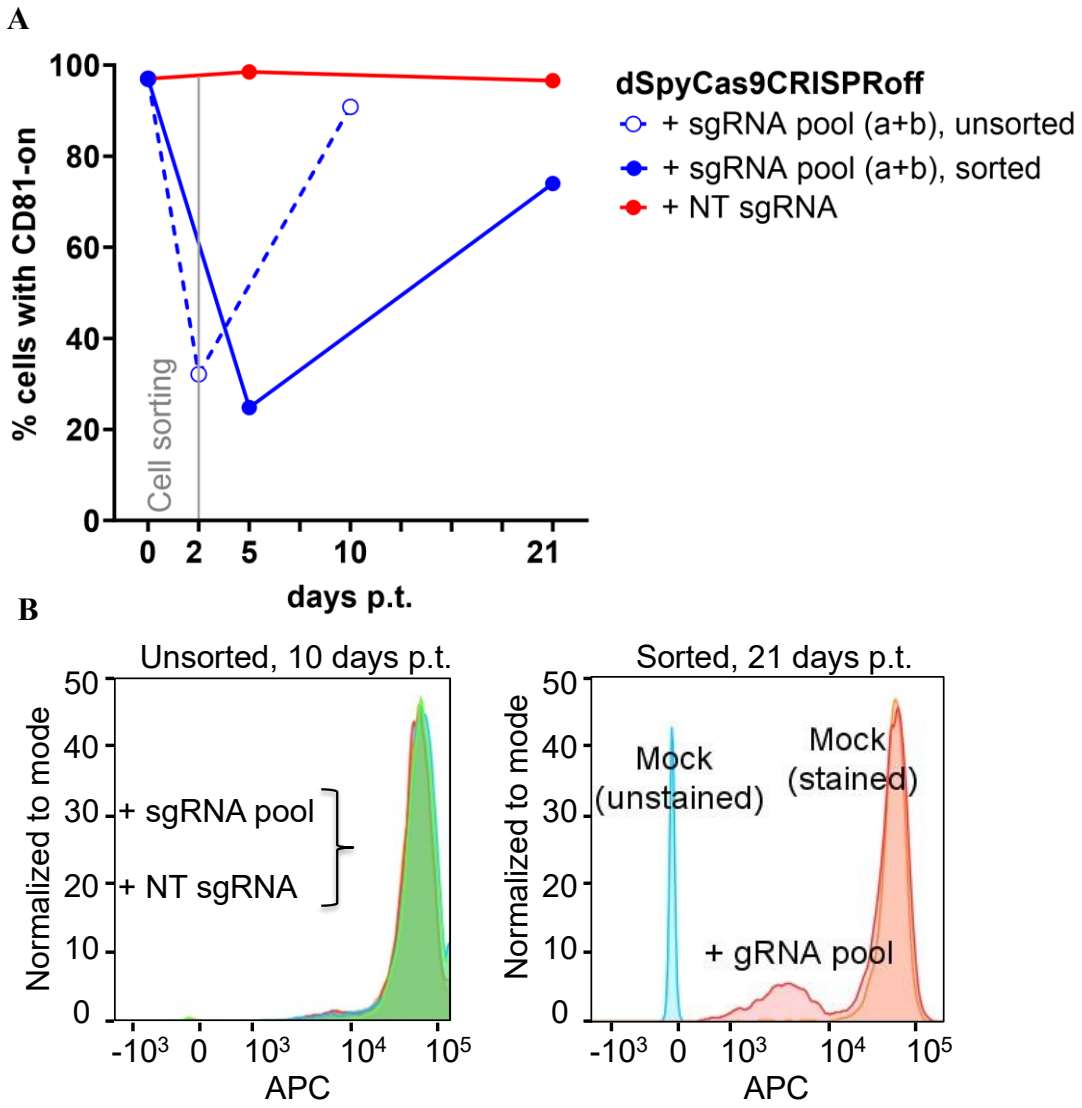

Figure 15: Enhanced dynamic range in epigenetic silencing assay through cell sorting. A) HEK293T cells were plasmid transfected with CRISPRoff and a sgRNA pool (a+b) targeting the *CD81* locus. BFP+ cells (transfected cells) were sorted 2 days p.t.. *CD81* silencing was monitored by live cell antibody staining followed by flow-cytometry analysis. A time-course study was conducted to measure *CD81* silencing over time (n = 1). **B)** A flow cytometry plot illustrating *CD81* expression in cells at 10 and 21 days p.t. comparing between experimental conditions were cells were measured in bulk (left, unsorted) or cell- sorted for BFP+ cells (right, transfected cells) 2 days p.t. (n = 1).

The second protocol adjustment comprised targeting the *CD81* promoter with a pool of 3 sgRNAs instead of 2 sgRNAs. CRISPRoff mediated stronger silencing 21 days p.t. with a pool of 3 sgRNAs (a+b+c) leading to 53% *CD81* reduction compared to 26% reduction with sgRNA pool (a+b) (Figure 16A). After 5 days pt., the application of 3 sgRNAs resulted in a homogenous population of *CD81*-silenced cells, as shown in Figure 16B (indicated in blue). In contrast, the treatment with 2 sgRNAs yielded a more heterogenous outcome, generating at least two distinct subpopulations of *CD81*-silenced cells, as shown in in Figure 16B (depicted in red). A subsequent read-out at 49 days p.t showed that 48% of cells treated with 3 sgRNAs maintained silenced.

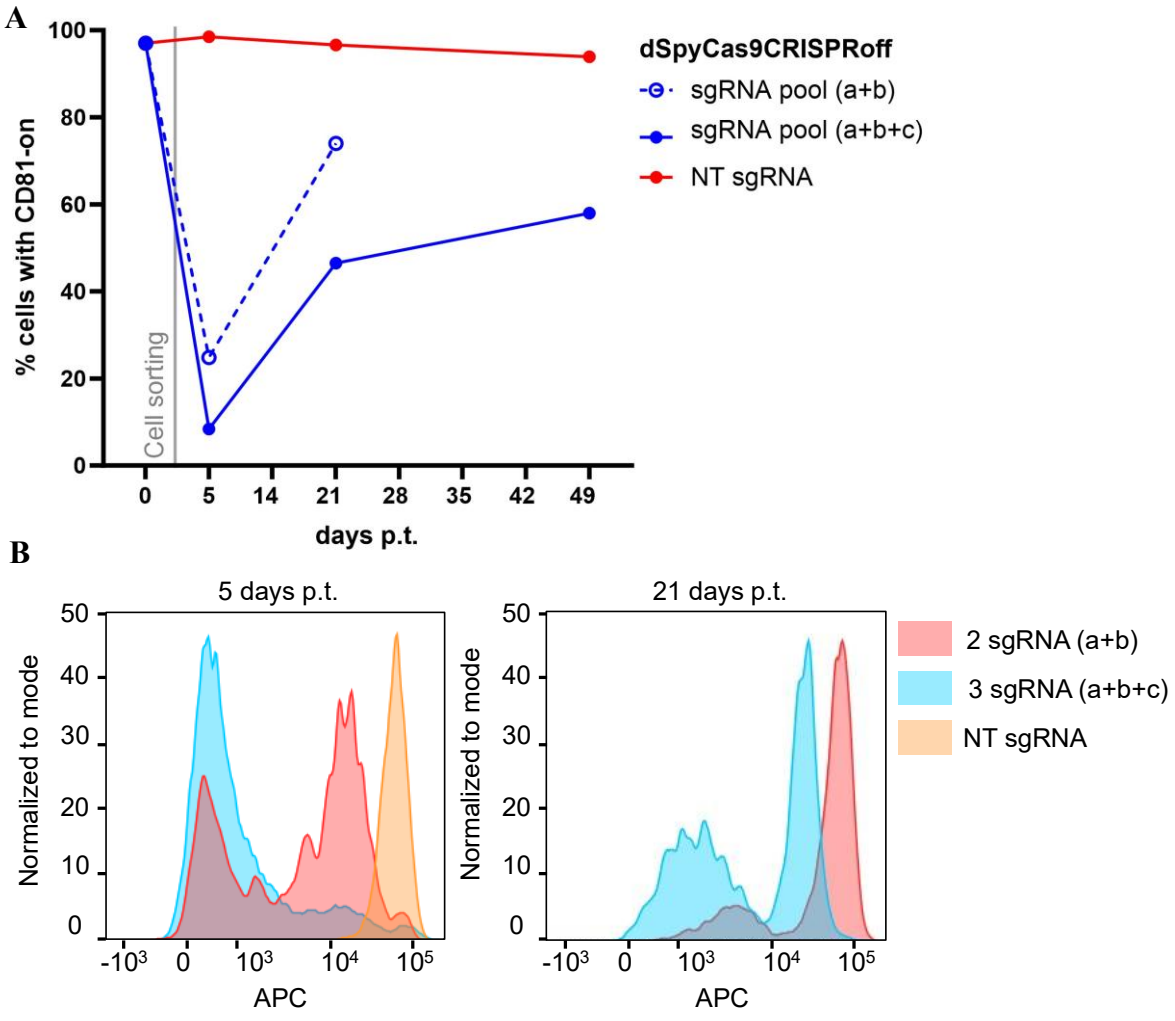

Figure 16: 3- instead of 2-sgRNAs increased silencing with CRISPRoff . A) A time-course was conducted to compare the efficacy of CD81 silencing by dSpyCas9CRISPRoff when targeted to two (sgRNA pool a+b) or three sites (sgRNA pool a+b+c) of the CD81 promoter (n = 1). **B)** Flow cytometry plots illustrating CD81 silencing with dSpyCas9CRISPRoff with sgRNA pool (a+b) (indicated in red) or (a+b+c) (indicated in blue) at 5 and 21 days p.t. (n = 1).

In the process of establishing an effective cell sorting protocol, we evaluated two different cell sorting machines, referred to as the 1st and 2nd cell sorting as indicated in Figure 17A. Cell

sorting was conducted at the indicated time points 21 and 49 days p.t.. Subsequent extended read-outs of the double-sorted cells indicated that approximately 70% of the population remained *CD81*-silenced four months p.t. (Figure 17A). Flow cytometry analysis revealed the presence of two distinct subpopulations of *CD81*-silenced cells, which varied in *CD81* signal strength ~4 month p.t.(119 days) (Figure 17A).

It is important to contextualize the following observations, as they may not be fully representative. During one of the initial cell sorting experiments, we noted that a significant proportion of cells underwent cell death. Consequently, it took several weeks for these surviving cells to recover and achieve a confluent state. Over a monitoring period of approximately three months, we assessed the silencing of *CD81* and observed complete silencing of >95%, as illustrated in Figure 17B. Flow cytometry analysis demonstrated that cells treated with the sgRNA pool (a+b+c) demonstrated a homogenous population with complete knockdown of *CD81* as shown in Figure 17B (indicated in blue).

Following the implementation of two critical adjustments - namely, the enrichment of transfected cells through sorting and the use of a three-guide RNAs targeting the *CD81* promoter - we observed 53% silencing levels at 21 days p.t. This range provided an adequate dynamic range to justify proceeding with the testing of the hypercompact EEs. Analysis over 3-4 month revealed permanent silencing although reactivation of gene expression was detectable.

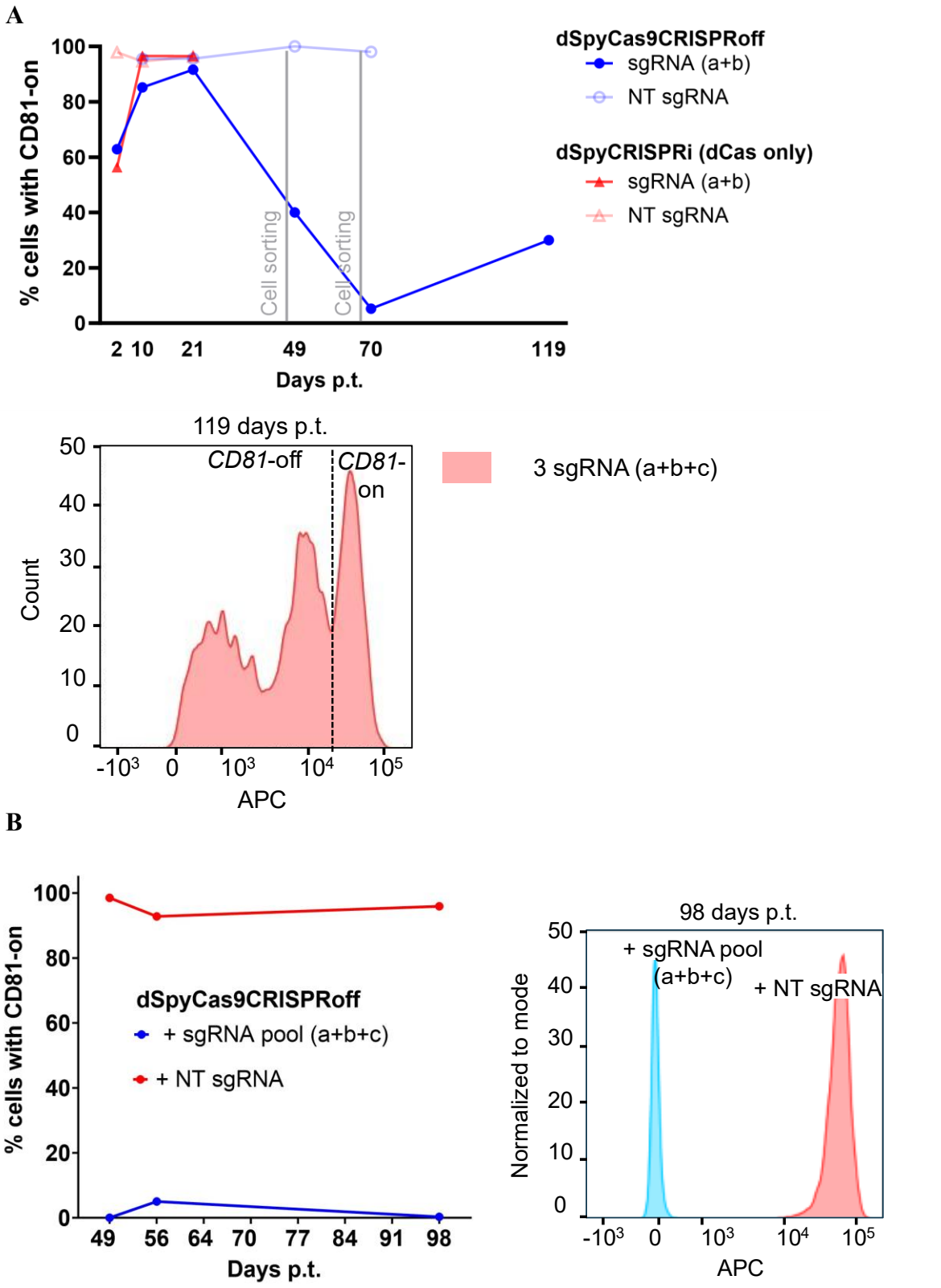

Figure 17: dSpyCas9CRISPRoff-mediated silencing lasted over 3-4 month. A) HEK293T cells were plasmid-transfected with dSpyCas9-CRISPRoff in combination with a sgRNA pool (a+b). During the establishment of protocols for cell sorting, we evaluated two cell sorting instruments at approximately 7- and 9-weeks p.t. as indicated in the graph. Silencing was monitored for up to 4 months p.t. (n = 1). A Flow-cytometry plot illustrates the proportion of *CD81*-silenced cells at 4 months p.t.. (n = 1). **B)** HEK293T cells were plasmid-transfected with dSpyCas9CRISPRoff in combination with a sgRNA pool (a+b). Cells were sorted for BFP+ cells 2 days p.t.. In this experiment, a significant number of cells underwent cell death. It took several weeks for the surviving cells to recover and reach a confluent state. The silencing of these surviving cells was monitored for approximately 3 months p.t. (n = 1). A Flow-cytometry plot illustrates the proportion of *CD81*-silenced cells at 4 months p.t. (n = 1).

3.1.2 Establishment of bisulfite sequencing for validating epigenetic modifications

To confirm that the observed silencing of *CD81* was indeed due to epigenetic modifications, we employed targeted bisulfite sequencing for analyzing DNA methylation (Li & Tollefsbol, 2011). To enhance the sequencing depth, we coupled targeted bisulfite sequencing with next-generation sequencing (NGS) technology to be able to investigate methylation in a quantitative manner. We conducted *in vitro* methylation of genomic DNA (gDNA) from HEK293T cells on targets with previously described bisulfite sequencing primers (Nuñez et al., 2021). Methylation levels of untreated gDNA were marginal around 0.5% for the targets *DYNC2LI1* and *H2B*; and around 20% for *LAMP*. We observed a steady increase in methylation with prolonged incubation time, ranging from approximately 60% methylation on the target MAPT to nearly 100% methylation on the target *LAMP* after 1 hour of *in vitro* methylation (Figure 18A).

Target *CD81* was suffering from low mapping efficiency (<5%) of the sequencing reads to the reference genome when using the *CD81* primers previously described by Nuñez et al., (2021). To address this challenge, we systematically tested multiple primer pairs with varying annealing temperatures, ultimately achieving specific amplification of the *CD81* promoter with fewer unspecific byproducts with amplicon 4, primer pair 2 (Figure 18B), Table 1. Despite this advancement, the NGS reads generated from the initial *CD81* amplicons were impaired by numerous sequencing errors, which we hypothesized were attributable to the presence of long stretches of cytosines (Cs) and guanines (Gs) within the amplified regions. To mitigate these errors, we adjusted the non-CG mismatch tolerance settings in the Bismark bisulfite mapper of the NGS reads to the reference sequence (Figure 18C).

A

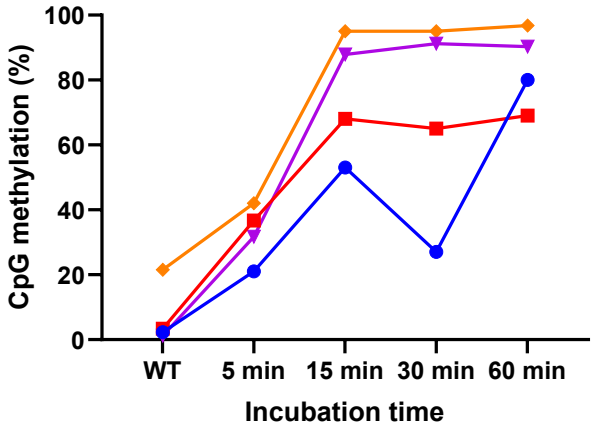

Target	Mapping efficiency
Lamp	7%-25%
DYNC2LI	97%-98%
MAPT	59%-82%
H2B locus 2	44%-86%

B

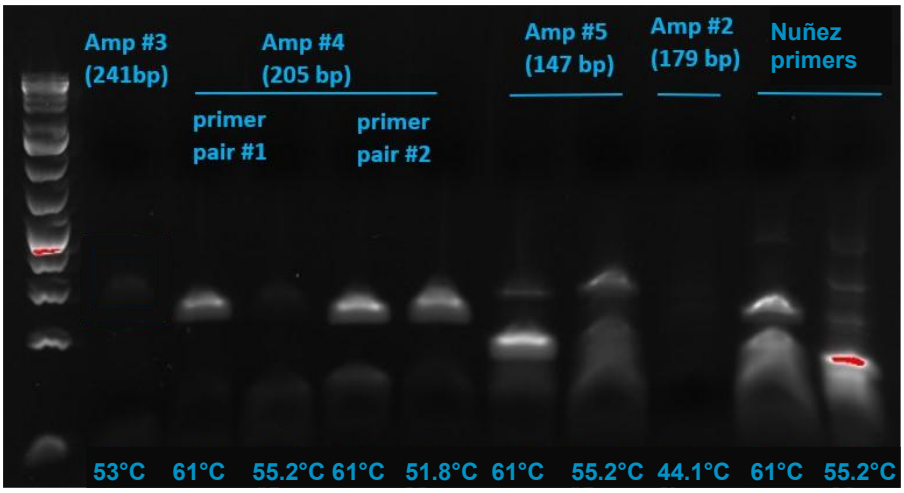

C

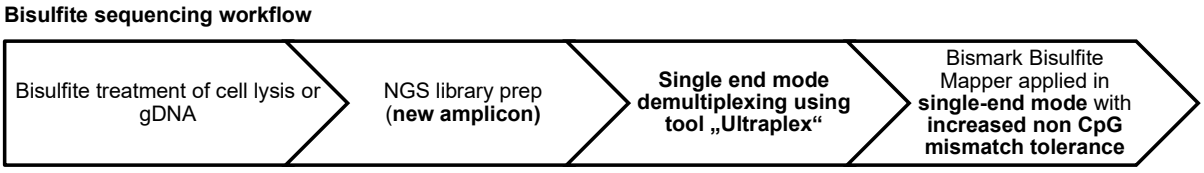

Figure 18: Establishment of bisulfite sequencing coupled to NGS analysis. A) CpG methylation levels of four loci after different duration of *in vitro* methylation of HEK293T gDNA. Methylation levels were analyzed through bisulfite sequencing coupled to NGS. Bisulfite sequencing primers previously described by Nuñez et al. (2021). The mapping efficiency of the NGS reads to the reference genome is presented in the accompanying table (n = 1). **B)** *CD81* promoter amplification with different primer pairs and different annealing temperatures (primer pair described by Nuñez et al. (2021) on the right). **C)** A schematic of the workflow to determine methylation levels using targeted bisulfite sequencing coupled to NGS. The optimization steps, introduced to compensate for the low mapping efficiency of *CD81* to the reference genome, are highlighted in bold.

To confirm the new analysis pipeline, we retested our in vitro methylated target *CD81*. There was a substantial improvement in mapping efficiency, now ranging between 36% and 41%. This refined approach yielded a wide dynamic range of CpG methylation. Initially we measured a limited dynamic range of CpG methylation that measured only 6% CpG methylation of the WT locus and 60% after in vitro methylation. The improvements increased the dynamic range now spanning from 1% in the WT locus to 95% in in vitro methylated samples (Table 2).

Table 2: Comparison of in vitro methylated *CD81* locus using the initial- and improved analysis pipeline.

		in vitro methylated	untreated
Initial workflow	Mapping efficiency [%]	1.1	1.9
	CpG methylation [%]	58.6	6.1
Adapted workflow	Mapping efficiency [%]	41	36
	CpG methylation [%]	95	1

Following treatment with the CRISPRoff system, we observed elevated levels of methylation within the *CD81* promoter, indicative of successful epigenetic modification. CRISPRoff treatment resulted in approximately 40%-60% methylated CpGs. In contrast, control samples treated with NT sgRNA exhibited methylation levels of less than 1% (Figure 19A). These findings align closely with the methylation levels reported by Nuñez et al. (2021). In comparison, the CRISPRi approach did not yield increased methylation levels (Figure 19C). This distinction underscores the unique capabilities of the CRISPRoff system in facilitating durable epigenetic changes for long-term gene regulation compared to transient regulation by CRISPRi. Subsequent NGS amplicon sequencing, a targeted DNA sequencing method used to analyze specific regions of a genome, of the *CD81* promoter region confirmed its integrity, revealing no disruptions or mutations following CRISPRoff treatment (Figure 19B).

In summary, we replicated and confirmed the findings of Nuñez et al., (2021) regarding stable epigenetic silencing of the cell surface protein *CD81*. Achieving this required critical assay optimizations, including the sorting of transfected cells and the utilization of a distinct gRNA pool consisting of three gRNAs instead of two. To validate that *CD81* silencing was a result of epigenetic modifications, we established and applied bisulfite sequencing coupled with NGS. This process required optimizations of the amplification protocol for the *CD81* promoter, as well as adaptations to the bioinformatics analysis pipeline. Taken together, these advancements enabled detect and quantify epigenetic editing. With these assays established, novel systems with previously unknown activity could be screened.

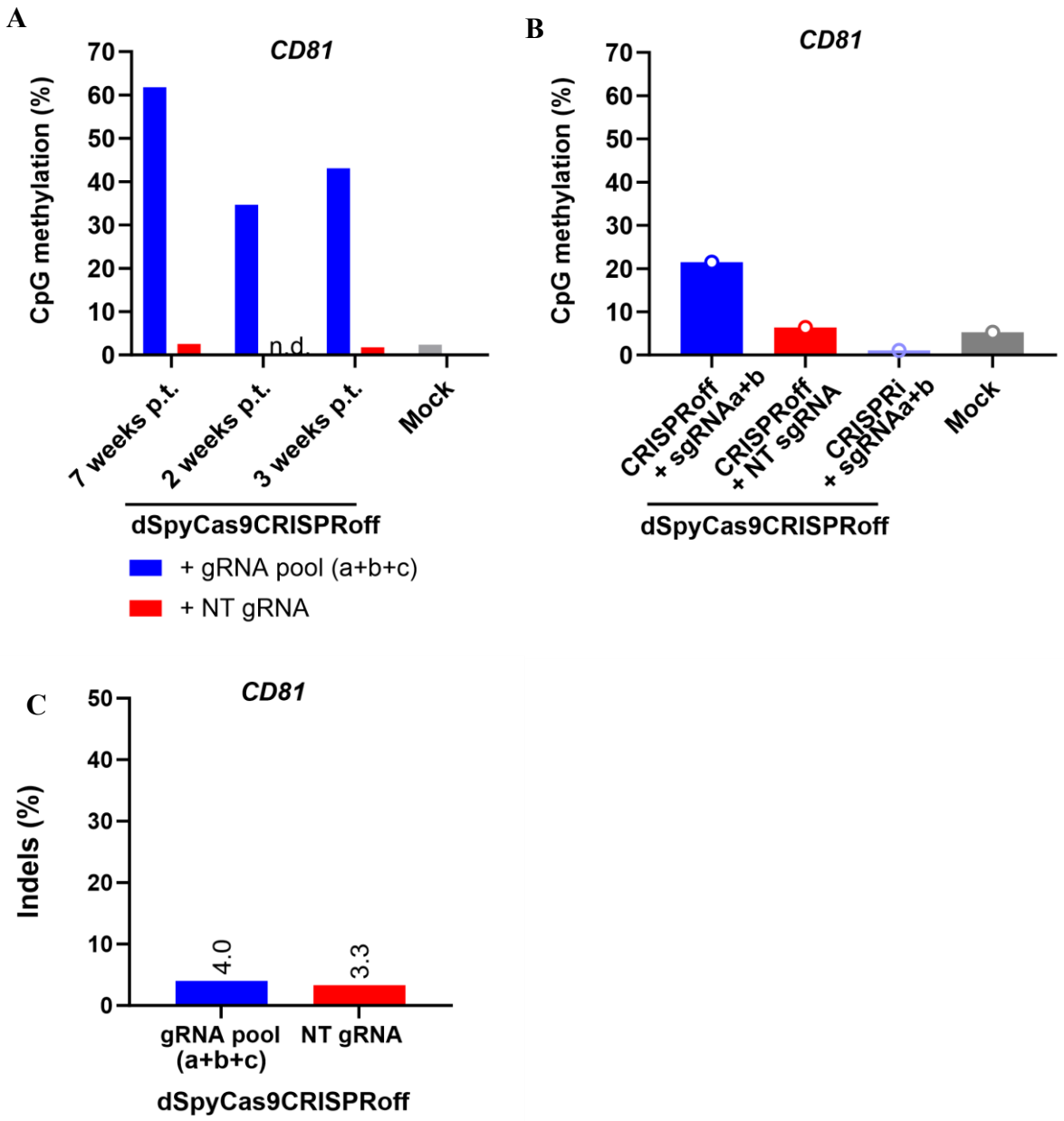

Figure 19: Amplicon sequencing and bisulfite sequencing of the *CD81* promoter. A) Samples which were previously analyzed for *CD81* silencing were subsequently subjected to bisulfite sequencing to confirm that silencing was due to epigenetic mark modifications. Bisulfite sequencing analysis was performed on a ~200 bp region of the *CD81* promoter. The samples of the different independent experimental repetitions were taken at different time points as indicated. (n.d.: not determined) **B)** Comparison of methylation levels of repeat n1 between CRISPRoff and CRISPRi 7 weeks p.t.. Samples were sorted for CD81-negative cells prior to bisulfite sequencing analysis (n = 1). **C)** NGS amplicon sequencing analysis was performed on a ~200 bp region of the *CD81* promoter to confirm that the promoter remained intact after CRISPRoff silencing 7 weeks p.t. (n = 1).

3.2 Identification of a novel hypercompact nuclease as a DNA binding platform

State-of-the art EE *CRISPRoff* mediates durable silencing across numerous targets; however, it suffers from its large size which restricts it from delivery via AAVs. We hypothesized to overcome the size limitation by replacing the large SpyCas9 nuclease with a smaller variant such as the recently described hypercompact nucleases from the Cas12f family. Studies from us and others have demonstrated that novel CRISPR systems can be effectively identified through microbial database mining (unpublished data from our group) (Pan et al., 2020; Panahi et al., 2024). This approach leverages computational methodologies to conduct extensive searches for CRISPR arrays in large internal microbial databases. Such efforts have proven effective in successfully identifying potential novel CRISPR nucleases. Identified candidates were evaluated through *in vitro* testing of nuclease activity to filter for potential candidates and subject them for evaluation in mammalian cells.

In this study, we selected 15 hypercompact Cas12f-like nucleases from our mining pipeline that showed promising *in vitro* DNA cleavage activity to test them as cutting deficient DNA binders in a transactivation assay adapted from Xu et al., (2021) as CRISPR activators (CRISPRa). We decided to initially test the system as CRISPRa instead of CRISPRoff because Xu et al. (2021) had previously demonstrated that Cas12f nucleases are functional within a CRISPRa architecture. However, it had not been established whether Cas12f nucleases would function effectively within a complex CRISPRoff architecture. Therefore, we adopted the CRISPRa architecture, which has been shown to be functional for dCasMini (dCasMini-VPR), to evaluate activity with alternative nucleases. They were catalytically inactivated by introducing two point mutations into the first and second cutting motif of the RuvC domain. These were identified by aligning the nucleases to the previously described Un1Cas12f (Figure 20) (Xu et al., 2021).

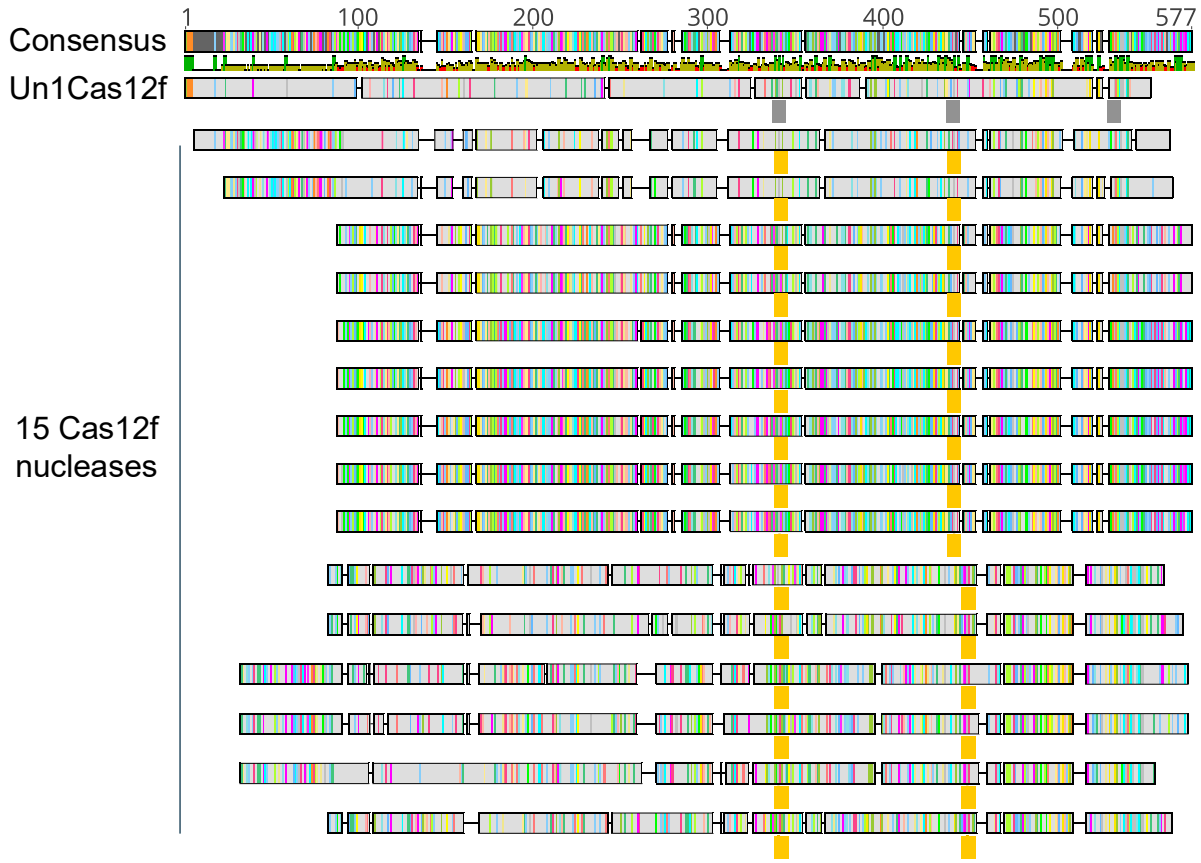

Figure 20: Sequence alignment of 15 Cas12f nucleases to Un1Cas12f. A set of 15 hypercompact Cas12f nucleases were selected from our mining pipeline for testing as DNA binders. The amino acid sequences of these nucleases were aligned to previously characterized Un1Cas12f to identify the cutting motifs of the RuvC domain (indicated as grey lines). Two-point mutations were introduced into the first and second cutting motif of the RuvC domain of the novel nucleases, thereby rendering them catalytically inactive (indicated as yellow lines).

The putatively catalytically inactive nuclease were fused with the tripartite activator VP64-p65-RTA (VPR) (Chavez et al., 2015; Xu et al., 2021). These CRISPRa constructs were targeted to a transiently transfected plasmid harboring the artificial promoter *TRE3G* fused to the dual reporter gene NanoLuc® luciferase (Nluc) and GFP (Figure 21A). Plasmids undergo chromatinization and are capable of recapitulating nuclear genome-encoded chromatin architectures (Mallory et al., 2025).

Although this system does not fully replicate an endogenous locus, it enables the differentiation between active and inactive nucleases. Furthermore, we hypothesized that the presence of seven *TRE3G* repeats amplifies the effect of each binding event, thereby enabling sensitive detection of even low levels of nuclease activity. We reasoned that an additional advantage is that the *TRE3G* target region of the reporter plasmid was tailored for each nuclease to align with their respective PAM specificities. This means an individual reporter plasmid was designed for each nuclease. This approach enhances the comparability across different nucleases, as opposed to targeting the nucleases to different binding sites in a promoter of an endogenous locus to

accommodate their specific PAM preferences. The PAM profiles are indicated in 24 hours p.t., we analyzed reporter gene activation by the CRISPRa constructs through Nluc luminescence read-out. As the assay was developed by Xu et al., (2021) for engineered Un1Cas12f (CasMini), we included it as positive control. We further incorporated the previously described Cas12f nuclease from *Parageobacillus thermoglucosidasius* (PtCas12f) which had shown PAM-dependent *in vitro* dsDNA cleavage and plasmid DNA interference in *E. coli* (Karvelis et al., 2020). Additionally we tested Cas12f from *Acidibacillus sulfuroxidans* (AsCas12f) which has previously shown activity in mammalian cells but had not been for CRISPRa (Kim et al., 2021). From the internal mining pipeline, Cas12b from *Brevibacillus reuszeri* (BreCas12b) was evaluated as well despite its large size because of its high DNA cleavage activity which indicates also strong DNA binding activity (patent WO 2022/258753 A1).

dBreCas12b mediated high reporter gene activation of Nluc which was 190-fold above NT sgRNA control which aligns with its cutting activity (previous data from our group). Among the 15 hypercompact nucleases evaluated in our study, dApCas12f emerged as a potent candidate, demonstrating the highest level of reporter gene activation, namely 72-fold, consistent with previous reports by our group on its cutting activity. In contrast, the remaining candidates exhibited minimal to negligible activity of 1-10-fold reporter gene activation (Figure 21B). dPtCas12f mediated moderate CRISPRa activity (19-fold activation) which also aligns with its moderate cutting activity (previous reports from our group). dAsCas12f did not mediate reporter gene activation. Highest CRISPRa activity was induced by dCasMini (389-fold), outperforming dSpyCas9 (375-fold). In summary, this screen identified ApCas12f and BreCas12b as promising DNA-binding platforms. These results allowed us to advance the engineering of EEs based on dApCas12f, dBreCas12b and dCasMini.

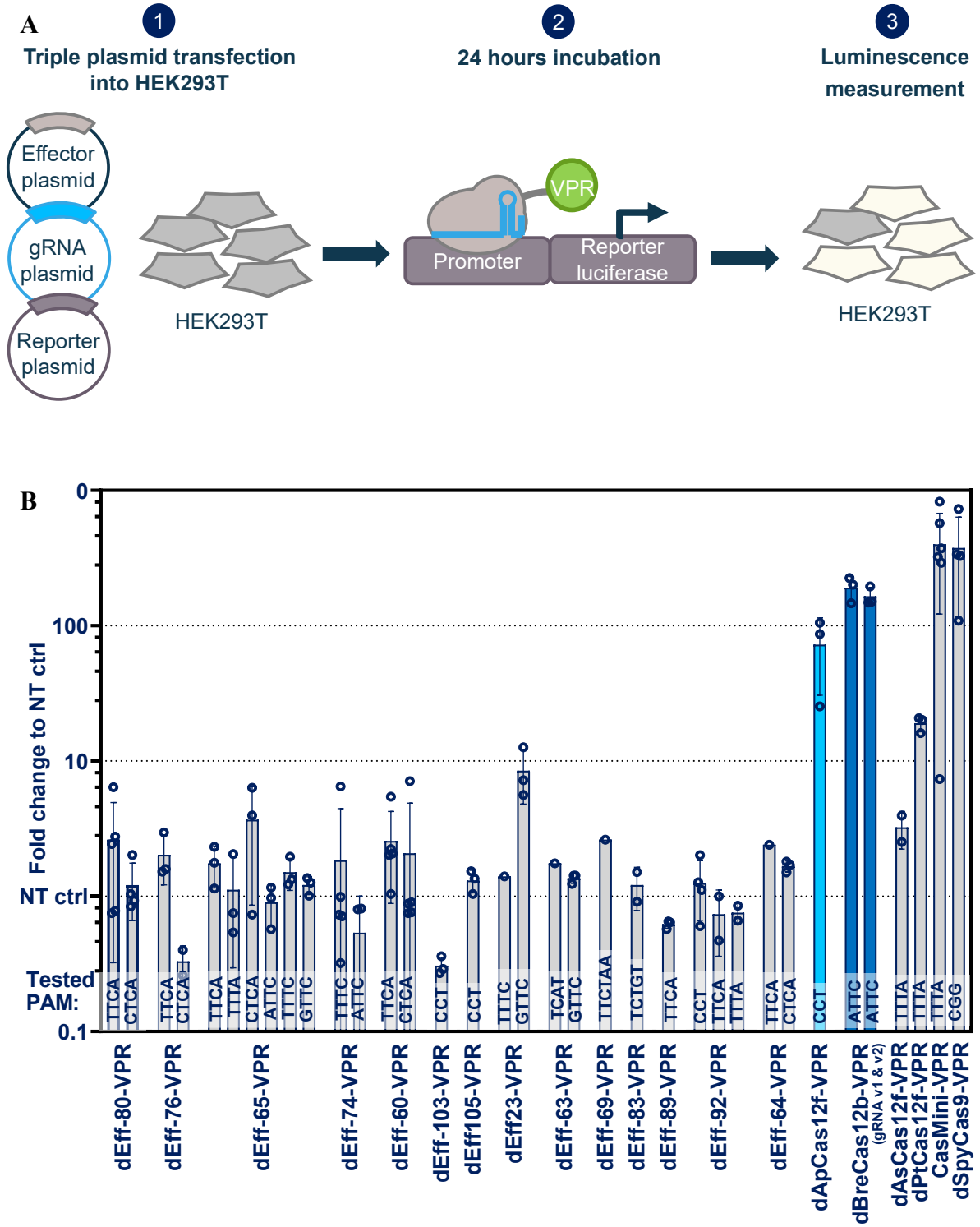

Figure 21: Screening Cas12f-like nucleases for DNA binding activity. A) A schematic illustration of the experimental setup. HEK293T cells were transfected with effector plasmid, sgRNA and reporter. The Cas12f nucleases were fused with the tripartite activator VPR and guided to the reporter plasmid to induce reporter gene activation in case of a DNA binding event. 24 hours p.t. reporter gene expression was analyzed through Nluc luminescence read-out. Reporter gene expression was compared between targeting and NT sgRNA. **B)** Reporter gene activation of the novel nucleases shown as fold changes to their respective NT sgRNA control. Each data point in the graph represents the average of three technical repeats (n = 3, each repeat was measured in three technical repeats).

3.3 Fusion of epigenetic domains with dApCas12f

After showing robust gene activation in a CRISPRa setup, we wanted to fuse dBreCas12b, dApCas12f and dCasMini with epigenetic modifiers, such as methyltransferases, to achieve targeted modifications of the epigenome.

3.3.1 Assessing baseline activity of dApCas12fCRISPRoff on *Snrpn*-reporter plasmid

We started by testing dBreCas12b, dApCas12f and CasMini in the state-of-the-art EE CRISPRoff context. After achieving positive results with a surrogate target, the *TRE3G* reporter plasmid described in chapter 3.2, we aimed to extend this approach to the screening of novel CRISPRoff systems. We hypothesized that such screening systems could facilitate more sensitive detection of initial silencing activity of CRISPRoff when utilizing alternative nucleases. Furthermore, the use of reporter genes allows for a simplified analysis compared to antibody-based readouts for *CD81* silencing. For that, we utilized an assay specifically described for screening EE for gene silencing capabilities (Kong et al., 2023; Nuñez et al., 2021). This assay uses a constitutively active, methylation-sensitive promoter coupled to a reporter gene cassette harboring the fluorescent protein GFP and the luciferase Nluc. Specifically, the promotors consisted of the constructs long *GAPDH-Snrpn* (Liu et al., 2016) or minimal *GAPDH-Snrpn* (Stelzer et al., 2015). Here, the terminology “long” and “minimal” refers to the respective stretches of the *GAPDH* region. We cloned the reporter cassettes into reporter plasmids. Although not classified as a hypercompact nuclease, dBreCas12b was included in our study despite its size being similar to that of SpyCas9, as it also belongs to the type V nucleases and functions as a monomer. This inclusion could potentially serve as a foundation for the transition of the epigenetic architecture from the type II nuclease SpyCas9 to the type V dimer of Cas12f nucleases. The dSpyCas9 sgRNAs targeting *GAPDH-Snrpn* were adapted from Nuñez et al., (2021). For dBreCas12b, dApCas12f and dCasMini, the sgRNA target sites were in proximity to the SpyCas9 binding sites but with necessary adjustments according to PAM recognition to simplify benchmarking the different nucleases among each other. The assay is based on a triple transfection of reporter plasmid, CRISPRoff plasmid (effector plasmid) and sgRNA plasmid. Silencing of the reporter plasmid was assayed at 72 hours and 96 hours p.t. (Figure 22A). Transfection efficiency was monitored by fluorescent analysis of a BFP tag on CRISPRoff.

The construct dSpyCas9CRISPRoff achieved approximately 90% silencing of the reporter plasmid at 72 hours p.t., with sustained effects observed even at 96 hours. ~20% silencing activity of dApCas12f was detected with sgRNA-1-3 after 96 hours; however, no to very low

silencing effects were observed at the earlier time points of 72 hours (Figure 22B). Similarly, dBreCas12b in conjunction with sgRNA-2 may induced a weak silencing effect of 20%, detected at 72- and 96 hours p.t.. It is important to note that the observed silencing effect was exclusive to sgRNA-2, as no activity was detected with sgRNA-1 and sgRNA-3. The dCasMiniCRISPRoff system did not mediate silencing with any of the tested sgRNAs. It is noteworthy that silencing of the reporter plasmid was also induced by dSpyCas9-only, without the involvement of additional fusion partner proteins, with both the long and minimal *GAPDH-Snrpn* promoters (Figure 22C). dSpyCas9CRISPRoff and dSpyCas9 induced a 6-fold reduction of the long *GAPDH-Snprn* reporter gene and a 3-fold reduction of the minimal *GAPDH-Snprn* reporter gene variant. The ability of dSpyCas9 to induce silencing without additional epigenetic domains complicates the read-out. It remains unclear whether the silencing mediated by the CRISPRoff system is a result of epigenetic mark modification or if it is primarily attributable to steric hinderance through dSpyCas9. To address this challenge, it is essential to implement longer readout periods in our experimental design. Utilizing a target on a reporter plasmid is not the ideal system for these investigations, as the target is only transiently available, limiting the ability to assess long-term silencing effects.

To enable long-term read-out, we generated reporter cell lines by stably integrating the long reporter cassette into the AAVS1 safe harbor locus in HEK293T cells to assess the longevity of the silencing effects induced by CRISPRoff. CRISPRoff-, sgRNA- and reporter plasmids were transfected, and silencing was analyzed at 3, 4 and 7 days p.t.. The dSpyCas9CRISPRoff system mediated 30%, 50% and 50% reporter gene silencing at 3, 4 and 7 days p.t., respectively. This silencing efficacy is weaker than the previously reported silencing levels of 80%-90% of the reporter plasmid (Figure 22D). Upon closer investigation to determine the reason for the reduced sensitivity, we observed that the polyclonal parent cell culture contained only 20% GFP-positive cells, rather than a homogeneous population in which every cell expressed the reporter gene. This state complicates the dynamic range, as it means that 80% of the cells already exhibit silencing of the GFP signal. Consequently, only the small population of 20% of cells, in which GFP expression is still active, is available for potential silencing by an EE. As a result, the ability to detect any additional silencing effects is compromised, leading to an underestimation of the true efficacy.

Taken together, we noted that silencing was observed with both dSpyCas9CRISPRoff and dSpyCas9-only, which complicated to differentiate whether the silencing effect stemmed from epigenetic modifications or steric hindrance. Furthermore, potentially weak silencing effects of

dApCas12fCRISPRoff could not be confirmed through subsequent readouts at later time points due to the transient nature of the reporter plasmid. To mitigate this limitation, we established cell lines with stably integrated reporter gene. Nonetheless, the cell line displayed a low dynamic range, which may hide any initial weak silencing effects associated with CRISPRoff and the alternative nucleases. As a result, the *GAPDH-Snrpn* locus was recognized to be an unsuitable system for evaluating epigenetic silencing. Consequently, we redirected our focus to the endogenous *CD81* locus for further investigation. We decided to focus our efforts on dApCas12f due to its small size and beneficial PAM preference5'-CCN-3'

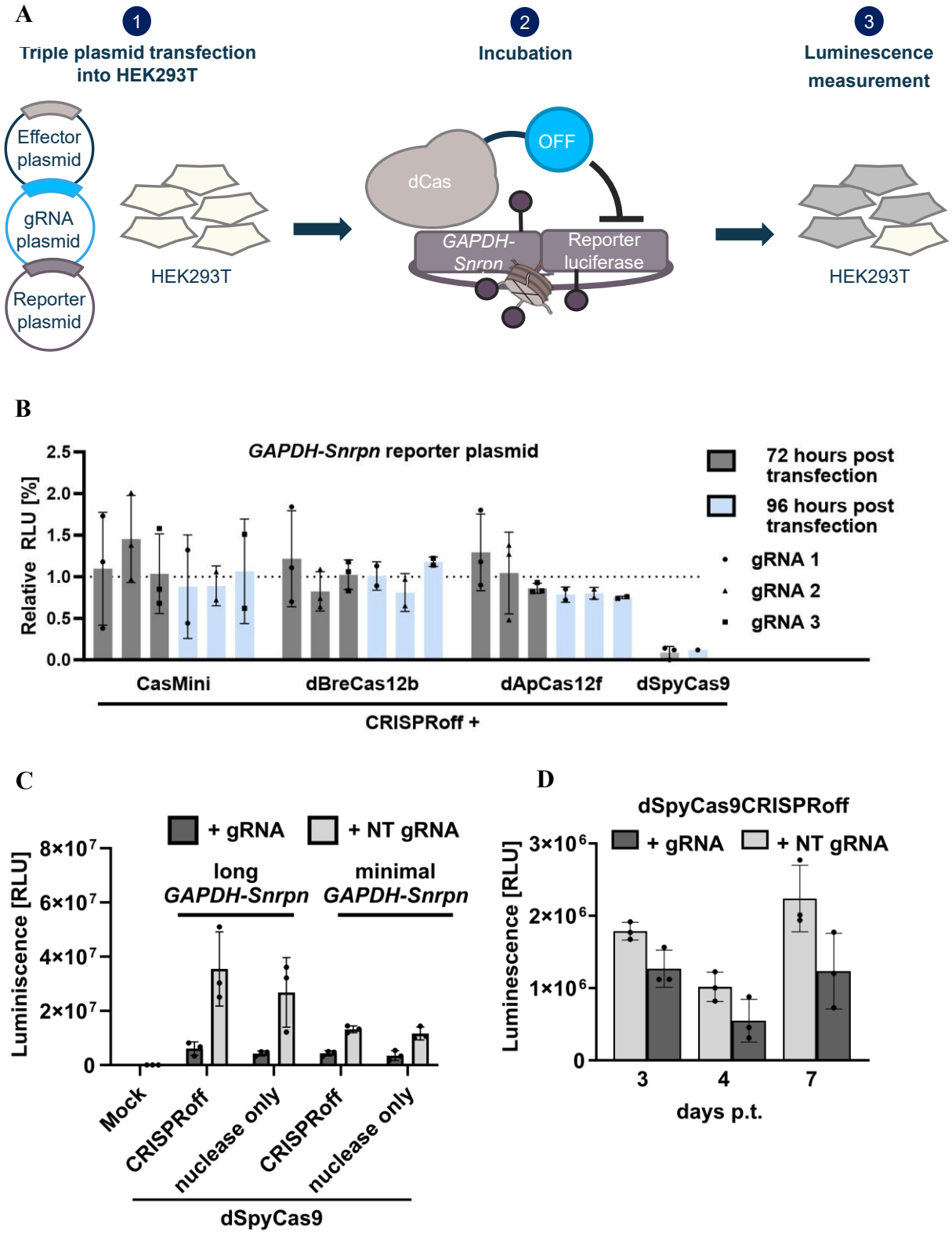

Figure 22: Silencing efficiency of CRISPRoff with different nucleases of the reporter plasmid harboring *GAPDH-Snrpn*. **A)** A schematic of the assay for epigenetic editing analysis. The assay consists of a plasmid-based triple transfection of effector plasmid, sgRNA and reporter plasmid harboring a long or minimal version of GAPDH-Snrpn. The effector plasmid encoded CRISPRoff with either dCasMini, dBreCas12b, dApCas12f or dSpyCas9. CRISPRoff was targeted to the reporter plasmid with constitutive active reporter gene. Silencing of the reporter gene was analyzed 72 and 96 hours p.t.. **B)** CRISPRoff-mediated silencing was calculated as fold change compared to the NT sgRNA of the long GAPDH-Snrpn reporter plasmid (n = 2 or 3, as indicated by the data points; each biological replicate was analyzed in technical triplicates). **C)** Silencing efficiency of dSpyCas9CRISPRoff and dSpyCas9-only was analyzed and compared 3 days p.t. (n = 1, tested in technical triplicates). **D)** Cell lines were generated with stably integrated reporter gene harboring long GAPDH-Snrpn. Over a time course of 7 days, silencing of dSpyCas9CRISPRoff was monitored at multiple time points (n = 1, tested in technical triplicates).

3.3.2 Lack of gene silencing of dApCas12fCRISPRoff in a sgRNA screen

We decided to return to the initially established assay where CRISPRoff silencing was measured though CD81 live cell antibody staining. Although the previous assay including the *GAPDH-Snrpn* reporter gene would have been advantageous and facilitated the analysis, it ultimately revealed multiple issues that outweighed the benefits. Therefore, we focused on the more reliable *CD81* silencing assay as we continue our optimization efforts. In initial testing on *GAPDH-Snrpn*, we observed that dApCas12fCRISPRoff induced no to minimal silencing.

SpyCas9 recognizes a 3' NGG PAM, while ApCas12f requires a 5' CCN 3' PAM. In theory, this property enables targeting of ApCas12f to any protospacer on the opposite strand relative to SpyCas9 including the gRNA pool (a+b+c) for *CD81*. However, a binding site that is effective for SpyCas9 does not necessarily guarantee functionality for ApCas12f. We constructed a panel of 13 alternative candidates to sgRNA-a. We specifically chose to start by substituting sgRNA-a because this guide binds in proximity to the transcriptional start site (TSS), as illustrated in Figure 23A. Previous studies have demonstrated that CRISPRoff achieves optimal silencing efficacy when targeted near the TSS, leading us to conclude that this particular sgRNA may be the most critical one (Nuñez et al., 2021). sgRNAs-b and -c were retained in their original form and were not modified with alternative sgRNAs to avoid altering multiple factors simultaneously. In total, we assessed the performance of dApCas12fCRISPRoff in conjunction with sgRNA pools consisting of sgRNA-b, sgRNA-c and one of the 13 alternative sgRNAs. HEK293T cells were transfected with both the effector plasmid and the sgRNA pools and tested for CD81 silencing as previously described in section 3.1.1. Our previous data has demonstrated while sorting is a crucial factor for sustained gene silencing, the initial signal strength 2-5 days p.t. is high, up to 70% silencing with dSpyCas9CRISPRoff (Figure 14A). To facilitate rapid screening, we did not sort the cells for transfection.

dApCas12fCRISPRoff was unable to induce CD81 silencing at 3 days p.t. with any tested sgRNA pool. Although we observed a slight decrease of approximately 5% in CD81-positive cells for all tested gRNA pools compared to the NT sgRNA control, this effect was markedly less than the positive control, where dSpyCas9CRISPRoff mediated approximate 50% CD81 reduction at 3 days p.t., slightly lower than 70% silencing in the previous repeat (Figure 23B). Taken together this data showed that the lack of activity of CRISPRoff with dApCas12f could not be resolved through a gRNA screening on *CD81*.

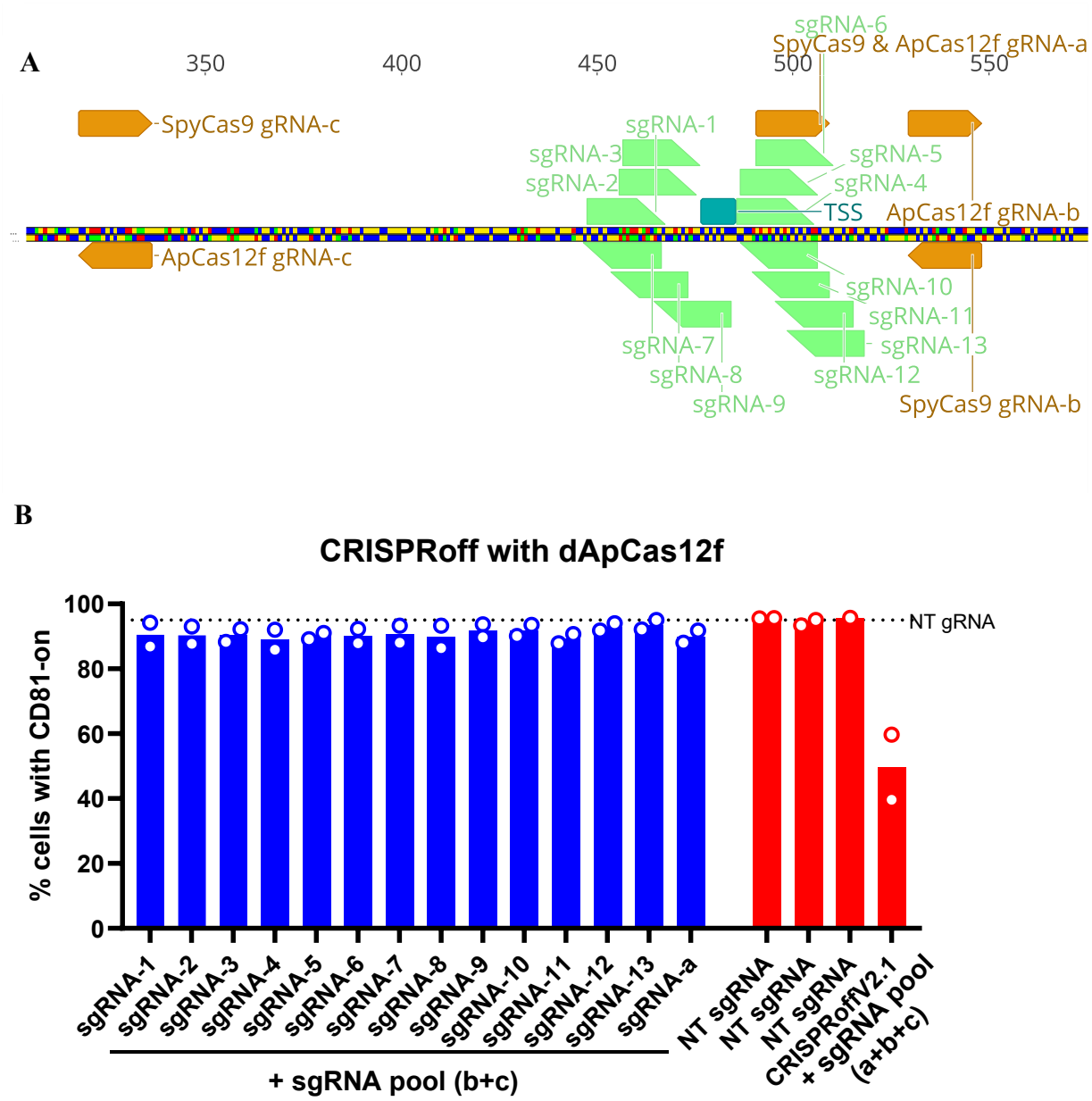

Figure 23: *CD81* sgRNA screen with dApCas12fCRISPRoff. A) A schematic representation of the *CD81* promoter with binding sites of the sgRNAs represented in orange. The sgRNA pool (a+b+c), as described by Nuñez et al. (2021), is highlighted in orange. Additionally, a set of 13 sgRNAs was designed as substitutes for sgRNA-a, which binds closest to the TSS. **B)** HEK293T cells were transfected with CRISPRoff fused with dApCas12f or dSpyCas9, and targeted to *CD81*. CRISPRoff with dApCas12f was combined with sgRNA pools consisting of sgRNA-b, sgRNA-c, and one of the sgRNAs-1-13. Silencing was assessed through live cell antibody staining of CD81 and flow cytometry measurement 3 days p.t (n = 1).

3.3.3 Alternative architectures EE1-EE17 fail to induce gene silencing of target *CD81*

The sgRNA screening did not resolve inactivity of dApCas12fCRISPRoff, prompting us to investigate the CRISPRoff architecture as a potential reason for the lack of activity. We aimed to achieve activity of dApCas12f-CRISPRoff through modifications of the CRISPRoff architecture. We constructed eleven alternative CRISPRoff architectures, designated as EE1 through EE11. These constructs differ in the fusion order of the epigenetic effector domains at

the N-terminus and/or C-terminus of dApCas12f, as illustrated in Figure 24. The design of these fusion protein architectures was partially informed by existing literature: All variants encode a nuclear localization signal (NLS) sequence at the N-terminus of ApCas12f, in contrast to CRISPRoff because previous studies have shown that the activity dCasMini-VPR is enhanced when NLS is present on the N-terminus (Xu et al., 2021). In the fusion construct of CasPhiCRISPRoff, which is a Cas12 nuclease, NLS were positioned at the N- and C-terminus of the nuclease (Liu et al., 2022). The constructs can be divided into three groups. The first category comprises EE1 and EE2 which are based on dApCas12f-VPR described in section 3.2.. In line with that architecture, both EE1 and EE2 feature a similar design, with all domains located in a serial arrangement at the C-terminus of the nuclease. This VPR-based CRISPRa fusion was established by Xu et al., (2021). The second group under investigation comprises constructs EE3 through EE5. Notably, EE3 and EE4 are characterized by the positioning of the KRAB domain and the Dnmt3A/L domains at opposite termini of the nuclease, in comparison to the configuration present in CRISPRoff. This arrangement allows for the assessment of the effects of domain positioning. In constructs EE1-EE5, we separated BFP from CRISPRoff by an intervening T2A sequence to reduce the construct size. Furthermore, by using the T2A sequence, the functionality of the CRISPRoff constructs is assessed independently of the BFP marker. Group 3 consists of construct EE6-EE11 which differentiate to CRISPRoff only by alternative N-terminal linkers and additional NLS.

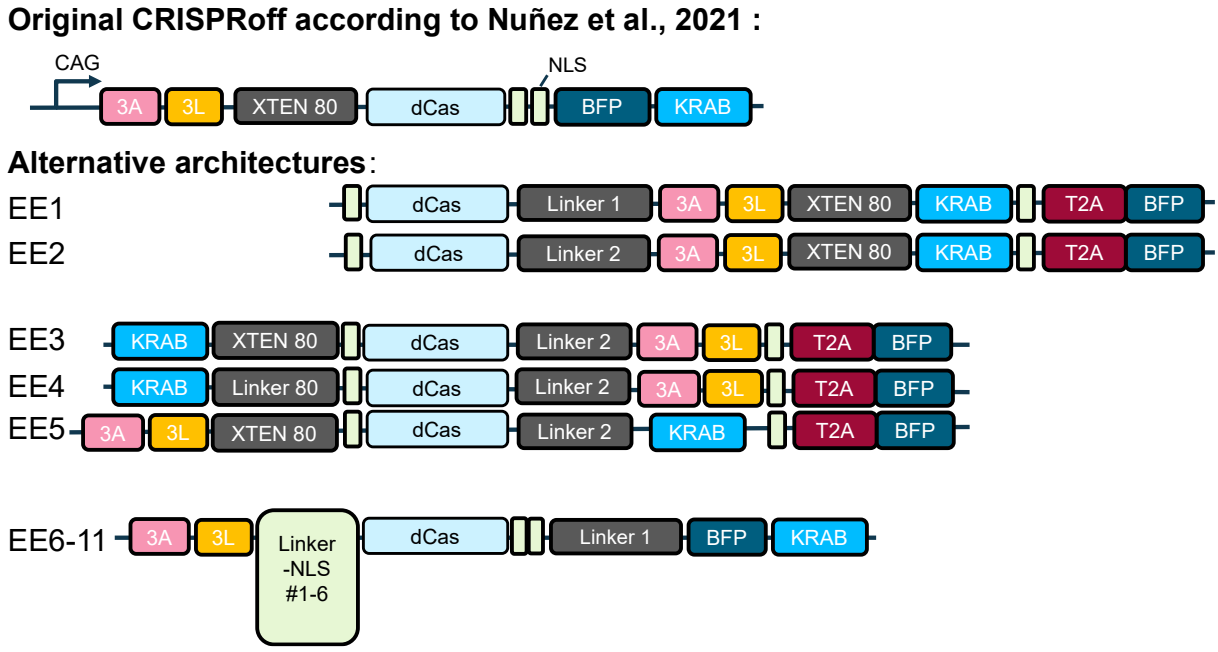

Figure 24: A schematic representation of the fusion proteins of EE1-EE11. The constructs vary in N- and C-terminal fusions of the catalytically inactive nuclease with the epigenetic effector domains DNMT3A, DNMT3L, and KRAB. All variants are supplemented with a NLS sequence at the N-terminus of the nuclease. Various linkers and NLS signals have been integrated, with BFP separated from the construct by a T2A sequence. Constructs EE6-11 include alternative linker and NLS sequences at the N-terminus of dCas.

We evaluated the alternative constructs for CD81 silencing as previously described using a pool of 3 sgRNAs (a+b+c) which bind to the complementary side of the SpyCas9 *CD81* sgRNAs. From each sample, a subset of cells was harvested for sorting of transfected cells two days p.t.to ensure maximum sensitivity of the assay. Furthermore, this allowed for a comparison between unsorted (blue) and sorted (red) cells (Figure 25A). At 5 days p.t., we observed a ~30% reduction in CD81-positive cells in the sorted population by EE8-EE10 (Figure 25A). For EE1-EE7 we detected a 10%-20% reduction of *CD81*-positive cells. We continued to culture the cells and conducted a follow-up measurement 14 days p.t.. We found no evidence of *CD81*-silenced cells at this later time point. In the unsorted population, no silencing was detected at any time point. Our positive control, dSpyCas9CRISPRoff, achieved 50% CD81 silencing (unsorted), consistent with previous results. We observed a high level of cell death in the sorted subpopulations 5 days p.t. treated with dSpyCas9 and dApCas12f. We noted cell death appeared as a *CD81* silencing signal in flow cytometry analysis, which poses a risk for false positive silencing by our EEs. To account for the possibility that the observed CD81 silencing in the sorted population was a consequence of cell death, we included an analysis that mirrored the sorting process through flow cytometry: We took the unsorted samples, which did not suffer from high cell death, and gated for transfected cells via BFP, as shown in Figure 25B (light

blue). However, silencing was undetectable for all dApCas12f EE constructs, even though silencing with dSpyCas9CRISPRoff increased from 50% CD81 silencing in the unsorted population to 80% CD81 silencing in the BFP+ gated cells. Taken together, this supports the conclusion that the low silencing effect of EE with dApCas12f at 5 days p.t. was not a result of gene silencing but due to cell death which decreased CD81 signal.

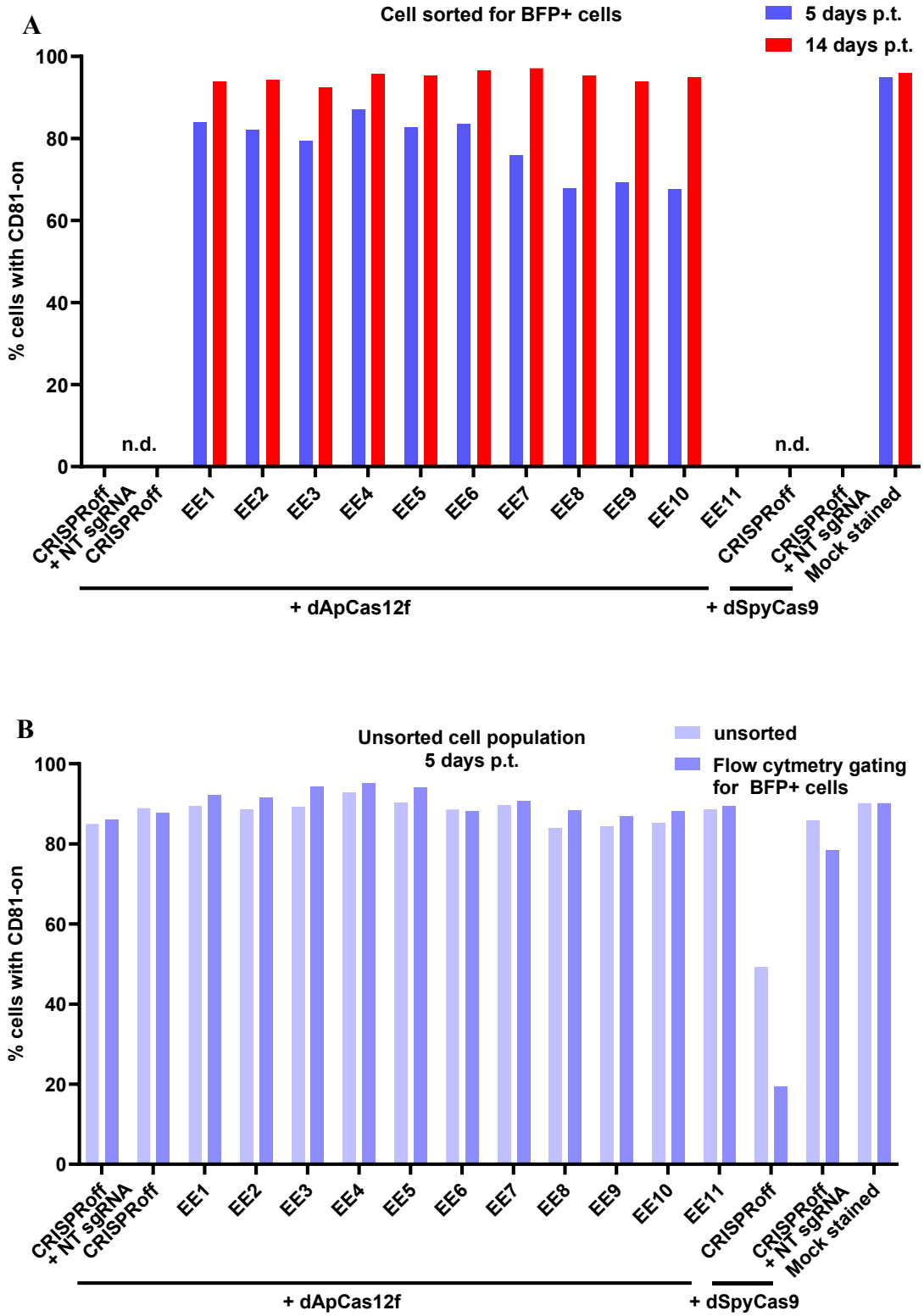

Figure 25: Evaluation of EE1-EE11 for epigenetic silencing of *CD81*. HEK293T cells were transfected with plasmids encoding constructs EE1-EE11 with a *CD81* sgRNA pool (a+b+c). 2 days p.t., the cells were divided into two subpopulations; one subpopulation underwent cell sorting (A), while the other was measured in bulk (B). Some samples underwent cell death and could not be measured, indicated in the graph as "not determined" (n.d.). **A)** The cells were continuously cultured by splitting them every 2-3 days. Silencing was analyzed at 5 and 14 days p.t. through live cell antibody staining and flow cytometry (n = 1). **B)** A subpopulation was taken to analyze the cells in bulk without sorting for transfected cells at 5 days p.t. (indicated in light blue). Additionally, the data was analyzed by flow cytometry gating for transfected cells (BFP+ cells), thereby mirroring the cell sorting process (indicated in dark blue) (n = 1).

Given the numerous possibilities for assembling the three epigenetic domains at the N-terminus, C-terminus, or in various combinations, along with the various options for linker sequences, we decided to start with a simpler architecture, similar to that used for CRISPRi. This architecture only includes one epigenetic domain (DNMT3A, DNMT3L or KRAB) and consequently mediates transient gene silencing. Starting from this CRISPRi architecture, we aimed gradually incorporate additional domains to transition from transient silencing to permanent silencing. The constructs were designed based on individual fusions of the silencing domains with dApCas12f, as illustrated in Figure 26.

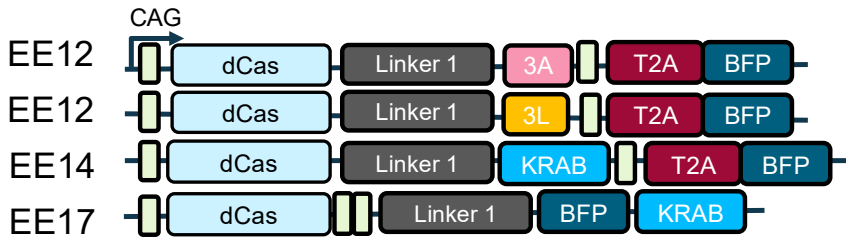

Figure 26: A schematic illustration of CRISPRi fusion variants.The constructs EE12-EE14 and EE17 are based on individual fusions of the epigenetic editing domains DNMT3A, DNMT3L and KRAB with a catalytically inactive nuclease.

Constructs EE12-14 and EE17 involved C-terminal fusions to dApCas12f, modeled after our previously established and validated dApCas12fCRISPRa constructs. It has been reported that C-terminal fusions, in comparison to N-terminal fusions, enhance efficacy in the context of dCasMiniCRISPRa and dSpyCas9CRISPRi (La Russa & Qi, 2015; Xu et al., 2021). We assessed *CD81* silencing as previously described, opting not to perform cell sorting in order to obtain a rapid impression of any potential activity. Our results indicated a complete absence of *CD81* silencing with dApCas12fCRISPRi 3 days p.t., as depicted in Figure 27. This lack of silencing was consistent for each construct (EE12-14 and EE17).

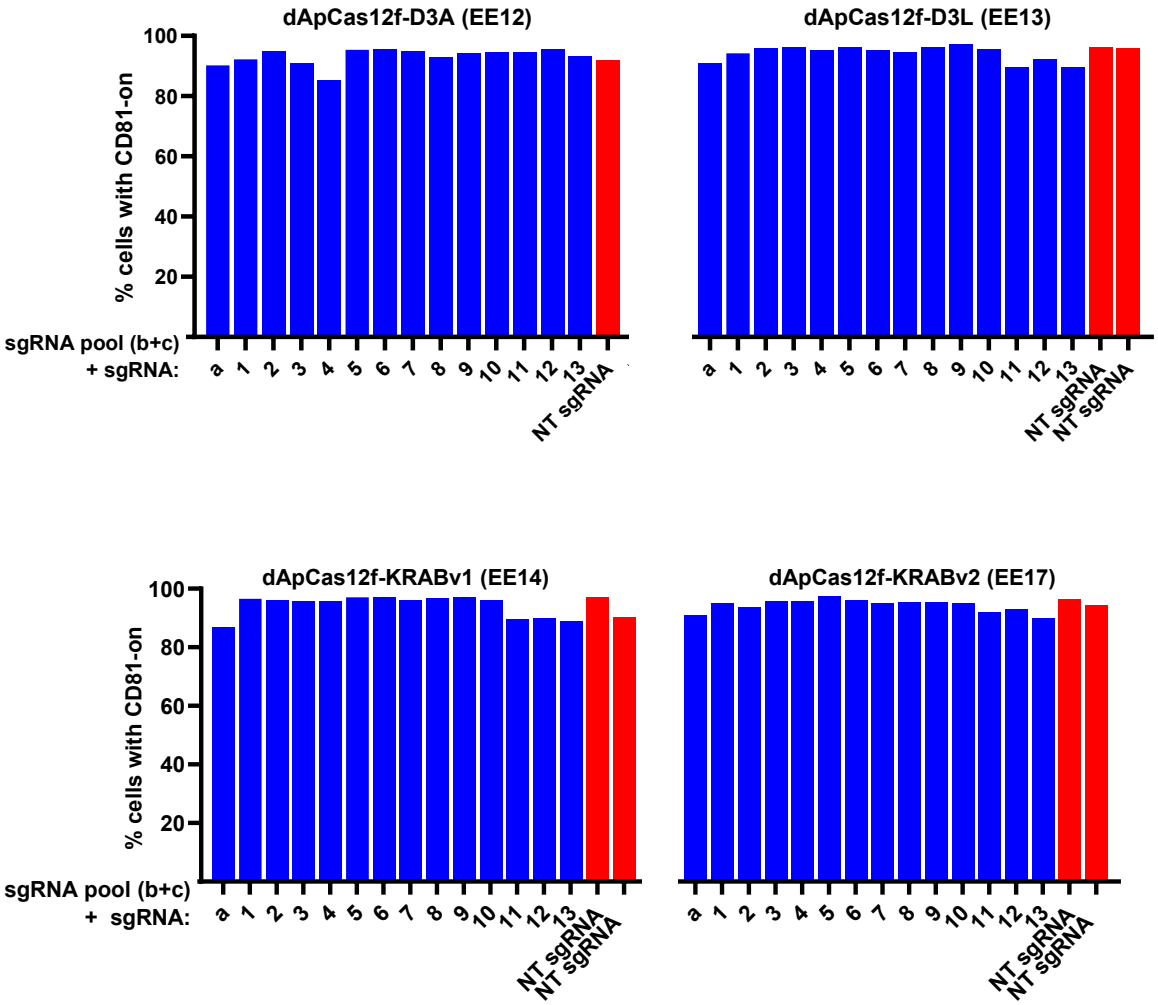

Figure 27: CRISPRi fusion variants tested with dApCas12f for silencing of *CD81*. HEK293T cells were plasmid transfected with plasmids encoding the CRISPRi variants (EE12-EE14 and EE17) and sgRNA pools targeting the CD81 promoter. The sgRNA pools consisted of sgRNA pool (b+c) and additionally a third sgRNA from a set consisting of sgRNA--1-13. 3 days p.t. silencing was analyzed by antibody staining of CD81 and flow cytometry read-out as previously described (n = 1).

CRISPRi fusion variants EE13-EE14 and EE17 with dSpyCas9 demonstrated approximately 50% reduction (Figure 28A). In comparison, construct EE12 with dSpyCas9 only mediated about 20% reduction. The activity of CRISPRi with dSpyCas9 shows that while the assay itself was functioning effectively, the dApCas12fCRISPRi constructs (EE12-14 and EE17) displayed no detectable activity in mediating *CD81* silencing. Of note, the dSpyCas9CRISPRi variants were additionally evaluated in conjunction with a pooled sgRNA set containing all three sgRNAs (a+b+c), as well as with individual sgRNA (a-c). sgRNA-a, sgRNA-b and the pool of sgRNA (a+b+c) all mediated ~50% CD81 silencing 3 days p.t.. However, we observed that sgRNA-c did not exhibit any silencing activity when tested as a standalone sgRNA (Figure 28B).

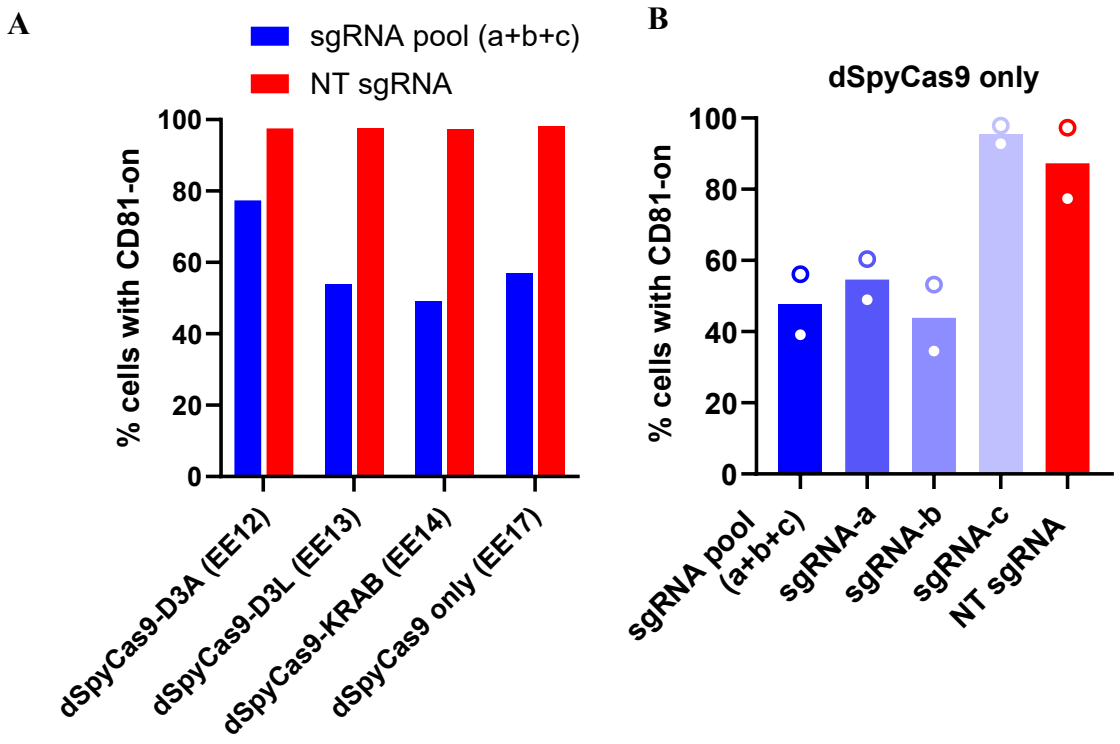

Figure 28: CRISPRi fusion variants tested with dSpyCas9 for silencing of *CD81*. HEK293T cells were plasmid transfected with plasmids encoding the CRISPRi variants and sgRNAs targeting the *CD81* promoter. 3 days p.t. silencing was analyzed by antibody staining of CD81 and flow cytometry read-out as previously described **A)** CRISPRi variants EE12-14 and EE17 with dSpyCas9 were combined with the sgRNA pool (a+b+c) (n = 1). **B)** dSpyCas9-only without additional fusion domains was combined with the single gRNAs-a-c aswell as the sgRNA pool (a+b+c) and tested for silencing as previously described (n = 2).

At this point, we faced two unknown variables: Whether the sgRNAs were ineffective or whether the architectures were not functional for our nuclease. We decided to address the gRNA questions first and tested sgRNAs for cleavage with catalytically active ApCas12f. The initial steps of CRISPR interference and DNA cleavage are analogous, encompassing the critical processes of PAM recognition and hybridization of the spacer to the protospacer in the event of a complementary (Gleditzsch et al., 2019). Therefore, it is reasonable to assume that DNA cleavage activity can be used as a proxy for DNA binding activity. Xu et al., (2021) have shown for CasMini that a sgRNA for binding also induces cleavage.

We co-transfected ApCas12f with sgRNAs-1-14 into HEK293T cells using lipid-mediated transfection and quantified DNA cleavage through NGS, as previously described (Figure 29A). All sgRNAs demonstrated extremely low activity levels, around background levels ranging from 1%-2%, with sgRNA-1 being the most active at 3%-4% indels (Figure 29B). For SpyCas9, sgRNA-a mediated approximately 60% indel frequency. The equivalent sgRNA-a for ApCas12f however only mediated 5% indel activity. Similarly, sgRNA-c, which displayed a

high indel frequency of 65% with SpyCas9, resulted in less than 1% activity for ApCas12f (Figure 29C). The activity of sgRNA-b could not be assessed, as no NGS amplicons could be established for that region. From this screen it can be concluded that one factor contributing to the lack of activity of the EEs can be potentially attributed to the low efficacy of the sgRNAs.

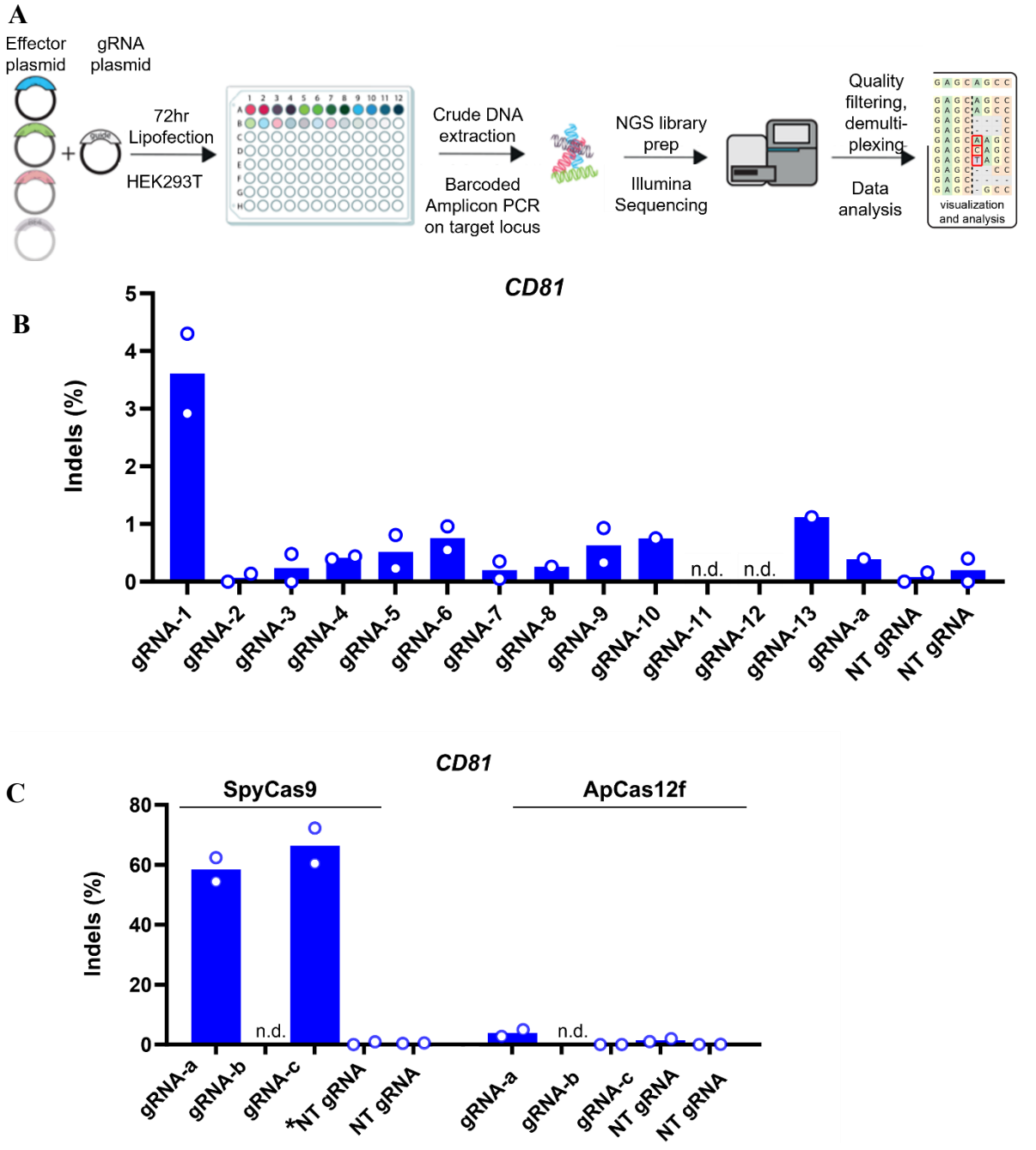

Figure 29: NGS demonstrates minimal cleavage activity of ApCas12f with *CD81* sgRNAs. A) Workflow to determine the indel frequencies of catalytically active ApCas12f and SpyCas9. HEK293T cells were transfected with an effector and sgRNA expression plasmid. 3 days p.t., DNA was extracted for barcoded amplification of the edited target followed by library preparation for subsequent NGS analysis. The generated fastq-files subjected to bioinformatic analysis. This included preprocessing such as quality filtering, demultiplexing and analyzing and characterizing the editing event. Figure from Dr. Christina Galonska. **B)** Indel frequencies of catalytically active ApCas12f across a panel of 14 *CD81* targeting sgRNAs (n = 1 or 2, as indicated by data points). **C)** Indel analysis of the *CD81* gRNA pool (a+b+c) mediated by SpyCas9 and ApCas12f. (gRNA-a binding site covered with amplicon 1, gRNA-c binding site covered with amplicon 27. The asterisk (*) indicates that there were only 1 k NGS reads).

3.4 Triple mutant en-ApCas12f shows increased nuclease activity

Previous studies from us and others have shown that mammalian activity of hypercompact nucleases can be improved by targeted protein and sgRNA engineering, for example CasMini and AsCas12f (Wu et al., 2023; Xu et al., 2021). To identify candidates for mutagenesis, the protein sequence of ApCas12f was aligned to engineered AsCas12f (enAsCAs12f). Single-point mutations which improved activity of AsCas12f were introduced at respective sites in the protein sequence of ApCas12f. This step was conducted by Dr. Philipp Knyphausen and Dr. Andreas Neerincx. This resulted in the three single point mutants T212K, I292R, D379R and a triple mutant harboring all three variants (T212K/I292R/D379R). First, we measured DNA cleavage activity. HEK293T cells were transfected with plasmids encoding engineered ApCas12f variants and analyzed for indels as previously described (Figure 29A). Besides target *CD81*, we chose to include into our analysis the targets fibrinogen alpha chain (*FGA*) and albumin (*ALB*), as our group had previously established ApCas12f sgRNAs with robust cleavage activity and NGS amplicons for both sites.

All single-point variants T212K, I292R and D379R as well as the triple mutant harboring all three mutations T212K/I292R/D379R showed 2-3-fold increased indel frequency over the WT on *CD81* (Figure 30). T212, I292R and T212K/I292R/D379R induced ~17% indels whereas the WT mediated 6%. Similarly, all mutants had increased indel rates on targets *FGA* and *ALB*. We observed an increase in activity of approximately 1.5-fold on *FGA* and approximately 1.5-2-fold on *ALB*. This was equivalent to indel rates of ~40% for T212, D379R and T212K/I292R/D379R on *FGA* whereas the WT induced 28%. On *ALB,* the mutants D379R and T212K/I292R/D379R induced ~27% indels compared to 14% indels with the WT. With the highest fold change of 3.17 over the WT on *CD81*, we selected the triple mutant for further optimizations, termed enhanced ApCas12f (en-ApCas12f).

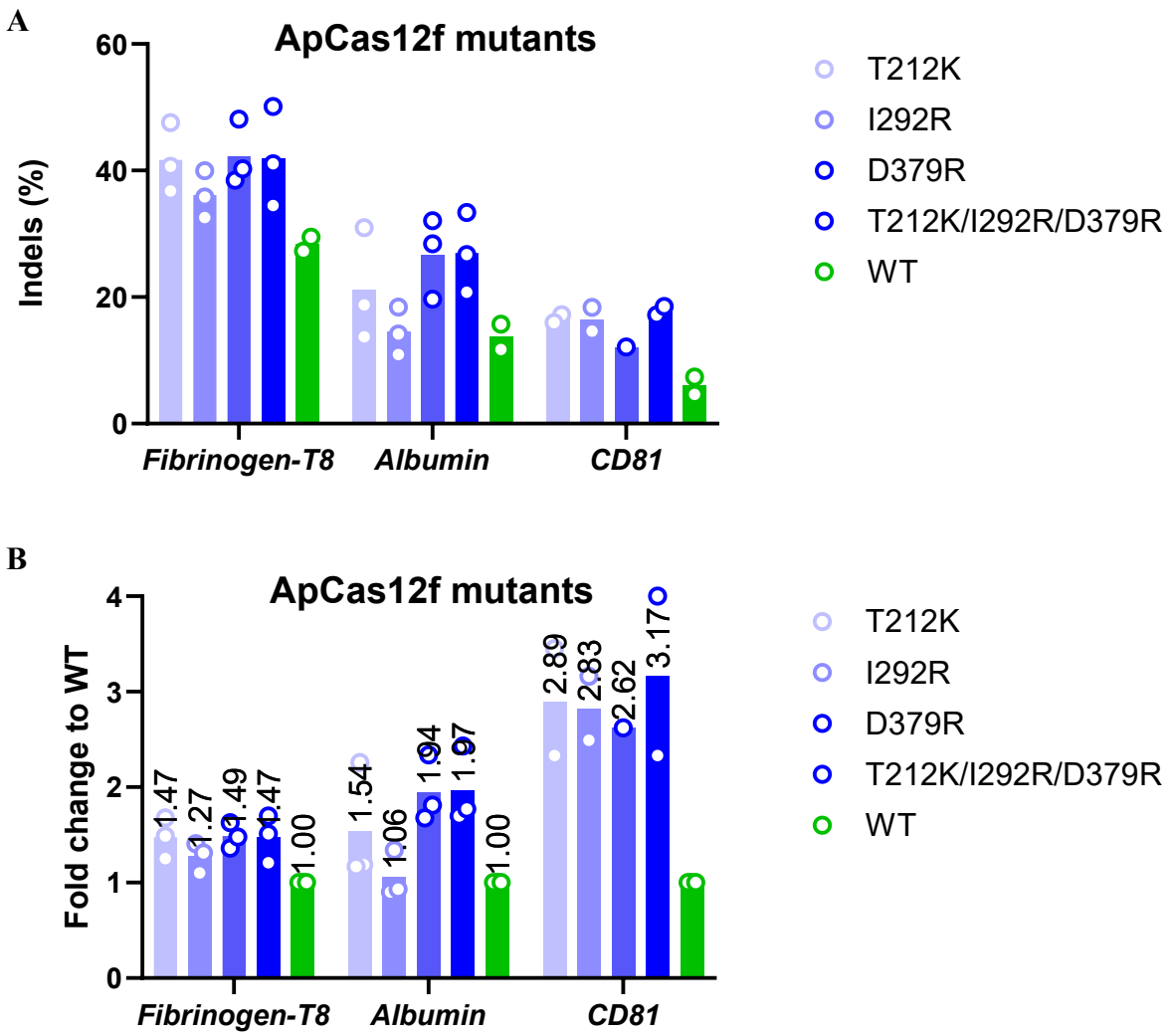

Figure 30: Protein engineering of ApCas12f based on engineered AsCas12f A) Plasmid transfection of HEK293T with ApCas12f mutants to analyze indel frequencies (%) on three targets. *CD81*: n = 2; *FGA* & *ALB:* n = 3. **B)** Fold change of indel frequencies compared to WT levels. *CD81*: n = 2; *FGA* & *ALB:* n = 3.

To further enhance the performance of the en-ApCas12f, especially on target *CD81*, we sought to draw insights from the recently engineered *Oscillibacter* sp OsCas12f (enOsCas12f) nuclease (Kong et al., 2023). We used an equivalent approach to our previous strategy for AsCas12f-based mutants. To identify candidates for mutagenesis, the protein sequence of ApCas12f was aligned with that of enOsCas12f. Specific mutations that had previously shown to improve the activity of enOsCas12f and were also present in our variant, were identified. The mutations E130E and D45R were selected. The identification of the mutations was conducted by Dr. Philipp Knyphausen. We incorporated the new candidates for mutagenesis into en-ApCas12f to further optimize the triple mutant variant, resulting in the ApCas12f candidates **E130R**/T212K/I292R/D379R, **D45R**/T212K/I292R/D379R and **E130R/D45R**/T212K/I292R/D379R. However, the introduction of additional mutations did not improve nuclease activity. Instead, we observed a significant loss of activity with each mutation

introduced. The indel rates decreased from 9% with the WT to 3% with **E130R**/T212K/I292R/D379R and fell below <1% with **D45R**/T212K/I292R/D379R and **E130R/D45R**/T212K/I292R/D379R (Figure 31).

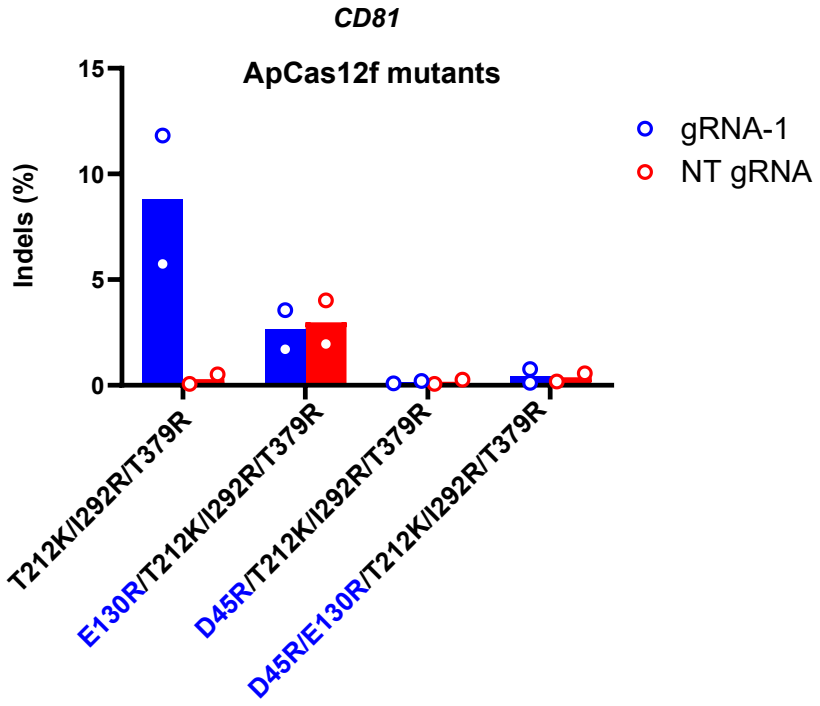

Figure 31: Cleavage activity of ApCas12f mutants derived from OsCas12f. Candidates for mutagenesis were derived from engineered OsCas12f. Mutations that enhanced OsCas12f were introduced into en-ApCas12f. HEK293T cells were plasmid-transfected with the mutants and cleavage activity was analyzed via NGS and compared to en-ApCas12f (n = 2).

Given that the mutations derived from the OsCas12f nuclease did not further enhance the activity of en-ApCas12f, we adopted a broader approach to identify beneficial mutations. Our colleague Dr. Florian Richter designed a novel set of candidates for mutagenesis. This consisted of analysing a structural homologue of ApCas12f for positions in functionally relevant regions and then analysing a family multiple sequence alignment (MSA) for consensus mutations at these positions. He derived a set of 91 single point mutants (SPMs). We decided to screen these mutants in WT ApCas12f rather than introducing them directly into en-ApCas12f to avoid detrimental effects of combinations as seen with quadruple and quintuple mutants derived from OsCas12f. Cloning was kindly carried out by our two colleagues Corinna Saalwächter and Dr. Andreas Neerincx. Point-mutations were introduced into WT ApCas12f by LDA cloning and subjected to automated mini-scale plasmid preparations.The mutants were screened in HEK293T cells on the targets *CD81*, *FGA* and *ALB*. When tested on target *CD81*, WT ApCas12f exhibited cleavage activity of 11%. In contrast, the best-performing mutants demonstrated indel rates of 19% (L177E), 19% (A307G) and 16% (K443I) indicating a notable

activity improvement of 1.5-1.7-fold (Figure 32). About half the of all tested mutants induced higher indel rates compared to the WT. On target *FGA*, WT ApCas12f displayed a cleavage activity of 25%. The best mutants N91Y and M144R reached cleavage efficiencies of 33% and 32%, respectively (1.3-fold improvement). This increase in indel activity was not as pronounced as that observed for *CD81*. It is noteworthy that results for target *FGA* yielded smaller differences in indel frequency across all mutants when compared to *CD81*. For target *ALB*, WT ApCas12f exhibited a cleavage activity of 18%. Again, the mutants N91Y and M144R demonstrated increases in indel rates, achieving 28% (1.6-fold) and 25% (1.4-fold), respectively. Additionally, the A247T mutant also exhibited high indel rate of 26% (1.4-fold). While these mutants were not the best performing candidates on *CD81*, with indel rates of 14% and 12% these mutants still showed an increase over the WT (11%).

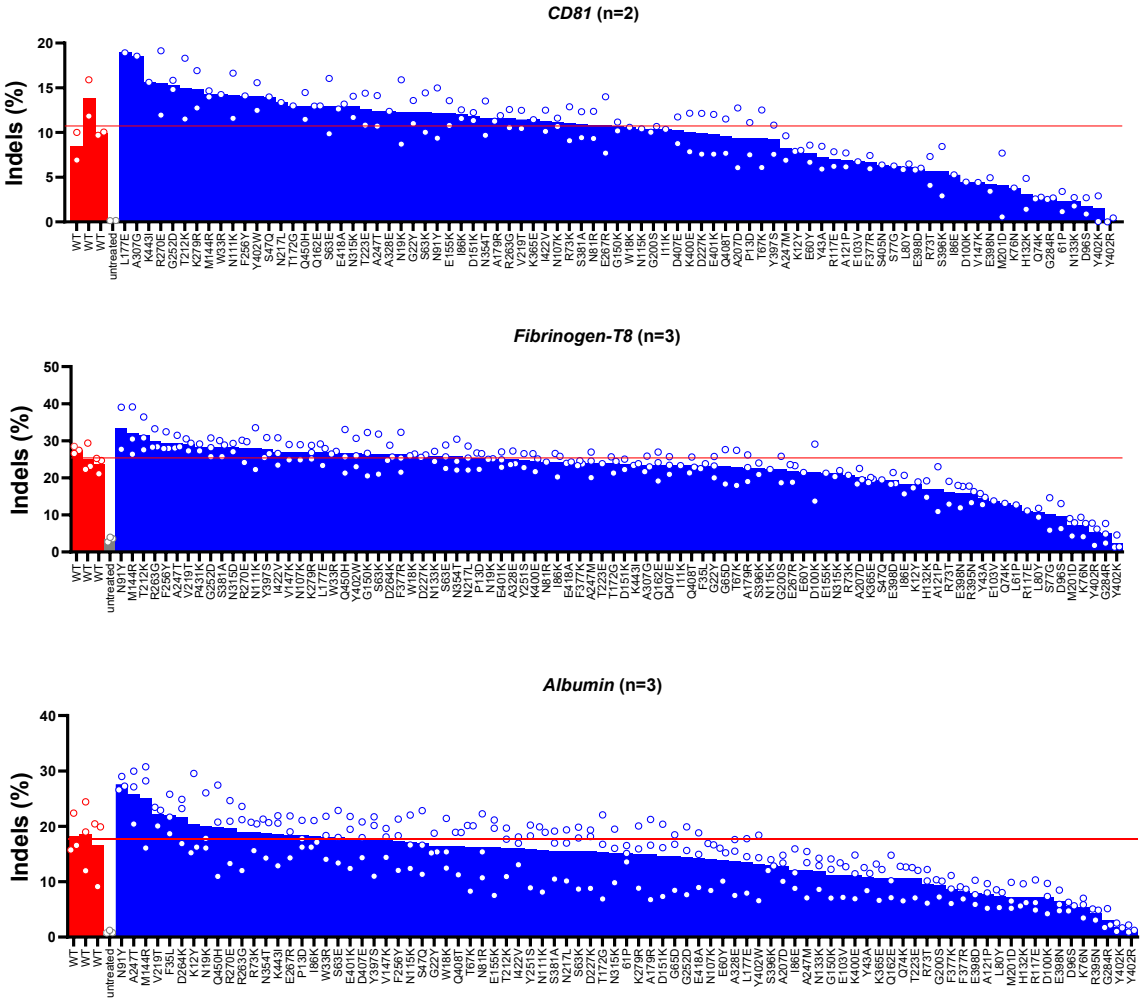

Figure 32: Cleavage activity of 91 SPMs of ApCas12f derived through MSA. ApCas12f candidates for mutagenesis were cloned by LDA and subjected to automated mini-scale plasmid preparations. HEK293T cells were plasmids transfected and cleavage activity was analyzed on three targets via NGS and compared to the WT. The red line indicates the average of the WT. *CD81*: n = 2; *FGA* & *ALB:* n = 3.

We selected all candidates that exhibited cleavage activity of at least one standard deviation greater than the WT across at least two of the three tested targets. This led to a list of ten candidates for further evaluation. Next, we sought to validate of our findings from the previous high-throughput screen by excluding the possibility that the observed improvements in indel rates were mere artifacts arising from variations e.g. in plasmid quality preparation. Results obtained from experiments using individual midi preparations of plasmid DNA were consistent with our initial findings that were based on automated mini-scale plasmid preparations. Indel rates were overall slightly higher across mutants and WT. Mutants M144R and N91Y were the best performing candidates on *FGA* and *ALB*. Specifically, mutant M144R mediated cleavage efficiencies of 62% (1.76-fold increase compared to WT) on *FGA* and 24% (1.36-fold increase compared to WT) on *ALB*. Likewise, mutant N91Y demonstrated cleavage activities of 57% (1.59-fold increase compared to WT) on *FGA* and 23% (1.38-fold increase compared to WT) on *ALB* (Figure 33). Taken together, this screen revealed several strong mutants. We noted that depending on the target, the mutants can vary in their activity profile. However, the best candidate was en-ApCas12f, which exhibited a fold increase of 1.47 and 1.97 on *FGA* and *ALB*, respectively. For the time being, we have decided to proceed with en-ApCas12f as the foundation for engineering an EE.

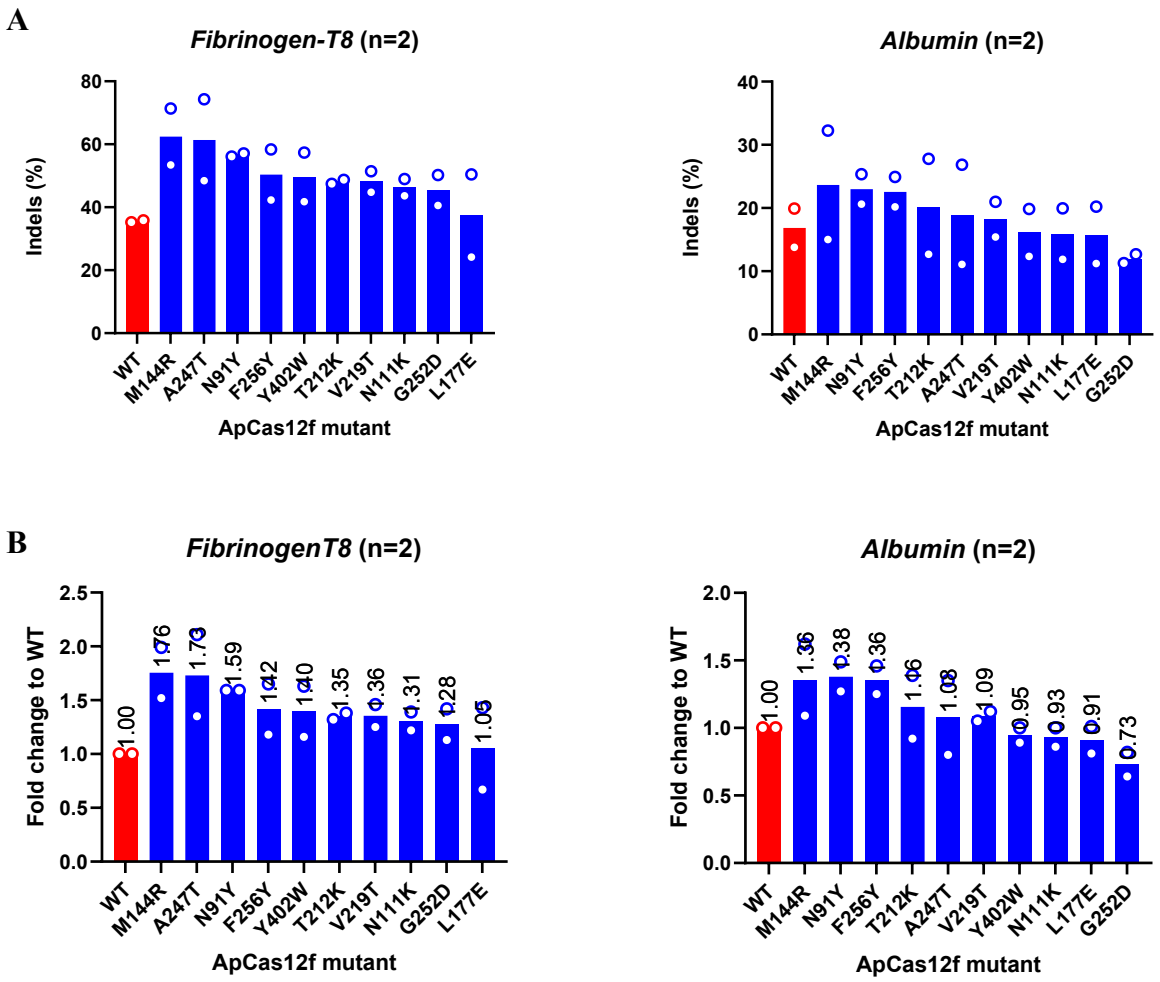

Figure 33: Evaluation of mutants with highest activity. A) HEK293T cells were plasmids transfected and cleavage activity was analyzed on two targets via NGS and compared to the WT. A set of selected mutants were tested again to confirm initial results from the high-throughput screen. Mutants with highest indel rates were transformed into *E. coli* and subjected to individual midi preparations of plasmid DNA to ensure varying levels of indel were not a result of plasmid quality. After that, the constructs were tested again for indel generation as described previously (n = 2). **B)** Indel activity of the mutants were calculated as fold change to WT ApCas12f (n = 2).

3.5 dApCas12fCRISPRoffCutter shows absence of DNA cleavage

We sought to gain a deeper understanding of the underlying causes of the observed lack of silencing activity. The sgRNAs represented at least one source of inefficiency. Another hypothesis suggested that the additional payload of three epigenetic domains might be contributing to this issue. We sought to address the question whether ApCas12f is still active when artificially fused to silencing domains. CRISPRa showed that this is indeed possible but could be different for silencing domains. To test this hypothesis, we incorporated nuclease active version of ApCas12f into both the original CRISPRoff construct and the CRISPRi constructs EE14 and EE17, termed CRISPRoffCutter and CRISPRiCutter. Our objective was to test whether the additional payload of these fusion constructs results in decreased indel rates compared to the respective nuclease without additional epigenetic domains. The efficiency of this binding was indirectly assessed through DNA cleavage analysis. For this experiment, HEK293T cells were transfected with the effector plasmid and sgRNA plasmid, and the resulting indels were analyzed using NGS, as previously described.

For the target *CD81*, we observed indel frequency of 46% with SpyCas9, compared to 34% for the SpyCas9CRISPRoffCutter. While this represents a notable reduction in activity, robust cutting efficiency remained and was comparable to that of the nuclease without fusion domains. In contrast, the ApCas12f nuclease exhibited indel levels of 9%, which were completely absent when utilizing the ApCas12fCRISPRoffCutter. This observation suggests either a minor reduction of approximately 10%, akin to the decrease noted with SpyCas9, or a complete loss of cleavage activity (Figure 34A). To further investigate this hypothesis, we introduced two additional targets for evaluation which provide a higher dynamic range, *FGA* and *ALB*. ApCas12fCRISPRoffCutter demonstrated a substantial reduction in cutting efficiency, with indel frequencies declining from 43% to 7% on *FGA* and from 15% to 3% on *ALB*. Furthermore, we included a CRISPRiCutter in our analysis. Indel rates were consistent between en-ApCas12f only and en-ApCas12f fused with KRAB at around 40% on *FGA* and ~ 20%-30% on *ALB* (in this case, engineered ApCas12f was employed) (Figure 34B).

In conjunction with the observation that the sgRNAs demonstrated nearly absent activity on *CD81*, these findings further support the notions that the lack of activity associated with dApCas12f EEs can be attributed to at least two factors: ineffective sgRNAs and a fusion protein architecture that is incompatible with our hypercompact Cas12f nuclease. This prompted us to further investigate alternative architectures to identify a design that would be suitable for dApCas12f.

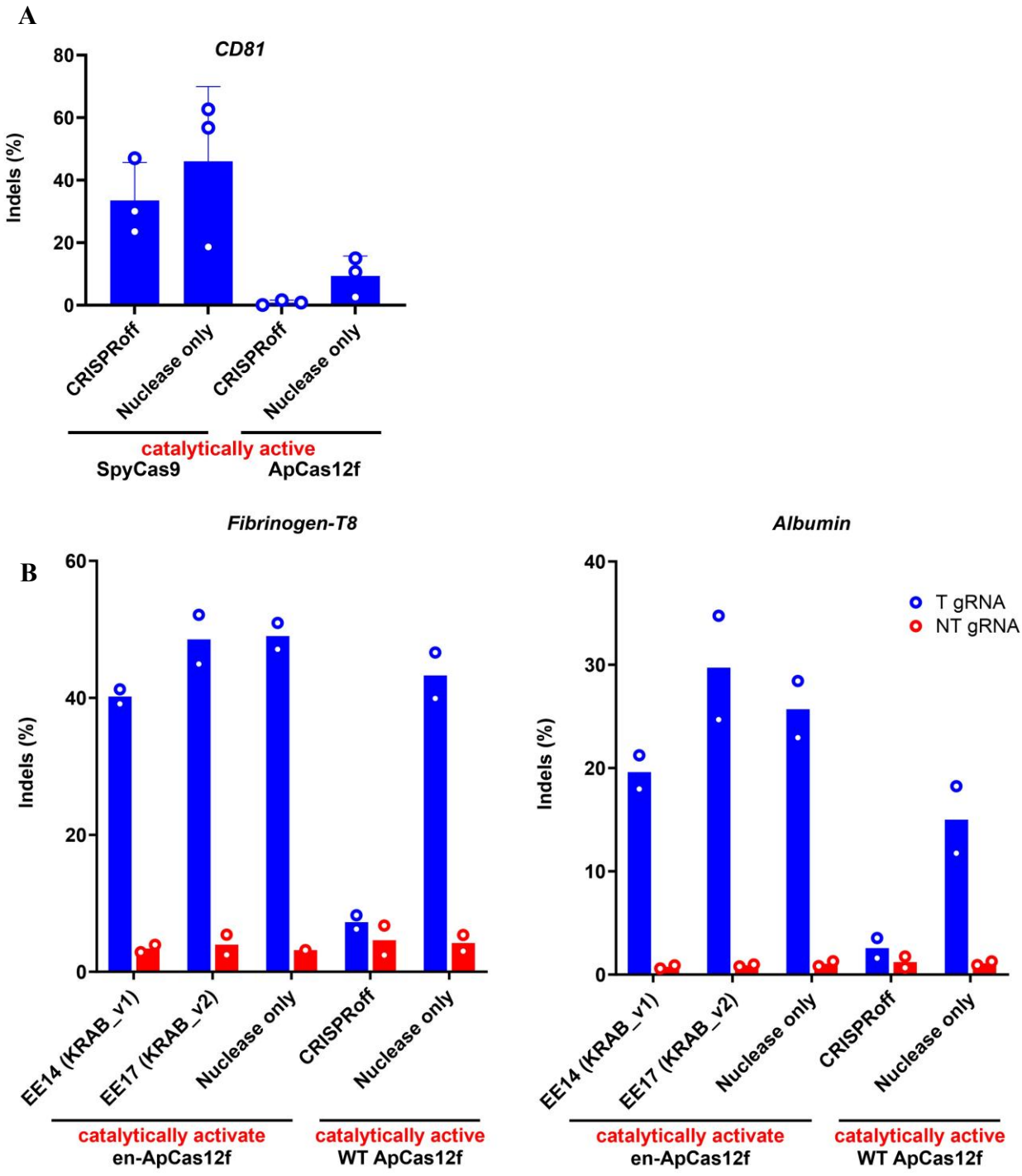

Figure 34: CRISPRi- and CRISPRoffCutter. Comparison of cutting efficiency between enApCas12f fused with KRAB (EE14 and EE17), ApCas12f/SpyCas9 fused with CRISPRoff and ApCas12f/SpyCas9 only. **A)** The cutting efficiency between CRISPRoff with catalytically active ApCas12f/SpyCas9 was compared to ApCas12f/SpyCas9-only. The constructs were introduced into HEK293T cells by plasmid transfection and targeted to *CD81* with gRNA-1. The Indel rates were analyzed by NGS (n = 3). **B)** The constructs EE14 and EE17 with catalytically active en-ApCas12f were tested for the introduction of indel (NGS analysis) into *FGA* and *ALB* and compared to en-ApCas12f-only. Additionally, the cutting efficiency between CRISPRoff with catalytically active ApCas12f was compared to ApCas12f-only. The experiment was based on HEK293T cells transfected with plasmids encoding the effectors and sgRNAs (n = 2).

3.6 EEs with dApCas12f mediated silencing of *TRE3G* reporter plasmid

Given the challenges we encountered with *CD81* as a target for ApCas12f due to the inability to identify a functional sgRNA, we faced a lack of effective sgRNAs and a non-functional effector. To address this, we aimed to utilize a modified version of the *TRE3G*-based assay for which we had previously established functional sgRNAs. The promoter *TRE3G*-minimalCMV exhibits basal activity that can be multiplied through CRISPRa. We sought to take advantage of this basal activity as it provides sufficient dynamic range to measure the silencing effects of EEs. The sgRNAs used for cleavage were not suitable for this purpose, as they targeted downstream regions in exons and not promoters as needed for gene regulation. Therefore, we adapted our previously established CRISPRa assay, which had shown that the sgRNA for dApCas12f was effective. The assay involved a triple plasmid transfection into HEK293T cells of an effector plasmid, a sgRNA plasmid, and a reporter plasmid.

We also incorporated our findings on cleavage activity improvement by using en-ApCas12f with the alternative EE architectures EE1-EE17. en-dApCas12fEE1-EE17 were directed towards the transiently available reporter plasmid harboring the artificial and constitutively active reporter cassette from our CRISPRa assay. Silencing of each EE variant was measured 3 days p.t.. In the FACS analysis, we gated for BFP+ cells and compared the median GFP expression to its respective NT gRNA control (Figure 35).

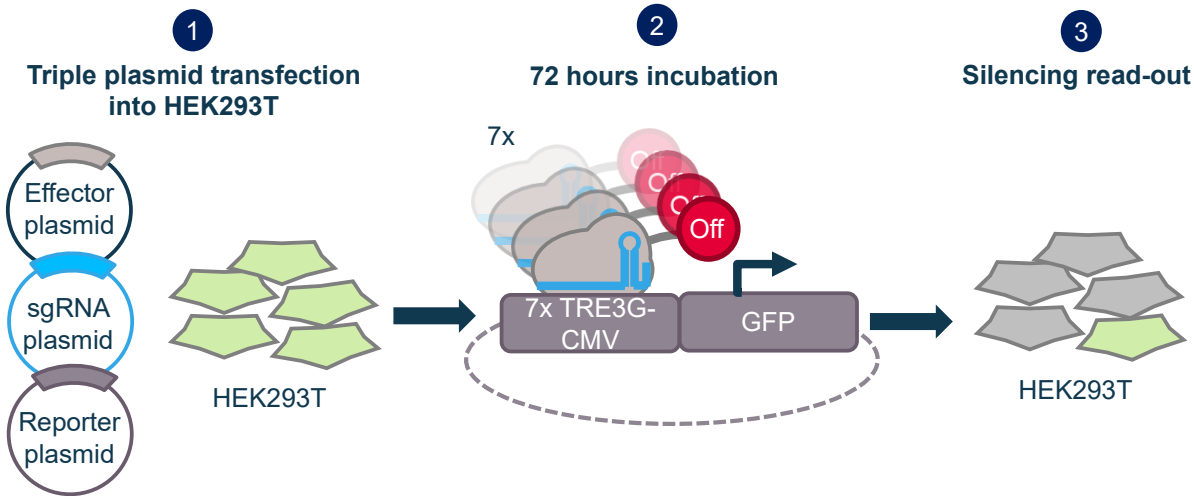

Figure 35: Experimental set up to evaluate EE1-EE17 for silencing of *TRE3G* reporter plasmid. To assess the silencing efficiency of the fusion constructs, HEK293T cells were triple transfected with an effector plasmid containing an EE variant, a sgRNA, and a reporter plasmid encoding TRE3G-GFP. Following a three-day incubation period, we conducted a subsequent analysis of reporter gene expression using flow cytometry. Silencing was evaluated by gating for BFP+ cells (transfected cells). Cells treated with a NT gRNA are provided as a benchmark for basal reporter gene expression.

Among the CRISPRi constructs, EE14 and EE11 exhibited strongest gene silencing, resulting in 6.51- and 4.5-fold reduction of GFP signal, respectively (Figure 36A). This corresponds to 80% and 73% signal reduction, respectively (Figure 36B). Notably, these levels of silencing were comparable to those achieved with CRISPRi construct EE17 with dSpyCas9, which demonstrated a 6.87-fold or an 84% reduction in GFP signal. Among the tested EE constructs, which incorporate all three epigenetic effector domains, construct EE2 emerged as the most effective, followed closely by construct EE1. These constructs achieved fold changes of 2.86 and 2.62, respectively, translating to approximately 50% reduction in GFP signal. In comparison, dSpyCas9CRISPRoff exhibited a 4.89-fold reduction, translating to a 78% reduction. The overall silencing effect of the candidates varied widely, ranging from those with strong activity to constructs exhibiting no silencing. Some candidates fell below the baseline activity of dApCas12fCRISPRoff, including constructs EE17, EE6, EE15, and EE9. Silencing with dSpyCas9-only, without the inclusion of additional epigenetic domains, did not induce gene silencing. Silencing of dApCas12f only varied between 1.1–1.7-fold reduction of GFP signal, however the baseline signal from samples treated with the NT sgRNA control were exceptionally low (Figure 36C).The baseline signal of the NT sgRNA control of EE1-EE17 ranged from 289-2578 (MFI). Collectively, this screening identified the architectures of EE1 and EE2 as suitable for dApCas12f.

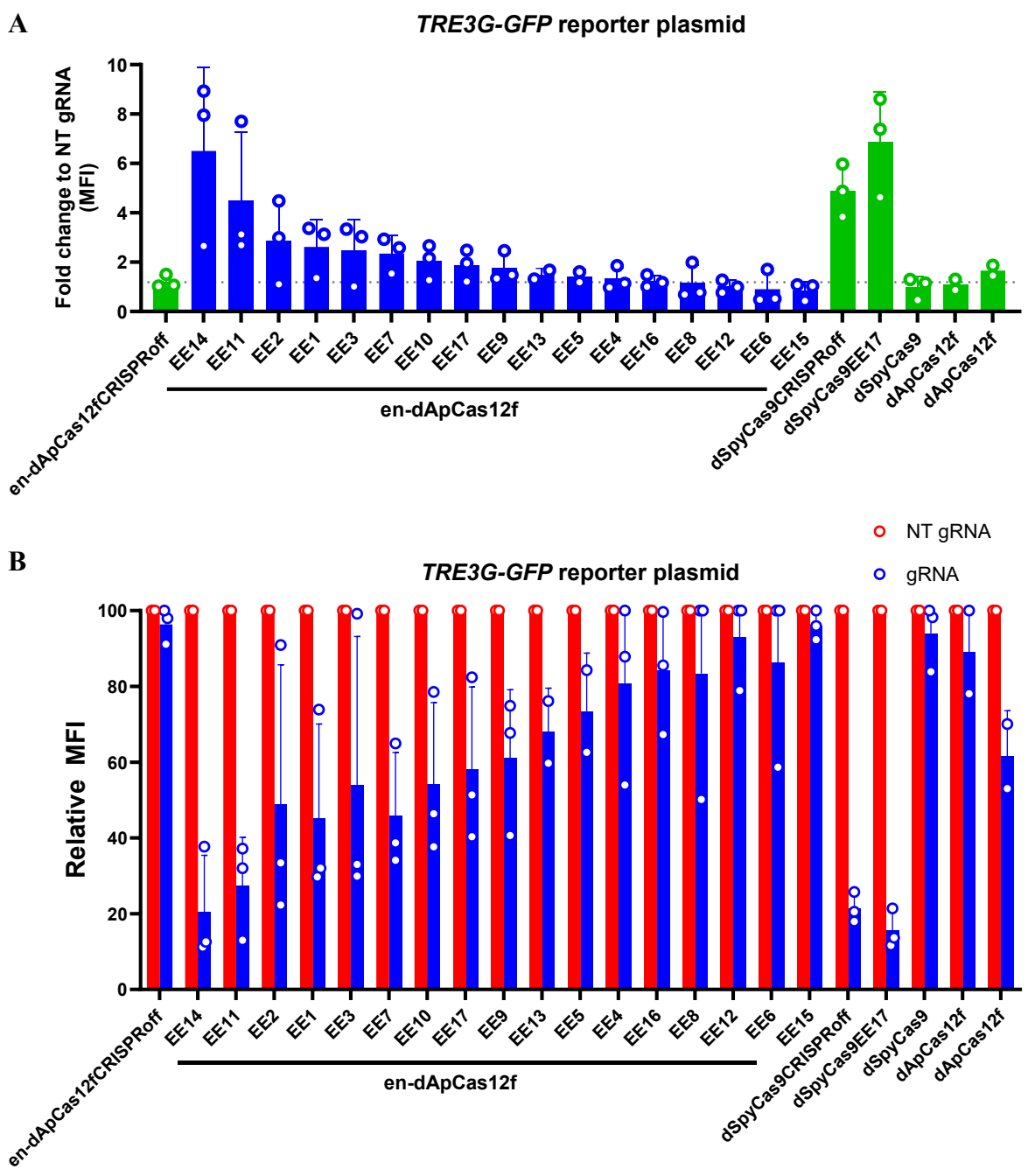

(Figure continued on next page)

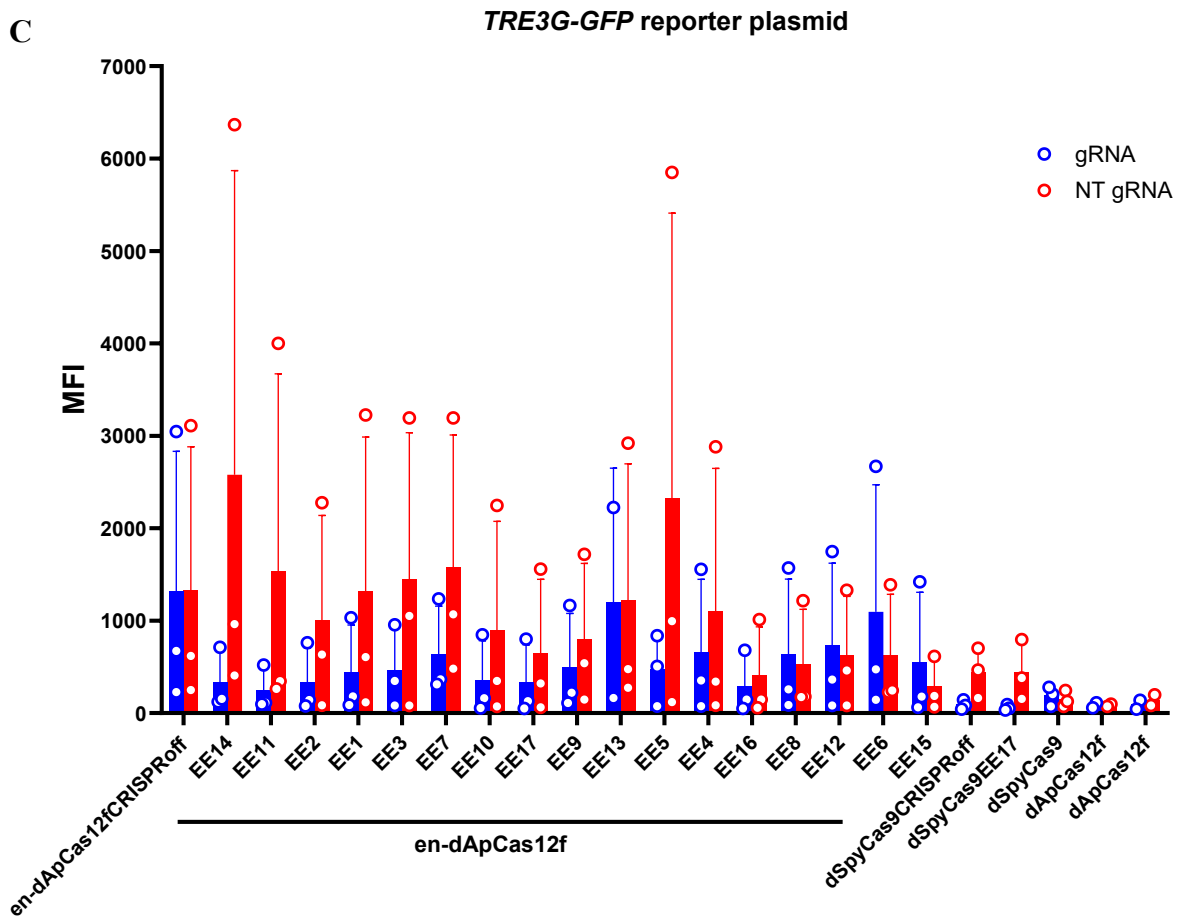

Figure 36: Evaluation of EE1-EE17 for silencing of *TRE3G* reporter plasmid A) Fold changes in median fluorescence intensity (MFI) were calculated between the active reporter gene (cells treated with NT gRNA) and the silenced reporter gene (cells treated with gRNA) (n = 3; each biological replicate was analyzed in technical triplicates). **B)** Analysis of silencing by epigenetic editors was based on relative silencing percentages (%) (n = 3; each biological replicate was analyzed in technical triplicates). **C)** Analysis of silencing was also conducted based on absolute values of GFP median. (n = 3; each biological replicate was analyzed in technical triplicates).

3.7 EE1 and EE2 with en-dApCas12 induce *PCSK9* methylation

The constructs en-dApCas12f EE1 and EE2, have demonstrated to be capable of mediating reporter plasmid silencing. However, transitioning from targeting a reporter plasmid to addressing endogenous targets presents a significant challenge. Previous studies have highlighted that while CRISPR systems may exhibit efficacy in plasmid contexts, they may necessitate additional modifications to achieve activity on an endogenous target (Lampe et al., 2024). Our investigations into reporter gene silencing have predominantly focused on protein-level outcomes. Consequently, we aimed to evaluate whether EE1 and EE2 can effectively induce methylation at endogenous targets, while also determining if the observed modifications are truly permanent. We selected proprotein convertase subtilisin/kexin type 9 (*PCSK9*) as the endogenous target for testing due to its well-established role in the liver and the extensive prior research conducted on this locus, including epigenetic editing studies (Cappelluti et al., 2024;

Tremblay et al., 2025; Whittaker et al., 2023). PCSK9 plays a critical role in the degradation of the LDL receptor, which is responsible for removing low-density lipoprotein cholesterol (LDL-C), commonly referred to as "bad" cholesterol, from the bloodstream. In the context of familial hypercholesterolemia, gain-of-function mutations in the PCSK9 gene lead to a harmful overexpression. Consequently, patients with familial hypercholesterolemia experience elevated levels of LDL-C, significantly increasing their risk of cardiac events. Previous studies have utilized the PCSK9 locus for various editing approaches. Notably, it has been shown that the PCSK9 locus in the HeLa cell line remains unmethylated but can be effectively methylated using dSpyCas9CRISPRoff with a combination of 2 sgRNAs, namely sgRNA-41 and -49. These sgRNAs were identified as the most effective candidates from a screening of 240 sgRNAs (Tremblay et al., 2025).

As previously shown in this study, a robustly active sgRNA pool is essential for successful epigenetic editing applications (section 3.1.1). Similar to the approach taken by Tremblay et al., (2025), we screened 90 sgRNAs targeting the *PCSK9* promoter to compile an effective sgRNA pool. We designed sgRNAs spanning 250 bp upstream and 250 bp downstream of the promoter region (Figure 37A). Nuñez et al. (2021) demonstrated that CRISPRoff exhibits the highest activity within this specific window. We tested these sgRNAs for cleavage activity using en-ApCas12f. During our screening of the sgRNAs, we included SpyCas9 with sgRNA-41 and sgRNA-49, which served as positive controls. Furthermore, we tested the same binding sites of the SpyCas9 sgRNAs for ApCas12f, ensuring that they were oriented in the complementary direction to align with the required PAM specificities.

The highest indel rates observed for en-ApCas12f were associated with sgRNA-61 and -21, both of which exceeded 50% indel activity. Some sgRNAs exhibited no activity at all. The top 20 sgRNAs displayed >15% cleavage activity. From this group, we selected six sgRNAs demonstrating the highest Indel rates that did not overlap in their binding sites. The selected sgRNA pool consisted of the following six sgRNAs: 56, 21, 45, 30, 52, and 88 with indels rates of 44%, 29%, 43%, 32% and 16% respectively. Notably, 88, which exhibited a relatively low activity rate of only 16%, was included because it was the only sgRNA to bind downstream of the TSS and this way ensured a greater coverage of the entire PCSK9 promoter. The indel activity of SpyCas9 with sgRNA-41 and -49 was around 31%. In the analysis, we excluded data points with fewer than 10,000 NGS reads per sample to maintain data quality. Therefore, for many tested sgRNAs there is only 1 data point (Figure 37B).

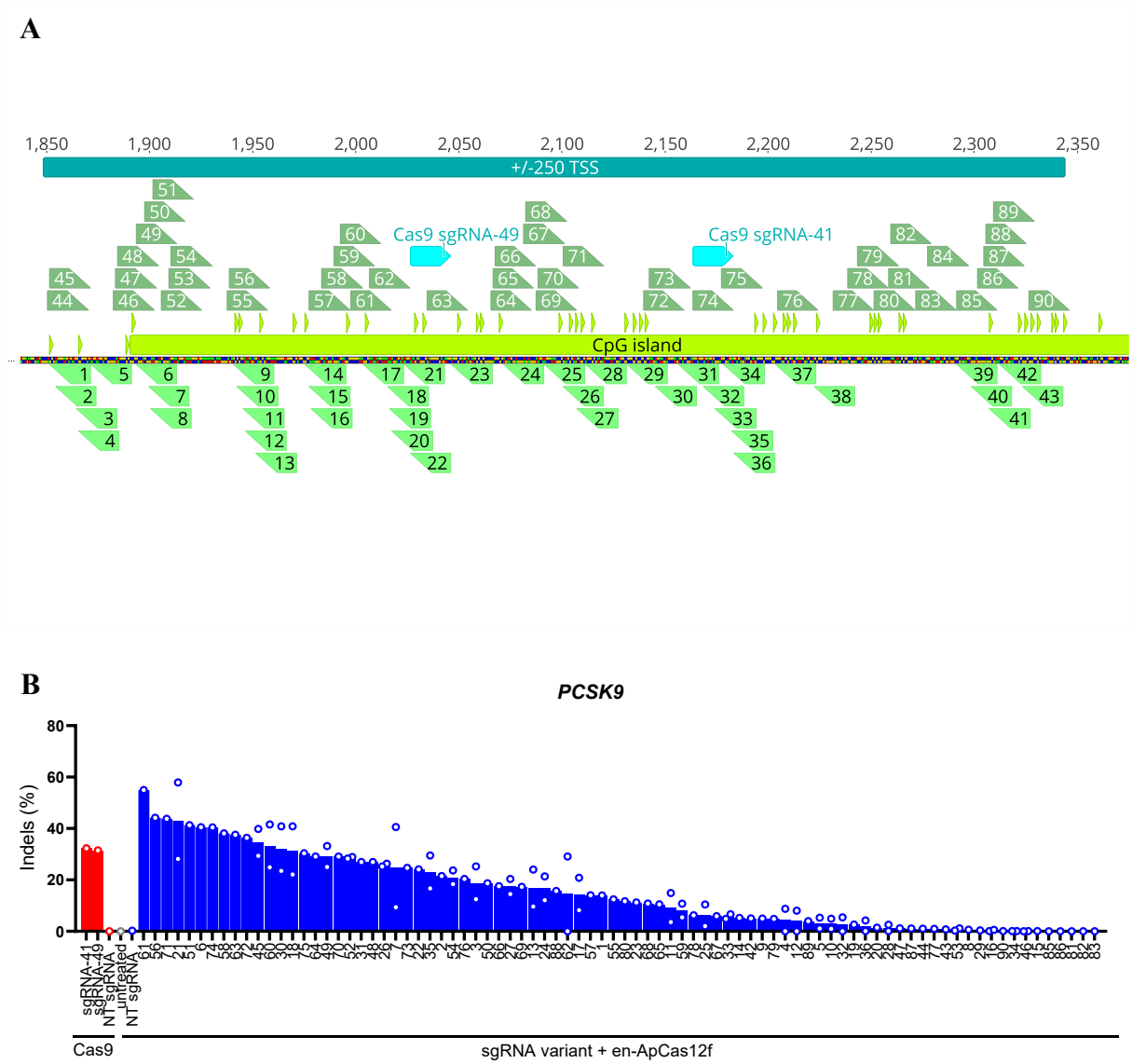

Figure 37: sgRNA screen for en-ApCas12f on *PCSK9*. A) Schematic of the PCSK9 promoter. A set of 90 sgRNAs (1-90) were designed to target PCSK9 250 bp upstream and 250 bp downstream of the TSS. sgRNAs are indicated in light and dark green. **B)** HeLa cells were plasmid-transfected with en-ApCas12f in combination with a panel of 90 sgRNAs targeting PCSK9. 3 days post-transfection, editing efficiency was assessed via NGS. Due to quality trimming to include only samples with more than 10,000 NGS reads, some gRNAs yielded only a single data point (n = 1 or 2, as indicated by the data points).

After identifying a robust sgRNA pool (Figure 38A), we wanted to determine whether the combination of these sgRNAs with EE1 and EE2 would induce promoter methylation. HeLa cells were co-transfected with effector plasmids and sgRNA plasmids. To enable long-term silencing analysis, cell sorting was performed 2-3 days p.t.. Methylation analyses were conducted 17 days p.t. with bisulfite sequencing coupled to NGS. Both EE1 and EE2 induced a strong increase in CpG methylation of the *PCSK9* promoter. While cells treated with the NT sgRNA exhibited 8% CpG methylation, levels increased to 31% and 42% with EE1 and EE2, respectively. Notably, EE2 demonstrated a slightly higher induction of methylation in both

experimental repeats, approximately 1.4-fold greater than that observed with EE1. EE2 induced a level of CpG methylation comparable to 39% mediated with dSpyCas9CRISPRoff. For WT dApCas12fCRISPRoff we detected 14% CpG methylation, slightly above baseline. With en-dApCas12fCRISPRoff we measured 9% methylation (Figure 38B).

In summary, a sgRNA screening on the *PCSK9* promoter utilizing catalytically active en-ApCas12f identified potent sgRNAs exhibiting high cleavage activity. We constructed a sgRNA pool that provided comprehensive promoter coverage while avoiding overlap among the sgRNAs. When combined with epigenetic editors EE1 and EE2, we observed that the constructs induced stable promoter methylation that persisted for up to 17 days p.t.. Our findings demonstrate that both EE1 and EE2 effectively introduce methylation of the *PCSK9* promoter, with EE2 achieving the highest levels of methylation.

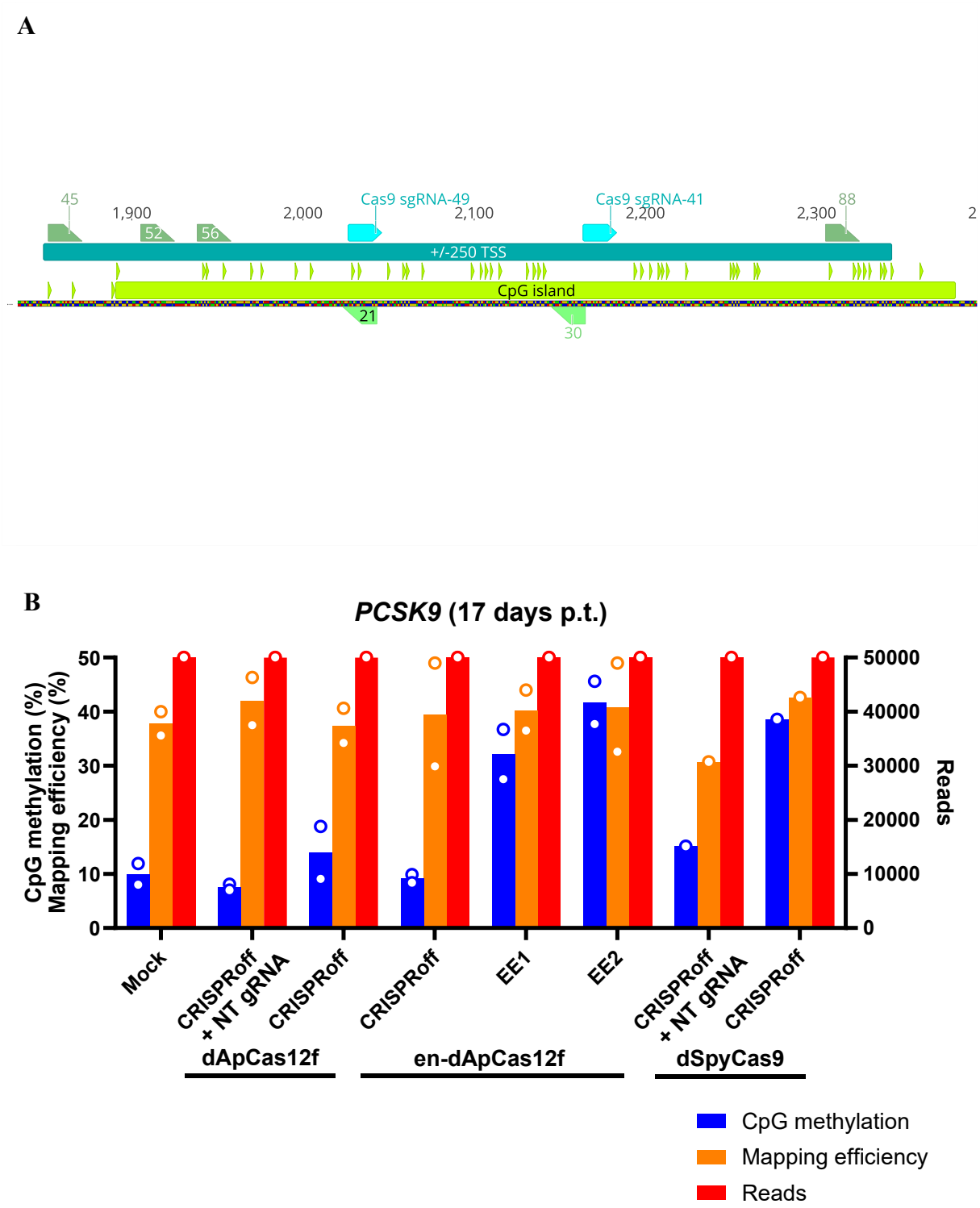

Figure 38: EE2 with en-dApCas12f induces DNA methylation of *PCSK9*. A) Schematic showing the binding sites of the sgRNA pool for en-dAsCas12f (light and dark green) and SpyCas9 (light blue). **B)** HeLa cells were transfected with plasmids encoding the effector plasmids and a sgRNA pool. Following transfection, cells were sorted for BFP+ cells (indicating successful transfection) and continued to be cultured by splitting the cells every 2-3 days. 17 days p.t., the cells were subjected to bisulfite sequencing to assess methylation levels. The percentage of methylated CG dinucleotides withing the PCSK9 promoter is indicated by the blue bars. The mapping efficiency of the NGS reads to the reference genome is represented in orange, while the NGS read count is shown in red. All samples were measured in biological replicates (n = 2), except for those treated with dSpyCas9-CRISPRoff, which were measured with a single replicate (n = 1).

4. Discussion

CRISPR technology is recognized as a transformative approach for addressing genetic diseases, offering unprecedented opportunities for therapeutic interventions based on targeted gene editing. DSBs associated with conventional genome editing may lead to chromosomal aberrations, including large deletions, rearrangements, or chromothripsis (Leibowitz et al., 2021; Nahmad et al., 2022; Turchiano et al., 2021). Technologies that utilize single-strand breaks in the DNA molecule, such as base editing (BE) and prime editing, may trigger genotoxicity, particularly when targeting multiple genes (multiplexing) (Fiumara et al., 2024; Stadtmauer et al., 2020; Turchiano et al., 2021). Epigenetic editing offers a potential safety advantage over conventional genome editing technologies by enabling durable changes in gene expression without altering the underlying DNA sequence, thereby significantly reducing the risks of chromosomal abnormalities (Trembley et al., 2021). The safety profile of epigenetic editing makes it especially attractive for *in vivo* applications. However, AAV-mediated approaches are inherently limited by their packaging capacity. To circumvent this limitation, we sought to replace the large SpyCas9 with a hypercompact nuclease from Aeribacillus pallidus identified through microbial genome mining.

4.1 Summary of results

In summary, we established assays for epigenetic editing read-out by reproducing a previously described assay from the literature which required significant optimization efforts until we achieved comparable levels of epigenetic silencing as demonstrated in the publication. To confirm that silencing of *CD81* was a result of targeted CpG methylation, we analyzed the genomic locus using bisulfite sequencing. Our data showed that CRISPRoff treatment led to a substantial increase in promoter methylation, lasting for weeks after treatment, indicating that silencing was a result of durable epigenetic modifications. Next, we screened hypercompact nucleases to assess their suitability as DNA binders. We identified dApCas12f, which exhibited a 72-fold reporter gene activation. In subsequent engineering efforts, we identified several mutations that increased its activity, resulting in the triple mutant en-ApCas12f. Initially, CRISPRoff with dApCas12f did not exhibit silencing activity. To address this lack of activity, we undertook multiple efforts to engineer dApCas12fCRISPRoff. This included screening of sgRNAs and testing a panel of eleven different ApCas12f-based EE variants, both approaches did not yield any detectable silencing activity. We then turned to simpler CRISPRi architectures which, again, did not display silencing activity. Testing of EE variants bearing active nucleases revealed comprised or complete lack of cleavage activity. This observation suggested that some

characteristics of the fusion construct limits the nuclease from binding to the DNA, preventing further downstream epigenetic editing events. To compensate for the lack of sgRNA activity, we repurposed our previously established CRISPRa assay, and the associated validated promoter-binding sgRNAs for ApCas12f. In this setup, we detected reporter gene silencing for EE1 and EE2 and CRISPRi EE14 and EE17. Recognizing the differences between the synthetic plasmid-based reporter gene target and endogenous targets, we aimed to test the ability of en-dApCas12fEE1 and en-dApCas12fEE2 to induce methylation and silencing of the endogenous locus *PCSK9*. In this assay, we observed a strong increase in promoter methylation compared to the WT promoter.

4.2 Development of hypercompact EE utilizing dApCas12f

The development of a CRISPR-based hypercompact EE that fits within the packaging limits of AAVs opens new avenues for delivering *in vivo* to distinct tissues and a variety of targets. To elude the initial absent silencing activity of CRISPRoff with ApCas12f, a panel of 14 *CD81* promoter sgRNAs were combined with catalytically active ApCas12f. Across all tested sgRNAs, a maximum of 3%-10% indel formation was conducted with sgRNA-1. One identified factor contributing to the lack of activity of the EE can be attributed to the low efficacy of the sgRNAs. This does not exclude the possibility of additional limiting factors, such as suboptimal architectural design. A distinctive characteristic of Cas12f nucleases is their functionality as asymmetric dimers, comprising a Cas12f1- and Cas12f2 monomer, bound to one sgRNA (Takeda et al., 2021; Xiao et al., 2021). The REC1 domain of Cas12f nucleases is essential for maintaining the dimer interface and is located at the N-terminus of Cas12f proteins, where the DNMT3A/L domain is positioned (Xiao et al., 2021). This fusion may disrupt the dimer interface. Another complication could stem from steric hinderance of the epigenetic domains to each other when positioned at both the N- and C-terminus (Figure 39A). In this scenario, the DNMT3A-DNMT3L complex of monomer Cas12f1 and the KRAB domain of monomer Cas12f2 come into proximity as depicted in Figure 39A, thereby potentially inhibiting their functionality. However, if the absence of silencing was solely due a potential steric hinderance of the epigenetic domains, ApCas12fCRISPRoffCutter would still be expected to generate indels, thus it can be hypothesized that dimer formation is also somewhat disrupted. This incompatibility of the architecture may prevent the epigenetic editing event at the initial stage of DNA binding. Notably, we observed that the single fusion of the KRAB domain at the C-terminus, as represented in constructs EE14 and EE17, did not impede the cutting event of the

CRISPRiCutter. These findings suggest that a less complex architecture may be beneficial for ApCas12f activity compared to a more complex three-epigenetic domain architecture.

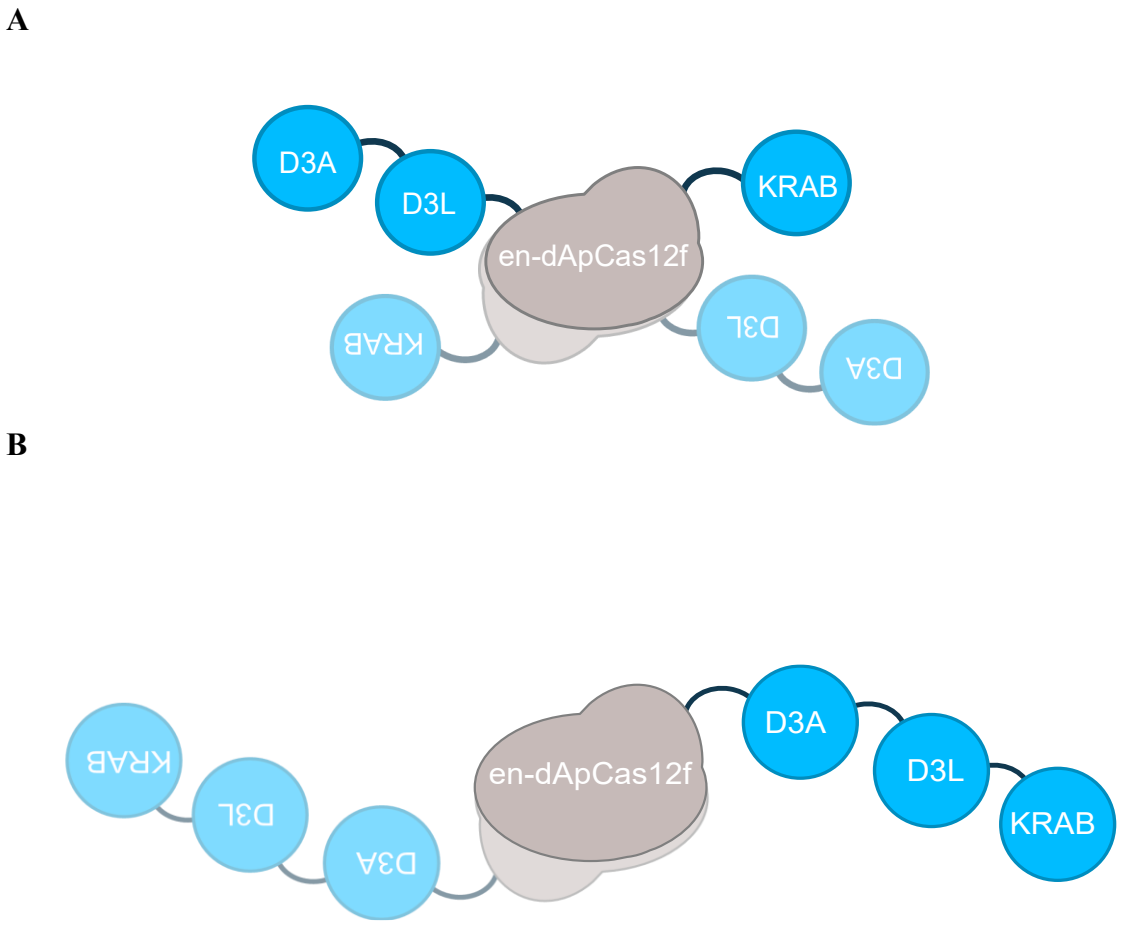

Figure 39: Schematic representation of CRISPRoff and EE1 or EE2 fused with ApCas12f.The diagram illustrates dimer formation of ApCas12f and arrangement of the epigenetic domains in: A) CRISPRoff and B) EE1 and EE2.

We report that the architecture of EE2 was superior for dApCas12f compared to the CRISPRoff architecture which had previously been optimized for SpyCas9. The main difference lies in the N- to C-terminal arrangement of the domains DNMT3A, DNMT3L and KRAB. EE1 and EE2 each feature only one side chain at the C-terminus, allowing all domains to be arranged in series, thereby potentially mitigating a steric hindrance (Figure 39B). Additionally, we added an NLS signal directly at the N-terminus of ApCas12f in EE1 and EE2 instead of only positioning one NLS at the C-terminus. Previous reports have shown that dCasMini fused with VPR mediates higher gene activation with NLS signals at both termini of the nuclease (Xu et al., 2021). In the same study, it was shown that C-terminal fusion of the nuclease with the CRISPRa domains were improved compared to N-terminal fusion. CRISPRi with miniCRa (an engineering variant of Un1Cas12f) was also engineered with NLS on both termini of the nuclease and also C-terminal fusion of the repressor with the nuclease (Wang, et al., 2024). CasMini-BE also only

induced weak editing of 8% in N-terminal fusion of the deaminase domain with the nuclease, however there was no direct comparison to C-terminal fusion therefore is not clear if the low activity stems from the N-terminal fusion or due to other factors such as suboptimal sgRNAs or linkers (Xu et al., 2021). Taken together, these reports on CasMini, miniCRa, and ApCas12f may hint towards a C-terminal preference for the fusion with additional domains of Cas12(f) proteins.

We observed that EE2 induced slightly higher methylation levels than EE1. While this difference may fall within the range of natural variations in methylation, it is noteworthy that EE2 also demonstrated slightly higher efficacy in inducing reporter gene silencing. These two constructs differ in the C-terminal linker connecting ApCas12f to the epigenetic domains. Linker substitution has been previously applied as engineering strategy for CRISPR editors such as base editors and epigenetic editors (Neumann et al., 2024; Nuñez et al., 2021; Tan et al., 2019). Compared to CRISPRoff where the 80 aa long XTEN80 linker connects the nuclease with the methyltransferases, both linkers of EE1 and EE2 are substantially shorter. EE1 harbors the same linker as the CRISPRa construct. This is a 17 aa long linker (aa sequence: SLGSGDGIGSGSNGSSL) rich in serin and glycine, expected to act as a flexible and hydrophilic linker (van Rosmalen et al., 2017). EE2 harbors a 34 aa long linker (aa sequence: AQAERQRILERTNEGRQEAMAKGVVFGRKRKIDR). It is low in serine and glycine and shows a more balanced profile of hydrophobic and hydrophilic aa. The more rigid linker of EE2 may lead to more precise positioning of the domains towards the DNA as previously shown in base editing (Tan et al., 2019). As Cas12f nucleases function as dimers, a rigid linker may positively influence this characteristic. It is important to consider that the C-terminus of DNMT3A forms a complex with the C-terminus of DNMT3L (Siddique et al., 2013) which seems to have been considered in the construction of CRISPRoff and CasPhiCRISPRoff (Liu et al., 2022; Nuñez et al., 2021). Therefore, dimerization was also considered across EE1-EE11. A key difference of EE1 and EE2 to CRISPRoff is that DNMT3A-DNMT3L are incorporated centrally of the construct. Nuñez et al., (2021) hypothesized that DNMT3A-DNMT3L may work best when fused at the N-terminus of SpyCas9 to provide open access to CpG sites for DNA methylation (Zhang et al., 2018). However, the group also showed that the dSpyCas9CRISPRoff still worked as efficiently in other formations. Our data supports the notions that DNMT3A and DNMT3L may dimerize when positioned centrally within the construct.

EE2 with en-dApCas12f demonstrated sustained DNA methylation 17 days p.t.. Silencing was demonstrated at the disease-relevant locus *PCSK9*, which is a target for the treatment of familiar hypercholesterolemia. Current treatment options of familiar hypercholesterolemia, such as statins, monoclonal antibodies and RNA interference (RNAi) necessitate regular redosing (Robinson et al., 2015; Sabatine et al., 2017; Wilkinson et al., 2024). A permanent treatment option involving CRISPR-based adenine base editing (ABE) has been developed, *VERVE-102*, which induces a premature stop codon in the *PCSK9* gene and is currently in clinical trials with promising results (Horie & Ono, 2024). Epigenetic editing of *PCSK9* may further add to the treatment options of familiar hypercholesterolemia with potential safety advantages. Cappelluti et al. (2024) showed that epigenetic editing was as efficient as conventional gene editing, reducing PCSK9 by up to 75% in mice. Additionally, Trembley et al., (2025) recently demonstrated a significant 90% reduction in PCSK9 levels with CRISPRoff in non-human primates. EE2 induced CpG methylation comparable to that mediated with dSpyCas9CRISPRoff. Of note, dSpyCas9CRISPRoff was applied with only two sgRNAs, as described by Trembley et al. (2025) whereas EE2 was combined with six sgRNAs. The use of 6 sgRNAs provided greater promoter coverage which may increase the efficiency of the overall system. It is important to note that the data on dSpyCas9CRISPRoff is still preliminary (n=1) and that further experimental validation is necessary to confirm these initial findings.

Besides overcoming the size limitations of dSpyCas9CRISPRoff, a major advantage of en-dApCas12f-EE2 compared to existing hypercompact systems such as EvoETR, and CHARM lies in its CRISPR-based programmability. Unlike the ZFN-based EE, which require labor-intensive and technically challenging protein engineering for each new target site, en-dApCas12f-EE2 can be redirected to theoretically any genomic locus by altering the short gRNA sequence. This capability simplifies testing multiple target sites, an essential step for effective epigenetic regulation. In addition, CRISPR/Cas ist inherently amenable to multiplexing: a single nuclease can be guided by multiple gRNAs in parallel, which is particularly beneficial for epigenome editing, where simultaneous targeting of several sites within a promoter may be required to achieve robust transcriptional repression. Finally, CRISPR technology in general has become highly accessible compared to ZFN, which remain technically demanding and costly to engineer. The simplicity of sgRNA design lowers the barrier to adoption and enables flexible and efficient implementation in a laboratory setting. In addition to these general advantages of CRISPR/Cas, the choice of ApCas12f as the DNA binding domain provides further benefits for epigenome editing. ApCas12f like other Cas12f nucleases is exceptionally compact, which facilitates vector delivery and broadens its potential

for *in vivo* applications. Moreover, the dimeric nature may improve recruitment of epigenetic effector domains to regulatory regions. Importantly, ApCas12f recognizes a PAM sequence that is rich in cytosines (PAM: 5'-CCN-3'). Other Cas12f nucleases typically have a preference for T-rich PAM profiles such as CasMini 5'-TTTA-3'. Since promoters frequently contain cytosine-rich regions, this PAM preference substantially increases the number of accessible binding sites within promoter contexts. This novel en-dApCas12f-EE2 system thus broadens the available toolkit of hypercompact EEs, providing a compact platform that can be easily directed to different target sequences.

4.3 ApCas12f protein engineering

ApCas12f demonstrated high reporter gene activation without prior engineering, in contrast to other Cas12f nucleases such as Un1Cas12f and AsCas12f, which required modifications to achieve activity in mammalian cells (Kim et al., 2021; Xu et al., 2021). The other tested Cas12f nucleases exhibited only moderate to no reporter gene activation, suggesting either a lack of activity in mammalian cells or an incompatibility with the implemented VPR fusion. The CRISPRa architecture utilized here has been optimized specifically for dCasMini, but not for SpyCas9 or other nucleases (Xu et al., 2021). We noted that ApCas12f mediated a maximum indel frequency of 3%-10% on the *CD81 locus,* across the panel of tested sgRNAs. Ineffectiveness among the panel of 16 tested sgRNAs may suggest reduced activity of the corresponding nuclease. This is particularly relevant given that the *CD81* locus appears to be an accessible target, as demonstrated by SpyCas9, which achieved up to 65% indels. Additionally, we noted that CasMini, which exhibited no activity in mammalian cells as a WT nuclease, induced nearly 400-fold reporter gene activation in our assays, outperforming wild type ApCas12f. Consequently, we decided to perform protein engineering. This lead to the identification of the triple mutant en-ApCas12f and the identification of the single mutants N91Y, M144R, T212K, F256Y and A247T. Interestingly, T212K was identified in both engineering approach consisting of alignment against engineered AsCas12f and MSA. N91Y consists of a substitution from asparagine, a polar, uncharged amino acid into tyrosine, an aromatic, hydrophobic amino acid. This mutation is located within the domain responsible for PAM interaction. Consequently, we speculate that this mutation not only enhances indel activity but also DNA binding, as PAM recognition represents the initial step in CRISPR nuclease-mediated gene editing. T212K, F256Y and A247T are situated within the domains responsible for sgRNA interaction, the R-loop, and the active site, respectively. However, the latter

mutation may not necessarily enhance DNA binding, as it is primarily involved in DNA cleavage activity.

4.4 Assay establishment for epigenetic editing analysis

Plasmids can undergo chromatinization and are capable of recapitulating nuclear genome-encoded chromatin architectures (Mallory et al., 2025). Therefore, we initially aimed to test silencing capabilities on a reporter plasmid harboring *GAPDH-Snrpn*. We detected low silencing by dBreCas12b and dApCas12f at the 96-hour mark, however, no to very low silencing effects were observed at the earlier timepoints. This delayed onset of activity raises the possibility that the observed silencing may represent an artifact rather than a real silencing effect. While silencing for CRISPRoff with dCasMini was absent, it is noteworthy that this and the other systems were only combined with a total of three sgRNAs. The sgRNAs had not been previously validated and did not stem from the literature, therefore there is a chance that the lack of activity does not originate from the system but from ineffective sgRNAs. This highlights the critical role that sgRNA design plays in the success of gene-editing applications.

The silencing of the reporter plasmid harboring *GAPDH-Snrpn* induced by dSpyCas9-only was surprising, as existing literature suggests that this effect is typically limited to prokaryotic systems. According to current understanding, additional functional domains are generally required to mediate effective silencing in mammalian cells (Bendixen et al., 2023; Vercauteren et al., 2024). Due to silencing mediated with dSpyCas9-only, it was unclear if silencing detected for CRISPRoff was due to epigenetic modifications or dSpyCas9-only. Our efforts to compensate this by generating reporter cells lines to monitor silencing over a longer period were not sufficient.

We established an epigenetic editing assay targeting the endogenous *CD81* locus. To determine whether *CD81* silencing resulted from epigenetic modifications, we implemented bisulfite sequencing. We measured the methylation levels of the targets *DYNC2LI1, H2B*, and *LAMP*, and found that the levels of methylation for these targets were consistent with those reported by Nuñez et al. (2021). However, the target *CD81* was suffering from low mapping efficiency of <5%. Notably, Nuñez and colleagues did not couple bisulfite sequencing with NGS, choosing Sanger sequencing instead. Consequently, the low mapping efficiency represents a novel issue that has arisen due to the incorporation of NGS in our analysis.

On the endogenous target *CD81,* we compared silencing of dSpyCas9CRISPRoff with the transient silencing mechanisms of CRISPRi and shRNA. Both methodologies are well-

documented in the literature for their efficacy in targeted gene expression, but only as long as the respective repressor is expressed. We observed a complete recovery of *CD81* expression several days p.t.. Furthermore, the CRISPRi approach did not yield increased methylation levels, indicating that the epigenetic domains associated with CRISPRoff are essential for the introduction of stable CpG methylation modifications. This distinction underscores the unique capabilities of the CRISPRoff system in facilitating enduring epigenetic changes for long-term gene regulation compared to transient regulation by CRISPRi.

Interestingly, despite absence of activity in context of CRISPRi experiments, sgRNA-c mediated high indel rates of 65%. This discrepancy may suggest either a technical artifact or serves as an example that a sgRNA demonstrating strong indel activity does not necessarily translate to effective CRISPRi activity. Many requirements for an effective sgRNA are similar between binding and cutting sgRNAs such as nucleosome positioning which inhibits access to the DNA (Hinz et al., 2015; Horlbeck, Witkowsky, et al., 2016; Isaac et al., 2016). However Horlbeck et al., (2016) described that nucleosome positioning may be particularly important for binding-based applications such as CRISPRi and CRISPRa, as they require sustained binding. This could explain why sgRNA-c may be sufficient to mediate indels but fails to mediate CRISPRi. This is in contrast to our experiments on the target *PCSK9*, as our screen of sgRNAs for indels delivered an efficient sgRNA pool for epigenetic editing at this locus.

The initial discrepancy of silencing of dSpyCas9CRISPRoff compared to reports by Nuñez et al., (2021) raises important questions regarding the variability in gene silencing outcomes across different experimental contexts. This underscores the necessity for further investigation into the underlying mechanisms that govern the efficiency of CRISPRoff-mediated gene regulation and let us to test and implement several assay optimizations. This included an alternative antibody staining protocol, modifications to the CRISPRoff plasmid backbone as well as testing an alternative codon usage of SpyCas9, alternative cell culture media, and the use of a HEK293T cell lines from a different provider. Additionally, we substituted HeLa cells for HEK293T cells. We report two key improvements. Firstly, we noticed that sorting for transfected cells greatly improves durability of gene silencing. Nuñez et al., (2021) described sorting for transfected cells, a step we initially overlooked. It underscores the importance of adhering closely to established protocols. Transfected cells often experience a degree of physiological stress that can confer a growth disadvantage relative to untransfected cells (Antczak et al., 2014; Carreño et al., 2024; Fiszer-Kierzkowska et al., 2011). Consequently, over time, the transfected cells may be diluted out of the sample population, leading to a

diminished representation of these cells in subsequent analyses. Another optimization included the use of a sgRNA pool consisting of 3 sgRNAs (a+b+c) targeting *CD81*, instead of two sgRNA (a+b) was found to be a central improvement in enabling durable silencing (Figure 16). Nuñez et al. (2021) described the use of three sgRNAs (a+b+c). The group reported that sgRNA-c mediates the weakest *CD81* silencing effect when tested individually - only half of the efficiency compared to sgRNA-a and sgRNA-b. After encountering cloning issues, we excluded sgRNA-c at that time. It seems however that sgRNA-c is critical for target *CD81.* sgRNA-c binds further upstream compared to sgRNA-a and b thus increasing the promoter region span (Figure 21). The need for multiple sgRNAs seems to be target dependent as single sgRNA approaches have shown to be sufficient for the silencing of the targets *H2B* with dCasMiniCRISPRi and *Snrpn* with dSpyCas9CRISPRoff (Nuñez et al., 2021; Wang et al., 2024). After the implementation of these assay optimization, we detected silencing levels that were comparable to those reported by Nuñez et al. (2021). Our results indicated 53% silencing, and the group reported 80% silencing 21 days p.t.. While we observed durable *CD81* silencing, NGS analysis revealed that the *CD81* promoter remained intact following CRISPRoff treatment. This further demonstrated that silencing was not a result of promoter destruction but was attributable to the introduction of stable epigenetic modifications.

While the optimizations greatly increased permanent gene silencing compared to the unoptimized experimental set-up, there was still some reactivation of gene expression detectable (Figure 16A and Figure 17A). In evaluating the factors that may induce unintended gene reactivation following CRISPRoff silencing, several considerations arise. During the cell sorting process, BFP-positive cells (indicating transfected cells) were selected. This approach could hypothetically enrich for cells that were transfected but did not achieve successful editing for various reasons. When sorting for BFP-positive cells, the effector could still get lost or degraded during cell division before stable epigenetic changes are fully established. Silencing may be more durable when sorting for *CD81*-negative cells, where the epigenetic silencing has already been conducted. Contrary, in one instance, where this approach was employed, a slight reactivation was still observed (Figure 17A). It is also essential to recognize that even with a cell sorting purity grade of 90%-95%, the sorted cell population still contains unedited cells. Nuñez et al., (2021) indicated that *CD81* does not impact cell proliferation or health, subtle effects may still manifest over extended periods, such as weeks or months. In this context, what is interpreted as reactivation may reflect the overgrowth of untreated cells. The untreated cells could possess a growth advantage, thereby diluting the CRISPRoff-silenced *CD81*-negative population over time. Besides that, the observed reactivation may be specific to the *CD81* locus,

with different dynamics potentially occurring at other loci. It is a known obstacle in the epigenetic editing field that efficacy may vary between loci. Another aspect to consider is that we observed a gradient between the silencing of cells with *CD81*-on or -off (Figure 16B and Figure 17A). The initial silencing strength may determine the overall durability. If the initial silencing induces a fully closed heterochromatin state, the likelihood of reactivation may be lower compared to scenarios where the chromatin remains loosely closed, allowing transcription factors to access the promoter and gradually destabilize the heterochromatin configuration over time. For example, in one of our initial sorting experiments, where a strong selection pressure occurred as most cells underwent cell death, the surviving cells exhibited complete and permanent *CD81* silencing without any reactivation over time (Figure 17 C/D).

Similar reports on varying degrees of epigenetic editing efficiency were reported by other groups. A group has reported half of the efficiency with CRISPRoff silencing of *CD81* 20 days p.t. using a similar experimental setup (Neumann et al., 2024). Whittaker et al., (2023) noted variability in the duration of gene silencing across different cardiovascular targets. Kong et al. (2023) encountered challenges with dSpyCas9CRISPRoff when tested on *Snrpn*. Similar to our findings, the group reported that silencing with dSpyCas9CRISPRoff was transient and returned to 80%-90% of baseline levels around 10 days p.t.. Taken together, these findings illustrate that while epigenetic editing offers several advantages, it remains an emerging technology that requires further research. The complexity of its application to disease targets and the experimental procedures in the laboratory present challenges, particularly in establishing effective assays. Furthermore, when transitioning to new targets, multiple sgRNAs must be identified, contrasting with the single effective sgRNA typically required in conventional gene editing. Additionally, the amplification of promoter regions for NGS analysis is often challenging due to their GC-rich nature.

4.5 Limitations & Outlook

In this section, we will examine the limitations of our study, including the challenges encountered during experimental design and execution that may affect the interpretation and applicability of our findings. Additionally, we will discuss the current limitations EE2 may face until it undergoes further optimization and improvement.

While silencing of dSpyCas9CRISPRoff was maintained over weeks, the initial level of *CD81* silencing did not persist. We noted that some cells reverted to gene activation of the targeted gene, and by 7 weeks p.t., only 40% of the cells remained silenced. Although this level of silencing is still substantial, consistent silencing is desired for therapeutic applications. Durable

silencing has been demonstrated by other studies, indicating that while we have optimized our experimental protocol extensively, there remains further potential for assay optimization.

When assessing the alternative constructs for silencing of *TRE3G* on the reporter plasmid, we observed that the baseline signal from some samples treated with the NT sgRNA control was exceptionally low, thereby constraining the dynamic range. In such a limited dynamic range, it can become challenging to distinguish natural fluctuations from gene editing-induced changes in gene expression. This was especially the case for the reporter plasmid with PAM requirements for SpyCas9. Consequently, the ranking of the 17 alternative EEs should be interpreted with caution, as the ranking may vary in a system with stronger expression of the reporter gene. To address this issue in future studies, it would be beneficial to consider strategies such as stably integrating the reporter gene or enhancing the expression through improved plasmid preparation. Alternatively, the concentration of transfected reporter plasmids could be increased.

Methylation is a strong indicator of durable silencing, as promoter methylation is associated with sustained gene repression. The observed increase in methylation by EE2 over a period of 17 days p.t. corresponds to ~13-23 cell doublings (Tang, 2019), demonstrating the stability of this epigenetic silencing mark. However, while we have tested silencing at the protein level for the surrogate target *TRE3G*, we have yet to evaluate similar silencing effects for the endogenous target *PCSK9*. Moving forward, it would be interesting to conduct an antibody-based quantification of *PCSK9* expression using an enzyme-linked immunosorbent assay (ELISA). Another aspect to clarify is whether the triple mutant en-ApCas12f enhances DNA binding activity or if it solely improves cutting efficiency. Our analysis relied on indel frequency as a surrogate measure for binding affinity. While EE2 incorporating the triple mutant demonstrated high efficacy, a direct comparison to EE2 with WT dApCas12f is currently lacking.

ApCas12f has not yet been tested within an AAV delivery system, and it is important to note that the delivery method can influence the efficiency of an editing system. Currently, EE2 is designed to fit within an AAV vector. The size of EE2 is 3.5 kb, with an additional 0.46 kb required for the U6 promoter-driven sgRNA. It is essential to account for the need to leave space for approximately 0.3 kb of inverted terminal repeat (ITR) sequences of the AAVs. Depending on the promoter, this configuration only allows for the inclusion of a single sgRNA which may reduce the overall efficiency of the system. The number of sgRNAs markedly improved *CD81* silencing efficiency by dSpyCas9CRISPRoff. This trend may similarly apply to EE2. Silencing of *PCSK9* was tested using EE2 in combination with a pool of six sgRNAs.

While the use of six sgRNAs is feasible for research purposes, it is not ideal for therapeutic applications due to the requirement for comprehensive off-target analysis for each sgRNA. In a therapeutic context, the treatment of familial hypercholesterolemia is unlikely to involve such a large number of sgRNAs. The payload for an AAV would be exceeded, and in other delivery systems, such as lipid nanoparticles (LNPs), incorporating six different RNA molecules would complicate production compared to using 1-2 sgRNAs**.**

To address the limitations, we propose the following next steps. It is critical to assess the durability of *PCSK9* promoter methylation by longer readout periods. en-ApCas12f should be assessed for off-target editing, as the increase in on-target editing raises the possibility of concurrent off-target effects. However, Mlambo et al., (2018) speculated that off-target editing may be less problematic in epigenetic editing compared to conventional gene editing. This is because epigenetic modifications may not induce functional outcomes when directed towards non-coding regions or gene bodies that are already in a methylated state. Additionally, the likelihood of targeting cis-regulatory regions is comparatively lower, as these regions constitute a smaller fraction of the overall genome. Besides off-target analysis, a comprehensive assessment of the safety and tolerability of en-ApCas12f-EE2 is necessary. Recent reports have highlighted the potential toxicity associated with the DNMT3A domain (Neumann et al., 2024). Notably, recent studies, including those by Neumann et al., (2024) and Nakamura et al., (2021), have demonstrated that the DNMT3A domain can be omitted without compromising functionality. This modification could further reduce the size of our system, enhancing its suitability for AAV delivery.

In conclusion, our findings highlight the potential of engineered EEs as a transformative approach for gene regulation and therapeutic interventions. Of note, the first-in-human study of *EPI-321*, an EE therapy targeting facioscapulohumeral muscular dystrophy (FSHD), commenced in 2025 and has recently dosed its first patient (ClinicalTrials.gov ID: NCT06907875), marking a significant milestone in the field. While challenges in optimizing the efficacy of epigenetic editing and fully understanding the underlying mechanisms persist, the encouraging results from our research lay a robust foundation for future investigations. The prospect of developing safe and effective treatments for genetic diseases highlights the critical importance of ongoing investigations in this dynamic area of research.

5. References

Bayer Ag, "Novel Small Type V RNA Programmable Endonuclease Systems," WO 2023/237587 A1, filed June 7, 2023, published December 14, 2023

Bayer Aktiengesellschaft, "Type V RNA Programmable Endonuclease Systems," WO2022258753A1, filed June 9, 2022, published December 15, 2022

Epicrispr Biotechnologies, Inc. (2025). *A first-in-human study of EPI-321 in facioscapulohumeral muscular dystrophy (FSHD)* (ClinicalTrials.gov ID: NCT06907875). ClinicalTrials.gov. https://clinicaltrials.gov/show/NCT06907875

Adikusuma, F., Piltz, S., Corbett, M. A., Turvey, M., McColl, S. R., Helbig, K. J., Beard, M. R., Hughes, J., Pomerantz, R. T., & Thomas, P. Q. (2018). Large deletions induced by Cas9 cleavage. *Nature*, *560*(7717), E8–E9. https://doi.org/10.1038/s41586-018-0380-z

Allis, C. D., & Jenuwein, T. (2016). The molecular hallmarks of epigenetic control. *Nature Reviews. Genetics*, *17*(8), 487–500. https://doi.org/10.1038/nrg.2016.59

Altucci, L., & Rots, M. G. (2016). Epigenetic drugs: From chemistry via biology to medicine and back. *Clinical Epigenetics*, *8*, 56. https://doi.org/10.1186/s13148-016-0222-5

Amabile, A., Migliara, A., Capasso, P., Biffi, M., Cittaro, D., Naldini, L., & Lombardo, A. (2016). Inheritable Silencing of Endogenous Genes by Hit-and-Run Targeted Epigenetic Editing. *Cell*, *167*(1), 219-232.e14. https://doi.org/10.1016/j.cell.2016.09.006

Amoasii, L., Long, C., Li, H., Mireault, A. A., Shelton, J. M., Sanchez-Ortiz, E., McAnally, J. R., Bhattacharyya, S., Schmidt, F., Grimm, D., Hauschka, S. D., Bassel-Duby, R., & Olson, E. N. (2017). Single-cut genome editing restores dystrophin expression in a new mouse model of muscular dystrophy. *Science Translational Medicine*, *9*(418), eaan8081. https://doi.org/10.1126/scitranslmed.aan8081

Anzalone, A. V., Randolph, P. B., Davis, J. R., Sousa, A. A., Koblan, L. W., Levy, J. M., Chen, P. J., Wilson, C., Newby, G. A., Raguram, A., & Liu, D. R. (2019). Search-and-replace genome editing without double-strand breaks or donor DNA. *Nature*, *576*(7785), 149–157. https://doi.org/10.1038/s41586-019-1711-4

Aronesty, E. (2013). Comparison of Sequencing Utility Programs. *The Open Bioinformatics Journal*, *7*(1). https://doi.org/10.2174/1875036201307010001

Barrangou, R., Fremaux, C., Deveau, H., Richards, M., Boyaval, P., Moineau, S., Romero, D. A., & Horvath, P. (2007). CRISPR provides acquired resistance against viruses in prokaryotes. *Science (New York, N.Y.)*, *315*(5819), 1709–1712. https://doi.org/10.1126/science.1138140

Barrangou, R., & Marraffini, L. A. (2014). CRISPR-Cas systems: Prokaryotes upgrade to adaptive immunity. *Molecular Cell*, *54*(2), 234–244. https://doi.org/10.1016/j.molcel.2014.03.011

Barski, A., Cuddapah, S., Cui, K., Roh, T.-Y., Schones, D. E., Wang, Z., Wei, G., Chepelev, I., & Zhao, K. (2007). High-resolution profiling of histone methylations in the human genome. *Cell*, *129*(4), 823–837. https://doi.org/10.1016/j.cell.2007.05.009

Bendixen, L., Jensen, T. I., & Bak, R. O. (2023). CRISPR-Cas-mediated transcriptional modulation: The therapeutic promises of CRISPRa and CRISPRi. *Molecular Therapy*, *31*(7), 1920–1937. https://doi.org/10.1016/j.ymthe.2023.03.024

Bétermier, M., Bertrand, P., & Lopez, B. S. (2014). Is non-homologous end-joining really an inherently error-prone process? *PLoS Genetics*, *10*(1), e1004086. https://doi.org/10.1371/journal.pgen.1004086

Bhat, K. P., Ümit Kaniskan, H., Jin, J., & Gozani, O. (2021). Epigenetics and beyond: Targeting writers of protein lysine methylation to treat disease. *Nature Reviews. Drug Discovery*, *20*(4), 265–286. https://doi.org/10.1038/s41573-020-00108-x

Bintu, L., Yong, J., Antebi, Y. E., McCue, K., Kazuki, Y., Uno, N., Oshimura, M., & Elowitz, M. B. (2016). Dynamics of epigenetic regulation at the single-cell level. *Science (New York, N.Y.)*, *351*(6274), 720–724. https://doi.org/10.1126/science.aab2956

Bolotin, A., Quinquis, B., Sorokin, A., & Ehrlich, S. D. (2005). Clustered regularly interspaced short palindrome repeats (CRISPRs) have spacers of extrachromosomal origin. *Microbiology (Reading, England)*, *151*(Pt 8), 2551–2561. https://doi.org/10.1099/mic.0.28048-0

Breunig, C. T., Köferle, A., Neuner, A. M., Wiesbeck, M. F., Baumann, V., & Stricker, S. H. (2021). CRISPR Tools for Physiology and Cell State Changes: Potential of Transcriptional Engineering and Epigenome Editing. *Physiological Reviews*, *101*(1), 177–211. https://doi.org/10.1152/physrev.00034.2019

Brouns, S. J. J., Jore, M. M., Lundgren, M., Westra, E. R., Slijkhuis, R. J. H., Snijders, A. P. L., Dickman, M. J., Makarova, K. S., Koonin, E. V., & van der Oost, J. (2008). Small CRISPR RNAs guide antiviral defense in prokaryotes. *Science (New York, N.Y.)*, *321*(5891), 960–964. https://doi.org/10.1126/science.1159689

Canver, M. C., Smith, E. C., Sher, F., Pinello, L., Sanjana, N. E., Shalem, O., Chen, D. D., Schupp, P. G., Vinjamur, D. S., Garcia, S. P., Luc, S., Kurita, R., Nakamura, Y., Fujiwara, Y., Maeda, T., Yuan, G.-C., Zhang, F., Orkin, S. H., & Bauer, D. E. (2015). BCL11A enhancer dissection by Cas9-mediated in situ saturating mutagenesis. *Nature*, *527*(7577), 192–197. https://doi.org/10.1038/nature15521

Cappelluti, M. A., Mollica Poeta, V., Valsoni, S., Quarato, P., Merlin, S., Merelli, I., & Lombardo, A. (2024). Durable and efficient gene silencing in vivo by hit-and-run epigenome editing. *Nature*, 1–8. https://doi.org/10.1038/s41586-024-07087-8

Chavez, A., Scheiman, J., Vora, S., Pruitt, B. W., Tuttle, M., P R Iyer, E., Lin, S., Kiani, S., Guzman, C. D., Wiegand, D. J., Ter-Ovanesyan, D., Braff, J. L., Davidsohn, N., Housden, B. E., Perrimon, N., Weiss, R., Aach, J., Collins, J. J., & Church, G. M. (2015). Highly efficient Cas9-mediated transcriptional programming. *Nature Methods*, *12*(4), 326–328. https://doi.org/10.1038/nmeth.3312

Chen, S., Zhou, Y., Chen, Y., & Gu, J. (2018). fastp: An ultra-fast all-in-one FASTQ preprocessor. *Bioinformatics (Oxford, England)*, *34*(17), i884–i890. https://doi.org/10.1093/bioinformatics/bty560

Cho, S. W., Kim, S., Kim, J. M., & Kim, J.-S. (2013). Targeted genome engineering in human cells with the Cas9 RNA-guided endonuclease. *Nature Biotechnology*, *31*(3), Article 3. https://doi.org/10.1038/nbt.2507

Cong, L., Ran, F. A., Cox, D., Lin, S., Barretto, R., Habib, N., Hsu, P. D., Wu, X., Jiang, W., Marraffini, L. A., & Zhang, F. (2013). Multiplex Genome Engineering Using CRISPR/Cas Systems. *Science (New York, N.Y.)*, *339*(6121), Article 6121. https://doi.org/10.1126/science.1231143

Deltcheva, E., Chylinski, K., Sharma, C. M., Gonzales, K., Chao, Y., Pirzada, Z. A., Eckert, M. R., Vogel, J., & Charpentier, E. (2011). CRISPR RNA maturation by trans-encoded small RNA and host factor RNase III. *Nature*, *471*(7340), Article 7340. https://doi.org/10.1038/nature09886

Deveau, H., Barrangou, R., Garneau, J. E., Labonté, J., Fremaux, C., Boyaval, P., Romero, D. A., Horvath, P., & Moineau, S. (2008). Phage response to CRISPR-encoded resistance in Streptococcus thermophilus. *Journal of Bacteriology*, *190*(4), 1390–1400. https://doi.org/10.1128/JB.01412-07

Doudna, J. A. (2020). The promise and challenge of therapeutic genome editing. *Nature*, *578*(7794), 229–236. https://doi.org/10.1038/s41586-020-1978-5

Doudna, J. A., & Charpentier, E. (2014). Genome editing. The new frontier of genome engineering with CRISPR-Cas9. *Science (New York, N.Y.)*, *346*(6213), 1258096. https://doi.org/10.1126/science.1258096

Du, J., Johnson, L. M., Jacobsen, S. E., & Patel, D. J. (2015). DNA methylation pathways and their crosstalk with histone methylation. *Nature Reviews. Molecular Cell Biology*, *16*(9), 519–532. https://doi.org/10.1038/nrm4043

Eden, S., & Cedar, H. (1994). Role of DNA methylation in the regulation of transcription. *Current Opinion in Genetics & Development*, *4*(2), 255–259. https://doi.org/10.1016/s0959-437x(05)80052-8

Edwards, J. R., Yarychkivska, O., Boulard, M., & Bestor, T. H. (2017). DNA methylation and DNA methyltransferases. *Epigenetics & Chromatin*, *10*(1), 23. https://doi.org/10.1186/s13072-017-0130-8

England, C. G., Ehlerding, E. B., & Cai, W. (2016). NanoLuc: A Small Luciferase is Brightening up the Field of Bioluminescence. *Bioconjugate Chemistry*, *27*(5), 1175–1187. https://doi.org/10.1021/acs.bioconjchem.6b00112

Engler, C., & Marillonnet, S. (2014). Golden Gate cloning. *Methods in Molecular Biology (Clifton, N.J.)*, *1116*, 119–131. https://doi.org/10.1007/978-1-62703-764-8_9

Fiumara, M., Ferrari, S., Omer-Javed, A., Beretta, S., Albano, L., Canarutto, D., Varesi, A., Gaddoni, C., Brombin, C., Cugnata, F., Zonari, E., Naldini, M. M., Barcella, M., Gentner, B., Merelli, I., & Naldini, L. (2024). Genotoxic effects of base and prime editing in human hematopoietic stem cells. *Nature Biotechnology*, *42*(6), 877–891. https://doi.org/10.1038/s41587-023-01915-4

Friskes, A., Koob, L., Krenning, L., Severson, T. M., Koeleman, E. S., Vergara, X., Schubert, M., van den Berg, J., Evers, B., Manjón, A. G., Joosten, S., Kim, Y., Zwart, W., & Medema, R. H. (2022). Double-strand break toxicity is chromatin context independent. *Nucleic Acids Research*, *50*(17), 9930–9947. https://doi.org/10.1093/nar/gkac758

Galonska, C., Charlton, J., Mattei, A. L., Donaghey, J., Clement, K., Gu, H., Mohammad, A. W., Stamenova, E. K., Cacchiarelli, D., Klages, S., Timmermann, B., Cantz, T., Schöler, H. R., Gnirke, A., Ziller, M. J., & Meissner, A. (2018). Genome-wide tracking of dCas9-methyltransferase footprints. *Nature Communications*, *9*(1), 597. https://doi.org/10.1038/s41467-017-02708-5

Garneau, J. E., Dupuis, M.-È., Villion, M., Romero, D. A., Barrangou, R., Boyaval, P., Fremaux, C., Horvath, P., Magadán, A. H., & Moineau, S. (2010). The CRISPR/Cas bacterial immune system cleaves bacteriophage and plasmid DNA. *Nature*, *468*(7320), Article 7320. https://doi.org/10.1038/nature09523

Gasiunas, G., Barrangou, R., Horvath, P., & Siksnys, V. (2012). Cas9-crRNA ribonucleoprotein complex mediates specific DNA cleavage for adaptive immunity in bacteria. *Proceedings of the National Academy of Sciences of the United States of America*, *109*(39), E2579-2586. https://doi.org/10.1073/pnas.1208507109

Gaudelli, N. M., Komor, A. C., Rees, H. A., Packer, M. S., Badran, A. H., Bryson, D. I., & Liu, D. R. (2017). Programmable base editing of A•T to G•C in genomic DNA without DNA cleavage. *Nature*, *551*(7681), Article 7681. https://doi.org/10.1038/nature24644

Gillmore, J. D., Gane, E., Taubel, J., Kao, J., Fontana, M., Maitland, M. L., Seitzer, J., O'Connell, D., Walsh, K. R., Wood, K., Phillips, J., Xu, Y., Amaral, A., Boyd, A. P., Cehelsky, J. E., McKee, M. D., Schiermeier, A., Harari, O., Murphy, A., … Lebwohl, D. (2021). CRISPR-Cas9 In Vivo Gene Editing for Transthyretin Amyloidosis. *The New England Journal of Medicine*. https://doi.org/10.1056/NEJMoa2107454

Gleditzsch, D., Pausch, P., Müller-Esparza, H., Özcan, A., Guo, X., Bange, G., & Randau, L. (2019). PAM identification by CRISPR-Cas effector complexes: Diversified mechanisms and structures. *RNA Biology*, *16*(4), 504–517. https://doi.org/10.1080/15476286.2018.1504546

Goll, M. G., & Bestor, T. H. (2005). Eukaryotic cytosine methyltransferases. *Annual Review of Biochemistry*, *74*, 481–514. https://doi.org/10.1146/annurev.biochem.74.010904.153721

Guo, X., Wang, L., Li, J., Ding, Z., Xiao, J., Yin, X., He, S., Shi, P., Dong, L., Li, G., Tian, C., Wang, J., Cong, Y., & Xu, Y. (2015). Structural insight into autoinhibition and histone H3-induced activation of DNMT3A. *Nature*, *517*(7536), 640–644. https://doi.org/10.1038/nature13899

Haapaniemi, E., Botla, S., Persson, J., Schmierer, B., & Taipale, J. (2018). CRISPR-Cas9 genome editing induces a p53-mediated DNA damage response. *Nature Medicine*, *24*(7), 927–930. https://doi.org/10.1038/s41591-018-0049-z

Han, H., Yang, Y., Jiao, Y., Qi, H., Han, Z., Wang, L., Dong, L., Tian, J., Vanhaesebroeck, B., Li, X., Liu, J., Ma, G., & Lei, H. (2023). Leverage of nuclease-deficient CasX for preventing pathological angiogenesis. *Molecular Therapy. Nucleic Acids*, *33*, 738–748. https://doi.org/10.1016/j.omtn.2023.08.001

Harrington, L. B., Burstein, D., Chen, J. S., Paez-Espino, D., Ma, E., Witte, I. P., Cofsky, J. C., Kyrpides, N. C., Banfield, J. F., & Doudna, J. A. (2018). Programmed DNA destruction by miniature CRISPR-Cas14 enzymes. *Science (New York, N.Y.)*, *362*(6416), 839–842. https://doi.org/10.1126/science.aav4294

Hinz, J. M., Laughery, M. F., & Wyrick, J. J. (2015). Nucleosomes Inhibit Cas9 Endonuclease Activity in Vitro. *Biochemistry*, *54*(48), 7063–7066. https://doi.org/10.1021/acs.biochem.5b01108

Horie, T., & Ono, K. (2024). VERVE-101: A promising CRISPR-based gene editing therapy that reduces LDL-C and PCSK9 levels in HeFH patients. *European Heart Journal. Cardiovascular Pharmacotherapy*, *10*(2), 89–90. https://doi.org/10.1093/ehjcvp/pvad103

Horlbeck, M. A., Gilbert, L. A., Villalta, J. E., Adamson, B., Pak, R. A., Chen, Y., Fields, A. P., Park, C. Y., Corn, J. E., Kampmann, M., & Weissman, J. S. (2016). Compact and highly active next-generation libraries for CRISPR-mediated gene repression and activation. *eLife*, *5*, e19760. https://doi.org/10.7554/eLife.19760

Horlbeck, M. A., Witkowsky, L. B., Guglielmi, B., Replogle, J. M., Gilbert, L. A., Villalta, J. E., Torigoe, S. E., Tjian, R., & Weissman, J. S. (2016). Nucleosomes impede Cas9 access to DNA in vivo and in vitro. *eLife*, *5*, e12677. https://doi.org/10.7554/eLife.12677

Horvath, P., Romero, D. A., Coûté-Monvoisin, A.-C., Richards, M., Deveau, H., Moineau, S., Boyaval, P., Fremaux, C., & Barrangou, R. (2008). Diversity, activity, and evolution of CRISPR loci in Streptococcus thermophilus. *Journal of Bacteriology*, *190*(4), 1401–1412. https://doi.org/10.1128/JB.01415-07

Hotchkiss, R. D. (1948). The quantitative separation of purines, pyrimidines, and nucleosides by paper chromatography. *The Journal of Biological Chemistry*, *175*(1), 315–332.

Hu, J. H., Davis, K. M., & Liu, D. R. (2016). Chemical Biology Approaches to Genome Editing: Understanding, Controlling, and Delivering Programmable Nucleases. *Cell Chemical Biology*, *23*(1), 57–73. https://doi.org/10.1016/j.chembiol.2015.12.009

Huang, Y.-H., Su, J., Lei, Y., Brunetti, L., Gundry, M. C., Zhang, X., Jeong, M., Li, W., & Goodell, M. A. (2017). DNA epigenome editing using CRISPR-Cas SunTag-directed DNMT3A. *Genome Biology*, *18*(1), 176. https://doi.org/10.1186/s13059-017-1306-z

Hustedt, N., & Durocher, D. (2016). The control of DNA repair by the cell cycle. *Nature Cell Biology*, *19*(1), 1–9. https://doi.org/10.1038/ncb3452

Hwang, W. Y., Fu, Y., Reyon, D., Maeder, M. L., Tsai, S. Q., Sander, J. D., Peterson, R. T., Yeh, J.-R. J., & Joung, J. K. (2013). Efficient genome editing in zebrafish using a CRISPR-Cas system. *Nature Biotechnology*, *31*(3), Article 3. https://doi.org/10.1038/nbt.2501

Isaac, R. S., Jiang, F., Doudna, J. A., Lim, W. A., Narlikar, G. J., & Almeida, R. (2016). Nucleosome breathing and remodeling constrain CRISPR-Cas9 function. *eLife*, *5*, e13450. https://doi.org/10.7554/eLife.13450

Jinek, M., Chylinski, K., Fonfara, I., Hauer, M., Doudna, J. A., & Charpentier, E. (2012a). A programmable dual-RNA-guided DNA endonuclease in adaptive bacterial immunity. *Science (New York, N.Y.)*, *337*(6096), 816–821. https://doi.org/10.1126/science.1225829

Jinek, M., Chylinski, K., Fonfara, I., Hauer, M., Doudna, J. A., & Charpentier, E. (2012b). A programmable dual-RNA-guided DNA endonuclease in adaptive bacterial immunity. *Science (New York, N.Y.)*, *337*(6096), Article 6096. https://doi.org/10.1126/science.1225829

Jinek, M., East, A., Cheng, A., Lin, S., Ma, E., & Doudna, J. (2013). RNA-programmed genome editing in human cells. *eLife*, *2*, e00471. https://doi.org/10.7554/eLife.00471

Kannan, S., Altae-Tran, H., Zhu, S., Xu, P., Strebinger, D., Oshiro, R., Faure, G., Moeller, L., Pham, J., Mears, K. S., Ni, H. M., Macrae, R. K., & Zhang, F. (2025). Evolution-guided protein design of IscB for persistent epigenome editing in vivo. *Nature Biotechnology*. https://doi.org/10.1038/s41587-025-02655-3

Karvelis, T., Bigelyte, G., Young, J. K., Hou, Z., Zedaveinyte, R., Budre, K., Paulraj, S., Djukanovic, V., Gasior, S., Silanskas, A., Venclovas, Č., & Siksnys, V. (2020). PAM recognition by miniature CRISPR-Cas12f nucleases triggers programmable double-stranded DNA target cleavage. *Nucleic Acids Research*, *48*(9), 5016–5023. https://doi.org/10.1093/nar/gkaa208

Kim, D. Y., Lee, J. M., Moon, S. B., Chin, H. J., Park, S., Lim, Y., Kim, D., Koo, T., Ko, J.-H., & Kim, Y.-S. (2021). Efficient CRISPR editing with a hypercompact Cas12f1 and engineered guide RNAs delivered by adeno-associated virus. *Nature Biotechnology*. https://doi.org/10.1038/s41587-021-01009-z

Klompe, S. E., Vo, P. L. H., Halpin-Healy, T. S., & Sternberg, S. H. (2019). Transposon-encoded CRISPR-Cas systems direct RNA-guided DNA integration. *Nature*, *571*(7764), Article 7764. https://doi.org/10.1038/s41586-019-1323-z

Koch, C. M., Andrews, R. M., Flicek, P., Dillon, S. C., Karaöz, U., Clelland, G. K., Wilcox, S., Beare, D. M., Fowler, J. C., Couttet, P., James, K. D., Lefebvre, G. C., Bruce, A. W., Dovey, O. M., Ellis, P. D., Dhami, P., Langford, C. F., Weng, Z., Birney, E., … Dunham, I. (2007). The landscape of histone modifications across 1% of the human genome in five human cell lines. *Genome Research*, *17*(6), 691–707. https://doi.org/10.1101/gr.5704207

Komor, A. C., Kim, Y. B., Packer, M. S., Zuris, J. A., & Liu, D. R. (2016). Programmable editing of a target base in genomic DNA without double-stranded DNA cleavage. *Nature*, *533*(7603), 420–424. https://doi.org/10.1038/nature17946

Kong, X., Zhang, H., Li, G., Wang, Z., Kong, X., Wang, L., Xue, M., Zhang, W., Wang, Y., Lin, J., Zhou, J., Shen, X., Wei, Y., Zhong, N., Bai, W., Yuan, Y., Shi, L., Zhou, Y., & Yang, H. (2023). Engineered CRISPR-OsCas12f1 and RhCas12f1 with robust activities and expanded target range for genome editing. *Nature Communications*, *14*, 2046. https://doi.org/10.1038/s41467-023-37829-7

Koonin, E. V., Makarova, K. S., & Zhang, F. (2017). Diversity, classification and evolution of CRISPR-Cas systems. *Current Opinion in Microbiology*, *37*, 67–78. https://doi.org/10.1016/j.mib.2017.05.008

Kosicki, M., Tomberg, K., & Bradley, A. (2018). Repair of double-strand breaks induced by CRISPR-Cas9 leads to large deletions and complex rearrangements. *Nature Biotechnology*, *36*(8), Article 8. https://doi.org/10.1038/nbt.4192

Kovalev, M. A., Mamaeva, N. Yu., Kristovskiy, N. V., Feskin, P. G., Vinnikov, R. S., Oleinikov, P. D., Sosnovtseva, A. O., Yakovlev, V. A., Glukhov, G. S., & Shaytan, A.

K. (2025). Epigenome Engineering Using dCas Systems for Biomedical Applications and Biotechnology: Current Achievements, Opportunities and Challenges. *International Journal of Molecular Sciences*, *26*(13), 6371. https://doi.org/10.3390/ijms26136371

Krenning, L., van den Berg, J., & Medema, R. H. (2019). Life or Death after a Break: What Determines the Choice? *Molecular Cell*, *76*(2), 346–358. https://doi.org/10.1016/j.molcel.2019.08.023

Krueger, F., & Andrews, S. R. (2011). Bismark: A flexible aligner and methylation caller for Bisulfite-Seq applications. *Bioinformatics (Oxford, England)*, *27*(11), 1571–1572. https://doi.org/10.1093/bioinformatics/btr167

La Russa, M. F., & Qi, L. S. (2015). The New State of the Art: Cas9 for Gene Activation and Repression. *Molecular and Cellular Biology*, *35*(22), 3800–3809. https://doi.org/10.1128/MCB.00512-15

Lampe, G. D., King, R. T., Halpin-Healy, T. S., Klompe, S. E., Hogan, M. I., Vo, P. L. H., Tang, S., Chavez, A., & Sternberg, S. H. (2024). Targeted DNA integration in human cells without double-strand breaks using CRISPR-associated transposases. *Nature Biotechnology*, *42*(1), 87–98. https://doi.org/10.1038/s41587-023-01748-1

Lee, Y.-H., Ren, D., Jeon, B., & Liu, H. (2023). S-Adenosylmethionine: More than just a methyl donor. *Natural Product Reports*, *40*(9), 1521–1549. https://doi.org/10.1039/d2np00086e

Lei, Y., Zhang, X., Su, J., Jeong, M., Gundry, M. C., Huang, Y.-H., Zhou, Y., Li, W., & Goodell, M. A. (2017). Targeted DNA methylation in vivo using an engineered dCas9-MQ1 fusion protein. *Nature Communications*, *8*, 16026. https://doi.org/10.1038/ncomms16026

Leibowitz, M. L., Papathanasiou, S., Doerfler, P. A., Blaine, L. J., Sun, L., Yao, Y., Zhang, C.-Z., Weiss, M. J., & Pellman, D. (2021). Chromothripsis as an on-target consequence of CRISPR-Cas9 genome editing. *Nature Genetics*, *53*(6), 895–905. https://doi.org/10.1038/s41588-021-00838-7

Lewis, J. D., Meehan, R. R., Henzel, W. J., Maurer-Fogy, I., Jeppesen, P., Klein, F., & Bird, A. (1992). Purification, sequence, and cellular localization of a novel chromosomal protein that binds to methylated DNA. *Cell*, *69*(6), 905–914. https://doi.org/10.1016/0092-8674(92)90610-o

Li, Bestor, T. H., & Jaenisch, R. (1992). Targeted mutation of the DNA methyltransferase gene results in embryonic lethality. *Cell*, *69*(6), 915–926. https://doi.org/10.1016/0092-8674(92)90611-f

Li, & Dahiya, R. (2002). MethPrimer: Designing primers for methylation PCRs. *Bioinformatics (Oxford, England)*, *18*(11), 1427–1431. https://doi.org/10.1093/bioinformatics/18.11.1427

Li, Y., & Tollefsbol, T. O. (2011). DNA methylation detection: Bisulfite genomic sequencing analysis. *Methods in Molecular Biology (Clifton, N.J.)*, *791*, 11–21. https://doi.org/10.1007/978-1-61779-316-5_2

Liao, Q., Yang, J., Ge, S., Chai, P., Fan, J., & Jia, R. (2023). Novel insights into histone lysine methyltransferases in cancer therapy: From epigenetic regulation to selective drugs. *Journal of Pharmaceutical Analysis*, *13*(2), 127–141. https://doi.org/10.1016/j.jpha.2022.11.009

Lieber, M. R. (2010). The mechanism of double-strand DNA break repair by the nonhomologous DNA end-joining pathway. *Annual Review of Biochemistry*, *79*, 181–211. https://doi.org/10.1146/annurev.biochem.052308.093131

Lister, R., Pelizzola, M., Dowen, R. H., Hawkins, R. D., Hon, G., Tonti-Filippini, J., Nery, J. R., Lee, L., Ye, Z., Ngo, Q.-M., Edsall, L., Antosiewicz-Bourget, J., Stewart, R., Ruotti, V., Millar, A. H., Thomson, J. A., Ren, B., & Ecker, J. R. (2009). Human DNA

methylomes at base resolution show widespread epigenomic differences. *Nature*, *462*(7271), 315–322. https://doi.org/10.1038/nature08514

Liu, Sretenovic, S., Fan, T., Cheng, Y., Li, G., Qi, A., Tang, X., Xu, Y., Guo, W., Zhong, Z., He, Y., Liang, Y., Han, Q., Zheng, X., Gu, X., Qi, Y., & Zhang, Y. (2022). Hypercompact CRISPR-Cas12j2 (CasΦ) enables genome editing, gene activation, and epigenome editing in plants. *Plant Communications*, *3*(6), 100453. https://doi.org/10.1016/j.xplc.2022.100453

Liu, W., Wu, G., Xiong, F., & Chen, Y. (2021). Advances in the DNA methylation hydroxylase TET1. *Biomarker Research*, *9*(1), 76. https://doi.org/10.1186/s40364-021-00331-7

Liu, Wu, H., Ji, X., Stelzer, Y., Wu, X., Czauderna, S., Shu, J., Dadon, D., Young, R. A., & Jaenisch, R. (2016). Editing DNA Methylation in the Mammalian Genome. *Cell*, *167*(1), 233-247.e17. https://doi.org/10.1016/j.cell.2016.08.056

Liu, Zhang, W., Xin, C., Yin, J., Shang, Y., Ai, C., Li, J., Meng, F.-L., & Hu, J. (2021). Global detection of DNA repair outcomes induced by CRISPR-Cas9. *Nucleic Acids Research*, *49*(15), 8732–8742. https://doi.org/10.1093/nar/gkab686

Madigan, V., Zhang, F., & Dahlman, J. E. (2023). Drug delivery systems for CRISPR-based genome editors. *Nature Reviews. Drug Discovery*, *22*(11), 875–894. https://doi.org/10.1038/s41573-023-00762-x

Makarova, K. S., Grishin, N. V., Shabalina, S. A., Wolf, Y. I., & Koonin, E. V. (2006). A putative RNA-interference-based immune system in prokaryotes: Computational analysis of the predicted enzymatic machinery, functional analogies with eukaryotic RNAi, and hypothetical mechanisms of action. *Biology Direct*, *1*, 7. https://doi.org/10.1186/1745-6150-1-7

Makarova, K. S., & Koonin, E. V. (2015). Annotation and Classification of CRISPR-Cas Systems. *Methods in Molecular Biology (Clifton, N.J.)*, *1311*, 47–75. https://doi.org/10.1007/978-1-4939-2687-9_4

Makarova, K. S., Wolf, Y. I., Iranzo, J., Shmakov, S. A., Alkhnbashi, O. S., Brouns, S. J. J., Charpentier, E., Cheng, D., Haft, D. H., Horvath, P., Moineau, S., Mojica, F. J. M., Scott, D., Shah, S. A., Siksnys, V., Terns, M. P., Venclovas, Č., White, M. F., Yakunin, A. F., … Koonin, E. V. (2020). Evolutionary classification of CRISPR-Cas systems: A burst of class 2 and derived variants. *Nature Reviews. Microbiology*, *18*(2), 67–83. https://doi.org/10.1038/s41579-019-0299-x

Makarova, K. S., Wolf, Y. I., & Koonin, E. V. (2013). The basic building blocks and evolution of CRISPR-CAS systems. *Biochemical Society Transactions*, *41*(6), 1392–1400. https://doi.org/10.1042/BST20130038

Mali, P., Yang, L., Esvelt, K. M., Aach, J., Guell, M., DiCarlo, J. E., Norville, J. E., & Church, G. M. (2013). RNA-guided human genome engineering via Cas9. *Science (New York, N.Y.)*, *339*(6121), Article 6121. https://doi.org/10.1126/science.1232033

Mallory, B. J., Tullius, T. W., Biar, C. G., Gustafson, J. A., Bohaczuk, S. C., Dubocanin, D., Starita, L. M., & Stergachis, A. B. (2025). *Principles and functional consequences of plasmid chromatinization in mammalian cells* (p. 2025.05.27.656122). bioRxiv. https://doi.org/10.1101/2025.05.27.656122

Marraffini, L. A., & Sontheimer, E. J. (2008). CRISPR interference limits horizontal gene transfer in staphylococci by targeting DNA. *Science (New York, N.Y.)*, *322*(5909), 1843–1845. https://doi.org/10.1126/science.1165771

McDonald, J. I., Celik, H., Rois, L. E., Fishberger, G., Fowler, T., Rees, R., Kramer, A., Martens, A., Edwards, J. R., & Challen, G. A. (2016). Reprogrammable CRISPR/Cas9-based system for inducing site-specific DNA methylation. *Biology Open*, *5*(6), 866–874. https://doi.org/10.1242/bio.019067

Mlambo, T., Nitsch, S., Hildenbeutel, M., Romito, M., Müller, M., Bossen, C., Diederichs, S., Cornu, T. I., Cathomen, T., & Mussolino, C. (2018). Designer epigenome modifiers

enable robust and sustained gene silencing in clinically relevant human cells. *Nucleic Acids Research*, *46*(9), 4456–4468. https://doi.org/10.1093/nar/gky171

Mojica, Díez-Villaseñor, C., García-Martínez, J., & Almendros, C. (2009). Short motif sequences determine the targets of the prokaryotic CRISPR defence system. *Microbiology (Reading, England)*, *155*(Pt 3), 733–740. https://doi.org/10.1099/mic.0.023960-0

Mojica, Díez-Villaseñor, C., García-Martínez, J., & Soria, E. (2005). Intervening sequences of regularly spaced prokaryotic repeats derive from foreign genetic elements. *Journal of Molecular Evolution*, *60*(2), 174–182. https://doi.org/10.1007/s00239-004-0046-3

Mojica, Juez, G., & Rodríguez-Valera, F. (1993). Transcription at different salinities of Haloferax mediterranei sequences adjacent to partially modified PstI sites. *Molecular Microbiology*, *9*(3), 613–621. https://doi.org/10.1111/j.1365-2958.1993.tb01721.x

Nahmad, A. D., Reuveni, E., Goldschmidt, E., Tenne, T., Liberman, M., Horovitz-Fried, M., Khosravi, R., Kobo, H., Reinstein, E., Madi, A., Ben-David, U., & Barzel, A. (2022). Frequent aneuploidy in primary human T cells after CRISPR-Cas9 cleavage. *Nature Biotechnology*, *40*(12), 1807–1813. https://doi.org/10.1038/s41587-022-01377-0

Nelson, C. E., Hakim, C. H., Ousterout, D. G., Thakore, P. I., Moreb, E. A., Castellanos Rivera, R. M., Madhavan, S., Pan, X., Ran, F. A., Yan, W. X., Asokan, A., Zhang, F., Duan, D., & Gersbach, C. A. (2016). In vivo genome editing improves muscle function in a mouse model of Duchenne muscular dystrophy. *Science (New York, N.Y.)*, *351*(6271), 403–407. https://doi.org/10.1126/science.aad5143

Neumann, E. N., Bertozzi, T. M., Wu, E., Serack, F., Harvey, J. W., Brauer, P. P., Pirtle, C. P., Coffey, A., Howard, M., Kamath, N., Lenz, K., Guzman, K., Raymond, M. H., Khalil, A. S., Deverman, B. E., Minikel, E. V., Vallabh, S. M., & Weissman, J. S. (2024). Brainwide silencing of prion protein by AAV-mediated delivery of an engineered compact epigenetic editor. *Science*, *384*(6703), ado7082. https://doi.org/10.1126/science.ado7082

Newell-Price, J., Clark, A. J., & King, P. (2000). DNA methylation and silencing of gene expression. *Trends in Endocrinology and Metabolism: TEM*, *11*(4), 142–148. https://doi.org/10.1016/s1043-2760(00)00248-4

Nguyen, T.-V., Yao, S., Wang, Y., Rolfe, A., Selvaraj, A., Darman, R., Ke, J., Warmuth, M., Smith, P. G., Larsen, N. A., Yu, L., Zhu, P., Fekkes, P., Vaillancourt, F. H., & Bolduc, D. M. (2019). The R882H DNMT3A hot spot mutation stabilizes the formation of large DNMT3A oligomers with low DNA methyltransferase activity. *The Journal of Biological Chemistry*, *294*(45), 16966–16977. https://doi.org/10.1074/jbc.RA119.010126

Nuñez, J. K., Chen, J., Pommier, G. C., Cogan, J. Z., Replogle, J. M., Adriaens, C., Ramadoss, G. N., Shi, Q., Hung, K. L., Samelson, A. J., Pogson, A. N., Kim, J. Y. S., Chung, A., Leonetti, M. D., Chang, H. Y., Kampmann, M., Bernstein, B. E., Hovestadt, V., Gilbert, L. A., & Weissman, J. S. (2021). Genome-wide programmable transcriptional memory by CRISPR-based epigenome editing. *Cell*, *184*(9), 2503-2519.e17. https://doi.org/10.1016/j.cell.2021.03.025

Nuñez, J. K., Kranzusch, P. J., Noeske, J., Wright, A. V., Davies, C. W., & Doudna, J. A. (2014). Cas1-Cas2 complex formation mediates spacer acquisition during CRISPR-Cas adaptive immunity. *Nature Structural & Molecular Biology*, *21*(6), 528–534. https://doi.org/10.1038/nsmb.2820

Nuñez, J. K., Lee, A. S. Y., Engelman, A., & Doudna, J. A. (2015). Integrase-mediated spacer acquisition during CRISPR–Cas adaptive immunity. *Nature*, *519*(7542), 193–198. https://doi.org/10.1038/nature14237

Okano, M., Bell, D. W., Haber, D. A., & Li, E. (1999). DNA methyltransferases Dnmt3a and Dnmt3b are essential for de novo methylation and mammalian development. *Cell*, *99*(3), 247–257. https://doi.org/10.1016/s0092-8674(00)81656-6

Pan, M., Nethery, M. A., Hidalgo-Cantabrana, C., & Barrangou, R. (2020). Comprehensive Mining and Characterization of CRISPR-Cas Systems in Bifidobacterium. *Microorganisms*, *8*(5), 720. https://doi.org/10.3390/microorganisms8050720

Panahi, B., Rostampour, M., Ghaffari, M. R., & Nami, Y. (2024). Genome mining approach reveals the CRISPR-Cas systems features and characteristics in Lactobacillus delbrueckii strains. *Heliyon*, *10*(22), e39920. https://doi.org/10.1016/j.heliyon.2024.e39920

Papathanasiou, S., Markoulaki, S., Blaine, L. J., Leibowitz, M. L., Zhang, C.-Z., Jaenisch, R., & Pellman, D. (2021). Whole chromosome loss and genomic instability in mouse embryos after CRISPR-Cas9 genome editing. *Nature Communications*, *12*(1), 5855. https://doi.org/10.1038/s41467-021-26097-y

Paschon, D. E., Lussier, S., Wangzor, T., Xia, D. F., Li, P. W., Hinkley, S. J., Scarlott, N. A., Lam, S. C., Waite, A. J., Truong, L. N., Gandhi, N., Kadam, B. N., Patil, D. P., Shivak, D. A., Lee, G. K., Holmes, M. C., Zhang, L., Miller, J. C., & Rebar, E. J. (2019). Diversifying the structure of zinc finger nucleases for high-precision genome editing. *Nature Communications*, *10*(1), 1133. https://doi.org/10.1038/s41467-019-08867-x

Pflueger, C., Tan, D., Swain, T., Nguyen, T., Pflueger, J., Nefzger, C., Polo, J. M., Ford, E., & Lister, R. (2018). A modular dCas9-SunTag DNMT3A epigenome editing system overcomes pervasive off-target activity of direct fusion dCas9-DNMT3A constructs. *Genome Research*, *28*(8), 1193–1206. https://doi.org/10.1101/gr.233049.117

Pinello, L., Canver, M. C., Hoban, M. D., Orkin, S. H., Kohn, D. B., Bauer, D. E., & Yuan, G.-C. (2016). Analyzing CRISPR genome editing experiments with CRISPResso. *Nature Biotechnology*, *34*(7), 695–697. https://doi.org/10.1038/nbt.3583

Pourcel, C., Salvignol, G., & Vergnaud, G. (2005). CRISPR elements in Yersinia pestis acquire new repeats by preferential uptake of bacteriophage DNA, and provide additional tools for evolutionary studies. *Microbiology (Reading, England)*, *151*(Pt 3), 653–663. https://doi.org/10.1099/mic.0.27437-0

Qi, L. S., Larson, M. H., Gilbert, L. A., Doudna, J. A., Weissman, J. S., Arkin, A. P., & Lim, W. A. (2013). Repurposing CRISPR as an RNA-guided platform for sequence-specific control of gene expression. *Cell*, *152*(5), 1173–1183. https://doi.org/10.1016/j.cell.2013.02.022

Razin, A., & Riggs, A. D. (1980). DNA methylation and gene function. *Science (New York, N.Y.)*, *210*(4470), 604–610. https://doi.org/10.1126/science.6254144

Robinson, J. G., Farnier, M., Krempf, M., Bergeron, J., Luc, G., Averna, M., Stroes, E. S., Langslet, G., Raal, F. J., El Shahawy, M., Koren, M. J., Lepor, N. E., Lorenzato, C., Pordy, R., Chaudhari, U., Kastelein, J. J. P., & ODYSSEY LONG TERM Investigators. (2015). Efficacy and safety of alirocumab in reducing lipids and cardiovascular events. *The New England Journal of Medicine*, *372*(16), 1489–1499. https://doi.org/10.1056/NEJMoa1501031

Rodenhiser, D., & Mann, M. (2006). Epigenetics and human disease: Translating basic biology into clinical applications. *CMAJ: Canadian Medical Association Journal = Journal de l'Association Medicale Canadienne*, *174*(3), 341–348. https://doi.org/10.1503/cmaj.050774

Roth, G. V., Gengaro, I. R., & Qi, L. S. (2024). Precision epigenetic editing: Technological advances, enduring challenges, and therapeutic applications. *Cell Chemical Biology*, *31*(8), 1422–1446. https://doi.org/10.1016/j.chembiol.2024.07.007

Sabatine, M. S., Giugliano, R. P., Keech, A. C., Honarpour, N., Wiviott, S. D., Murphy, S. A., Kuder, J. F., Wang, H., Liu, T., Wasserman, S. M., Sever, P. S., Pedersen, T. R., &

FOURIER Steering Committee and Investigators. (2017). Evolocumab and Clinical Outcomes in Patients with Cardiovascular Disease. *The New England Journal of Medicine*, *376*(18), 1713–1722. https://doi.org/10.1056/NEJMoa1615664

San Filippo, J., Sung, P., & Klein, H. (2008). Mechanism of eukaryotic homologous recombination. *Annual Review of Biochemistry*, *77*, 229–257. https://doi.org/10.1146/annurev.biochem.77.061306.125255

Saunderson, E. A., Stepper, P., Gomm, J. J., Hoa, L., Morgan, A., Allen, M. D., Jones, J. L., Gribben, J. G., Jurkowski, T. P., & Ficz, G. (2017). Hit-and-run epigenetic editing prevents senescence entry in primary breast cells from healthy donors. *Nature Communications*, *8*(1), 1450. https://doi.org/10.1038/s41467-017-01078-2

Schönberg, P. Y., Ding, L., & Buchholz, F. (2023). Genom-Editierung ohne die DNA-Sequenz zu verändern—Geht das? *BIOspektrum*, *29*(1), 46–48. https://doi.org/10.1007/s12268-023-1882-2

Siddique, A. N., Nunna, S., Rajavelu, A., Zhang, Y., Jurkowska, R. Z., Reinhardt, R., Rots, M. G., Ragozin, S., Jurkowski, T. P., & Jeltsch, A. (2013). Targeted methylation and gene silencing of VEGF-A in human cells by using a designed Dnmt3a-Dnmt3L single-chain fusion protein with increased DNA methylation activity. *Journal of Molecular Biology*, *425*(3), 479–491. https://doi.org/10.1016/j.jmb.2012.11.038

Stadtmauer, E. A., Fraietta, J. A., Davis, M. M., Cohen, A. D., Weber, K. L., Lancaster, E., Mangan, P. A., Kulikovskaya, I., Gupta, M., Chen, F., Tian, L., Gonzalez, V. E., Xu, J., Jung, I.-Y., Melenhorst, J. J., Plesa, G., Shea, J., Matlawski, T., Cervini, A., … June, C. H. (2020). CRISPR-engineered T cells in patients with refractory cancer. *Science (New York, N.Y.)*, *367*(6481), eaba7365. https://doi.org/10.1126/science.aba7365

Stark, J. M., Pierce, A. J., Oh, J., Pastink, A., & Jasin, M. (2004). Genetic steps of mammalian homologous repair with distinct mutagenic consequences. *Molecular and Cellular Biology*, *24*(21), 9305–9316. https://doi.org/10.1128/MCB.24.21.9305-9316.2004

Stelzer, Y., Shivalila, C. S., Soldner, F., Markoulaki, S., & Jaenisch, R. (2015). Tracing dynamic changes of DNA methylation at single-cell resolution. *Cell*, *163*(1), 218–229. https://doi.org/10.1016/j.cell.2015.08.046

Stepper, P., Kungulovski, G., Jurkowska, R. Z., Chandra, T., Krueger, F., Reinhardt, R., Reik, W., Jeltsch, A., & Jurkowski, T. P. (2017). Efficient targeted DNA methylation with chimeric dCas9-Dnmt3a-Dnmt3L methyltransferase. *Nucleic Acids Research*, *45*(4), 1703–1713. https://doi.org/10.1093/nar/gkw1112

Sternberg, S. H., LaFrance, B., Kaplan, M., & Doudna, J. A. (2015). Conformational control of DNA target cleavage by CRISPR-Cas9. *Nature*, *527*(7576), Article 7576. https://doi.org/10.1038/nature15544

Strecker, J., Ladha, A., Gardner, Z., Schmid-Burgk, J. L., Makarova, K. S., Koonin, E. V., & Zhang, F. (2019). RNA-guided DNA insertion with CRISPR-associated transposases. *Science (New York, N.Y.)*, *365*(6448), Article 6448. https://doi.org/10.1126/science.aax9181

Suetake, I., Shinozaki, F., Miyagawa, J., Takeshima, H., & Tajima, S. (2004). DNMT3L stimulates the DNA methylation activity of Dnmt3a and Dnmt3b through a direct interaction. *The Journal of Biological Chemistry*, *279*(26), 27816–27823. https://doi.org/10.1074/jbc.M400181200

Tabebordbar, M., Zhu, K., Cheng, J. K. W., Chew, W. L., Widrick, J. J., Yan, W. X., Maesner, C., Wu, E. Y., Xiao, R., Ran, F. A., Cong, L., Zhang, F., Vandenberghe, L. H., Church, G. M., & Wagers, A. J. (2016). In vivo gene editing in dystrophic mouse muscle and muscle stem cells. *Science (New York, N.Y.)*, *351*(6271), 407–411. https://doi.org/10.1126/science.aad5177

Takeda, S. N., Nakagawa, R., Okazaki, S., Hirano, H., Kobayashi, K., Kusakizako, T., Nishizawa, T., Yamashita, K., Nishimasu, H., & Nureki, O. (2021). Structure of the

miniature type V-F CRISPR-Cas effector enzyme. *Molecular Cell*, *81*(3), 558-570.e3. https://doi.org/10.1016/j.molcel.2020.11.035

Tan, J., Zhang, F., Karcher, D., & Bock, R. (2019). Engineering of high-precision base editors for site-specific single nucleotide replacement. *Nature Communications*, *10*(1), Article 1. https://doi.org/10.1038/s41467-018-08034-8

Tang, L. (2019). Investigating heterogeneity in HeLa cells. *Nature Methods*, *16*(4), 281. https://doi.org/10.1038/s41592-019-0375-1

Tou, C. J., Orr, B., & Kleinstiver, B. P. (2023). Precise cut-and-paste DNA insertion using engineered type V-K CRISPR-associated transposases. *Nature Biotechnology*, *41*(7), 968–979. https://doi.org/10.1038/s41587-022-01574-x

Tremblay, F., Xiong, Q., Shah, S. S., Ko, C.-W., Kelly, K., Morrison, M. S., Giancarlo, C., Ramirez, R. N., Hildebrand, E. M., Voytek, S. B., El Sebae, G. K., Wright, S. H., Lofgren, L., Clarkson, S., Waters, C., Linder, S. J., Liu, S., Eom, T., Parikh, S., … Jaffe, A. B. (2025). A potent epigenetic editor targeting human PCSK9 for durable reduction of low-density lipoprotein cholesterol levels. *Nature Medicine*, 1–10. https://doi.org/10.1038/s41591-025-03508-x

Turchiano, G., Andrieux, G., Klermund, J., Blattner, G., Pennucci, V., El Gaz, M., Monaco, G., Poddar, S., Mussolino, C., Cornu, T. I., Boerries, M., & Cathomen, T. (2021). Quantitative evaluation of chromosomal rearrangements in gene-edited human stem cells by CAST-Seq. *Cell Stem Cell*, *28*(6), 1136-1147.e5. https://doi.org/10.1016/j.stem.2021.02.002

van Rosmalen, M., Krom, M., & Merkx, M. (2017). Tuning the Flexibility of Glycine-Serine Linkers To Allow Rational Design of Multidomain Proteins. *Biochemistry*, *56*(50), Article 50. https://doi.org/10.1021/acs.biochem.7b00902

Vercauteren, S., Fiesack, S., Maroc, L., Verstraeten, N., Dewachter, L., Michiels, J., & Vonesch, S. C. (2024). The rise and future of CRISPR-based approaches for high-throughput genomics. *FEMS Microbiology Reviews*, *48*(5), fuae020. https://doi.org/10.1093/femsre/fuae020

Vickaryous, M. K., & Hall, B. K. (2006). Human cell type diversity, evolution, development, and classification with special reference to cells derived from the neural crest. *Biological Reviews of the Cambridge Philosophical Society*, *81*(3), 425–455. https://doi.org/10.1017/S1464793106007068

Vojta, A., Dobrinić, P., Tadić, V., Bočkor, L., Korać, P., Julg, B., Klasić, M., & Zoldoš, V. (2016). Repurposing the CRISPR-Cas9 system for targeted DNA methylation. *Nucleic Acids Research*, *44*(12), 5615–5628. https://doi.org/10.1093/nar/gkw159

Wakap, S., Lambert, D. M., Olry, A., Rodwell, C., Gueydan, C., Lanneau, V., Murphy, D., Le Cam, Y., & Rath, A. (2020). Estimating cumulative point prevalence of rare diseases: Analysis of the Orphanet database. *European Journal of Human Genetics: EJHG*, *28*(2), 165–173. https://doi.org/10.1038/s41431-019-0508-0

Walton, R. T., Christie, K. A., Whittaker, M. N., & Kleinstiver, B. P. (2020). Unconstrained genome targeting with near-PAMless engineered CRISPR-Cas9 variants. *Science (New York, N.Y.)*, *368*(6488), Article 6488. https://doi.org/10.1126/science.aba8853

Wang, F., Jin, Y., Wang, M., Luo, H.-Y., Fang, W.-J., Wang, Y.-N., Chen, Y.-X., Huang, R.-J., Guan, W.-L., Li, J.-B., Li, Y.-H., Wang, F.-H., Hu, X.-H., Zhang, Y.-Q., Qiu, M.-Z., Liu, L.-L., Wang, Z.-X., Ren, C., Wang, D.-S., … Xu, R.-H. (2024). Combined anti-PD-1, HDAC inhibitor and anti-VEGF for MSS/pMMR colorectal cancer: A randomized phase 2 trial. *Nature Medicine*, *30*(4), 1035–1043. https://doi.org/10.1038/s41591-024-02813-1

Wang, Guo, R., Du, Z., Bai, L., Li, L., Cui, J., Li, W., Hoffman, A. R., & Hu, J.-F. (2018). Epigenetic Targeting of Granulin in Hepatoma Cells by Synthetic CRISPR dCas9 Epi-

suppressors. *Molecular Therapy. Nucleic Acids*, *11*, 23–33. https://doi.org/10.1016/j.omtn.2018.01.002

Wang, J. Y., Pausch, P., & Doudna, J. A. (2022). Structural biology of CRISPR–Cas immunity and genome editing enzymes. Nature Reviews Microbiology, 1–16. https://doi.org/10.1038/s41579-022-00739-4

Wang, Li, L., Guo, L., Feng, Y., Du, Z., Jiang, W., Wu, X., Zheng, J., Xiao, X., Zheng, H., Sun, Y., & Ma, H. (2024). Robust Miniature Cas-based Transcriptional Modulation by Engineering Un1Cas12f1 and Tethering Sso7d. *Molecular Therapy*. https://doi.org/10.1016/j.ymthe.2024.02.013

Wei, Y., Chesne, M. T., Terns, R. M., & Terns, M. P. (2015). Sequences spanning the leader-repeat junction mediate CRISPR adaptation to phage in Streptococcus thermophilus. *Nucleic Acids Research*, *43*(3), 1749–1758. https://doi.org/10.1093/nar/gku1407

Weinberg, D. N., Papillon-Cavanagh, S., Chen, H., Yue, Y., Chen, X., Rajagopalan, K. N., Horth, C., McGuire, J. T., Xu, X., Nikbakht, H., Lemiesz, A. E., Marchione, D. M., Marunde, M. R., Meiners, M. J., Cheek, M. A., Keogh, M.-C., Bareke, E., Djedid, A., Harutyunyan, A. S., … Lu, C. (2019). The histone mark H3K36me2 recruits DNMT3A and shapes the intergenic DNA methylation landscape. *Nature*, *573*(7773), 281–286. https://doi.org/10.1038/s41586-019-1534-3

Whittaker, M. N., Testa, L. C., Quigley, A., Jindal, I., Cortez-Alvarado, S. V., Qu, P., Yang, Y., Alameh, M.-G., Musunuru, K., & Wang, X. (2023). Epigenome Editing Durability Varies Widely Across Cardiovascular Disease Target Genes. *Arteriosclerosis, Thrombosis, and Vascular Biology*, *43*(10), 2075–2077. https://doi.org/10.1161/ATVBAHA.123.319748

Wilkins, O. G., Capitanchik, C., Luscombe, N. M., & Ule, J. (2021). Ultraplex: A rapid, flexible, all-in-one fastq demultiplexer. *Wellcome Open Research*, *6*, 141. https://doi.org/10.12688/wellcomeopenres.16791.1

Wilkinson, M. J., Bajaj, A., Brousseau, M. E., & Taub, P. R. (2024). Harnessing RNA Interference for Cholesterol Lowering: The Bench-to-Bedside Story of Inclisiran. *Journal of the American Heart Association*, *13*(6), e032031. https://doi.org/10.1161/JAHA.123.032031

Wu, T., Liu, C., Zou, S., Lyu, R., Yang, B., Yan, H., Zhao, M., & Tang, W. (2023). An engineered hypercompact CRISPR-Cas12f system with boosted gene-editing activity. *Nature Chemical Biology*. https://doi.org/10.1038/s41589-023-01380-9

Wu, W. Y., Adiego-Pérez, B., & van der Oost, J. (2024). Biology and applications of CRISPR–Cas12 and transposon-associated homologs. *Nature Biotechnology*, *42*(12), 1807–1821. https://doi.org/10.1038/s41587-024-02485-9

Wu, Zhang, Y., Yu, H., Pan, D., Wang, Y., Wang, Y., Li, F., Liu, C., Nan, H., Chen, W., & Ji, Q. (2021). Programmed genome editing by a miniature CRISPR-Cas12f nuclease. *Nature Chemical Biology*, *17*(11), 1132–1138. https://doi.org/10.1038/s41589-021-00868-6

Xiao, R., Li, Z., Wang, S., Han, R., & Chang, L. (2021). Structural basis for substrate recognition and cleavage by the dimerization-dependent CRISPR-Cas12f nuclease. *Nucleic Acids Research*, *49*(7), 4120–4128. https://doi.org/10.1093/nar/gkab179

Xu, Chemparathy, A., Zeng, L., Kempton, H. R., Shang, S., Nakamura, M., & Qi, L. S. (2021). Engineered miniature CRISPR-Cas system for mammalian genome regulation and editing. *Molecular Cell*, *81*(20), 4333-4345.e4. https://doi.org/10.1016/j.molcel.2021.08.008

Xu, Liu, M., Zhou, X. E., Liang, G., Zhao, G., Xu, H. E., Melcher, K., & Jones, P. A. (2020). Structure of nucleosome-bound DNA methyltransferases DNMT3A and DNMT3B. *Nature*, *586*(7827), 151–155. https://doi.org/10.1038/s41586-020-2747-1

Xu, W., Li, J., Rong, B., Zhao, B., Wang, M., Dai, R., Chen, Q., Liu, H., Gu, Z., Liu, S., Guo, R., Shen, H., Wu, F., & Lan, F. (2020). DNMT3A reads and connects histone H3K36me2 to DNA methylation. *Protein & Cell*, *11*(2), 150–154. https://doi.org/10.1007/s13238-019-00672-y

Yeh, C. D., Richardson, C. D., & Corn, J. E. (2019). Advances in genome editing through control of DNA repair pathways. *Nature Cell Biology*, *21*(12), 1468–1478. https://doi.org/10.1038/s41556-019-0425-z

Yoganand, K. N., Muralidharan, M., Nimkar, S., & Anand, B. (2019). Fidelity of prespacer capture and processing is governed by the PAM-mediated interactions of Cas1-2 adaptation complex in CRISPR-Cas type I-E system. *The Journal of Biological Chemistry*, *294*(52), 20039–20053. https://doi.org/10.1074/jbc.RA119.009438

Zhang, Z.-M., Lu, R., Wang, P., Yu, Y., Chen, D., Gao, L., Liu, S., Ji, D., Rothbart, S. B., Wang, Y., Wang, G. G., & Song, J. (2018). Structural basis for DNMT3A-mediated de novo DNA methylation. *Nature*, *554*(7692), 387–391. https://doi.org/10.1038/nature25477

Zuccaro, M. V., Xu, J., Mitchell, C., Marin, D., Zimmerman, R., Rana, B., Weinstein, E., King, R. T., Palmerola, K. L., Smith, M. E., Tsang, S. H., Goland, R., Jasin, M., Lobo, R., Treff, N., & Egli, D. (2020). Allele-Specific Chromosome Removal after Cas9 Cleavage in Human Embryos. *Cell*, *183*(6), 1650-1664.e15. https://doi.org/10.1016/j.cell.2020.10.025

V. Appendix

Coding sequence of EE2 with en-dAsCas12f

MGPKKKRKVGSGSMTTKVVKIEIIKPINDTWNVLGQVLRDIQYQTWKFANKAIQMY
WDFSNFSYSYKKRFGEELLSKGKTLPNGYRQVKSDILNEHKEIINKLNSNSKDALIDM
VEKKWNADFNDIINGRKSIANFKRDLPIELHNKQFMNSKKQLMLYVENGDYYAEINL
ISRQYAKELGKKSTAFKLLLAVKDNYQKVIVDRLISGEYKLGMSKITKAKKGKKKW
YLNLVYSFTEKKDNSLDPNKVMGIALGVNIPAALAIYGDKYFKEFVGDRDEIENFRK
QIEARKRKLQRQGKWCGEGRRGHGIKTRIKPLEKLAGKIANFKNTKNHCWSRYIVDA
AVKNKCGVIQMADLSGIAEENTFLKNWTYYDLQQKIKYKAEEKGIKVVFIRPSYTSA
RCNKCGHIHRSYEKKEYRPSQDQFICQSCGHKENADINAARNIATPNIEKIIKDQLEKQ
EKEMKQNLKYIIGAYPYDVPDYAAQAERQRILERTNEGRQEAMAKGVVFGRKRKID
RMNHDQEFDPPKVYPPVPAEKRKPIRVLSLFDGIATGLLVLKDLGIQVDRYIASEVCE
DSITVGMVRHQGKIMYVGDVRSVTQKHIQEWGPFDLVIGGSPCNDLSIVNPARKGLY
EGTGRLFFEFYRLLHDARPKEGDDRPFFWLFENVVAMGVSDKRDISRFLESNPVMID
AKEVSAAHRARYFWGNLPGMNRPLASTVNDKLELQECLEHGRIAKFSKVRTITTRSN
SIKQGKDQHFPVFMNEKEDILWCTEMERVFGFPVHYTDVSNMSRLARQRLLGRSWS
VPVIRHLFAPLKEYFACVSSGNSNANSRGPSFSSGLVPLSLRGSHMGPMEIYKTVSAW
KRQPVRVLSLFRNIDKVLKSLGFLESGSGSGGGTLKYVEDVTNVVRRDVEKWGPFDL
VYGSTQPLGSSCDRCPGWYMFQFHRILQYALPRQESQRPFFWIFMDNLLLTEDDQET
TTRFLQTEAVTLQDVRGRDYQNAMRVWSNIPGLKSKHAPLTPKEEEYLQAQVRSRS
KLDAPKVDLLVKNCLLPLREYFKYFSQNSLPLGGPSSGAPPPSGGSPAGSPTSTEEGTS
ESATPESGPGTSTEPSEGSAPGSPAGSPTSTEEGTSTEPSEGSAPGTSTEPSERTLVTFKD
VFVDFTREEWKLLDTAQQIVYRNVMLENYKNLVSLGYQLTKPDVILRLEKGEEPHM
GGGSGEDPAAKRVKLDGGEGRGSLLTCGDVEENPGPEFSELIKENMHMKLYMEGTV
DNHHFKCTSEGEGKPYEGTQTMRIKVVEGGPLPFAFDILATSFLYGSKTFINHTQGIPD
FFKQSFPEGFTWERVTTYEDGGVLTATQDTSLQDGCLIYNVKIRGVNFTSNGPVMQK
KTLGWEAFTETLYPADGGLEGRNDMALKLVGGSHLIANIKTTYRSKKPAKNLKMPG
VYYVDYRLERIKEANNETYVEQHEVAVARYCDLPSKLGHKLNSRSASTVPSSCQPSV
VCPSPVPSLTLEGATPTVLS*

Primer for mutagenesis of ApCas12f through LDA cloning

Table 3: LDA primer for site directed mutagenesis

Mutant	LDA primer
I11K	GGTAGTCAAGATCGAGATTAAGAAGCCAATCAACGACACCTG
K12Y	AGTCAAGATCGAGATTATCTACCCAATCAACGACACCTGGAA
P13D	CAAGATCGAGATTATCAAGGACATCAACGACACCTGGAACGT
W18K	CAAGCCAATCAACGACACCAAGAACGTGTTGGGTCAAGTTCT
N19K	GCCAATCAACGACACCTGGAAGGTGTTGGGTCAAGTTCTTAG
G22Y	CGACACCTGGAACGTGTTGTACCAAGTTCTTAGAGACATCCA
W33R	AGACATCCAGTACCAGACTAGAAAGTTTGCCAACAAGGCAAT
F35L	CCAGTACCAGACTTGGAAGCTGGCCAACAAGGCAATTCAAAT
Y43A	CAACAAGGCAATTCAAATGGCCTGGGATTTCAGCAACTTTTC
S47Q	TCAAATGTATTGGGATTTCCAGAACTTTTCTTACAGCTACAA
E60Y	CAAGAAACGGTTCGGCGAGTACCTCCTGTCCAAAGGAAAGAC
61P	GAAACGGTTCGGCGAGGAGCCCCTGTCCAAAGGAAAGACACT
S63E	GTTCGGCGAGGAGCTCCTGGAGAAAGGAAAGACACTGCCTAA
S63K	GTTCGGCGAGGAGCTCCTGAAGAAAGGAAAGACACTGCCTAA
G65D	CGAGGAGCTCCTGTCCAAAGACAAGACACTGCCTAATGGCTA
T67K	GCTCCTGTCCAAAGGAAAGAAGCTGCCTAATGGCTACAGGCA
R73K	GACACTGCCTAATGGCTACAAGCAGGTGAAGTCAGACATCCT
R73T	GACACTGCCTAATGGCTACACCCAGGTGAAGTCAGACATCCT
Q74K	ACTGCCTAATGGCTACAGGAAGGTGAAGTCAGACATCCTCAA
K76N	TAATGGCTACAGGCAGGTGAACTCAGACATCCTCAACGAACA
S77G	TGGCTACAGGCAGGTGAAGGGCGACATCCTCAACGAACATAA
80Y	GCAGGTGAAGTCAGACATCTACAACGAACATAAGGAAATTAT
N81R	GGTGAAGTCAGACATCCTCAGAGAACATAAGGAAATTATCAA
I86E	CCTCAACGAACATAAGGAAGAGATCAACAAGCTGAATTCTAA
I86K	CCTCAACGAACATAAGGAAAAGATCAACAAGCTGAATTCTAA
N91Y	GGAAATTATCAACAAGCTGTACTCTAATTCAAAGGATGCGCT
D96S	GCTGAATTCTAATTCAAAGAGCGCGCTCATCGATATGGTGGA
D100K	TTCAAAGGATGCGCTCATCAAGATGGTGGAAAAGAAATGGAA
E103V	TGCGCTCATCGATATGGTGGTGAAGAAATGGAATGCCGACTT
N107K	TATGGTGGAAAAGAAATGGAAGGCCGACTTCAACGACATTAT
N111K	GAAATGGAATGCCGACTTCAAGGACATTATTAACGGCCGAAA
N115K	CGACTTCAACGACATTATTAAGGGCCGAAAATCAATCGCCAA
R117E	CAACGACATTATTAACGGCGAGAAATCAATCGCCAATTTCAA
A121P	TAACGGCCGAAAATCAATCCCCAATTTCAAGCGAGATCTCCC
H132K	AGATCTCCCTATAGAACTCAAGAACAAACAATTTATGAATTC
N133K	TCTCCCTATAGAACTCCACAAGAAACAATTTATGAATTCCAA
M144R	GAATTCCAAGAAGCAGCTGAGACTGTACGTGGAGAATGGGGA
G150K	GATGCTGTACGTGGAGAATAAGGATTATTATGCAGAGATCAA
D151K	GCTGTACGTGGAGAATGGGAAGTATTATGCAGAGATCAATCT

E155K	GAATGGGGATTATTATGCAAAGATCAATCTGATCTCTCGCCA
Q162E	GATCAATCTGATCTCTCGCGAGTACGCGAAGGAACTGGGGAA
T172G	GGAACTGGGGAAGAAGTCTGGCGCGTTCAAGCTTCTCCTCGC
L177E	GTCTACTGCGTTCAAGCTTGAGCTCGCGGTCAAAGACAACTA
A179R	TGCGTTCAAGCTTCTCCTCAGAGTCAAAGACAACTACCAAAA
G200S	TTCAGGAGAGTACAAGCTGAGCATGTCCAAGATAACAAAAGC
M201D	AGGAGAGTACAAGCTGGGCGACTCCAAGATAACAAAAGCTAA
A207D	CATGTCCAAGATAACAAAAGACAAGAAAGGAAAGACCAAGTG
T212K	AAAAGCTAAGAAAGGAAAGAAGAAGTGGTACCTCAACCTCGT
N217L	AAAGACCAAGTGGTACCTCCTGCTCGTGTACTCTTTCACCGA
V219T	CAAGTGGTACCTCAACCTCACCTACTCTTTCACCGAGAAGAA
T223E	CAACCTCGTGTACTCTTTCGAGGAGAAGAAGGACAACTCACT
D227K	CTCTTTCACCGAGAAGAAGAAGAACTCACTCGATCCAAATAA
A247M	TGGGGTGAATATACCTGCCATGCTGGCTATCTACGGTGACAA
Y251S	ACCTGCCGCTCTGGCTATCAGCGGTGACAAATACTTTAAGGA
G252D	TGCCGCTCTGGCTATCTACGACGACAAATACTTTAAGGAATT
F256Y	TATCTACGGTGACAAATACTACAAGGAATTTGTCGGGGACCG
R263G	TAAGGAATTTGTCGGGGACGGCGATGAAATCGAGAACTTCCG
D264K	GGAATTTGTCGGGGACCGGAAGGAAATCGAGAACTTCCGCAA
E267R	CGGGGACCGGGATGAAATCAGAAACTTCCGCAAACAAATTGA
R270E	GGATGAAATCGAGAACTTCGAGAAACAAATTGAGGCCCGCAA
K279R	AATTGAGGCCCGCAAAAGAAGATTGCAGCGACAAGGCAAATG
G284R	AAGAAAGTTGCAGCGACAAAGAAAATGGTGTGGCGAGGGGCG
A307G	CAAGCCTCTTGAAAAGCTCGGCGGCAAGATTGCGAACTTCAA
N315D	CAAGATTGCGAACTTCAAGGACACCAAGAACCACTGTTGGTC
N315K	CAAGATTGCGAACTTCAAGAAGACCAAGAACCACTGTTGGTC
A328E	GTCACGTTACATAGTGGACGAGGCCGTGAAGAATAAGTGTGG
K365E	CGACTTGCAACAAAAGATCGAGTACAAAGCCGAGGAGAAGGG
F377K	GAAGGGGATCAAGGTGGTGAAGATCGACCCCAGCTACACAAG
S381A	GGTGGTGTTCATCGACCCCGCCTACACAAGCGCCCGATGCAA
Y397S	TGGCCACATTCACCGCAGCAGCGAGAAGAAGGAGTATAGACC
E398N	CCACATTCACCGCAGCTACAACAAGAAGGAGTATAGACCTTC
Y402R	CAGCTACGAGAAGAAGGAGAGAAGACCTTCTCAAGACCAATT
Y402W	CAGCTACGAGAAGAAGGAGTGGAGACCTTCTCAAGACCAATT
E418A	TCAGTCCTGCGGGCACAAGGCCAACGCAGACATCAATGCCGC
P431K	CGCGAGGAACATAGCGACTAAGAATATCGAGAAGATCATCAA
K443I	CATCAAGGACCAGCTGGAAATCCAAGAAAAGGAGATGAAGCA
Q450H	GCAAGAAAAGGAGATGAAGCACAACCTGAAGTACATCATC
A247T	TGGGGTGAATATACCTGCCACCCTGGCTATCTACGGTGACAA
F377R	GAAGGGGATCAAGGTGGTGAGAATCGACCCCAGCTACACAAG
R395N	CAAGTGTGGCCACATTCACAACAGCTACGAGAAGAAGGAGTA
S396K	GTGTGGCCACATTCACCGCAAGTACGAGAAGAAGGAGTATAG

E398D	CCACATTCACCGCAGCTACGACAAGAAGGAGTATAGACCTTC
K400E	TCACCGCAGCTACGAGAAGGAGGAGTATAGACCTTCTCAAGA
E401K	CCGCAGCTACGAGAAGAAGAAGTATAGACCTTCTCAAGACCA
Y402K	CAGCTACGAGAAGAAGGAGAAGAGACCTTCTCAAGACCAATT
S405N	GAAGAAGGAGTATAGACCTAACCAAGACCAATTCATTTGTCA
D407E	GGAGTATAGACCTTCTCAAGAGCAATTCATTTGTCAGTCCTG
Q408T	GTATAGACCTTCTCAAGACACCTTCATTTGTCAGTCCTGCGG
I422V	GCACAAGGAAAACGCAGACGTGAATGCCGCGAGGAACATAGC
N354T	GGAAAACACATTCCTTAAGACCTGGACTTACTACGACTTGCA
V147K	GAAGCAGCTGATGCTGTACAAGGAGAATGGGGATTATTATGC

Copyright information

Figure 6) Reprinted from *CMAJ*, 174 (3), Rodenhiser, D., Mann, M., Epigenetics and human disease: translating basic biology into clinical applications, 341-348, Copyright © 2006, with permission from the Canadian Medical Association.

Permission granted by Isabelle Laurendau, Business Development Manager, CMAJ Group, 06.11.2025.

Figure 9) Reprinted from *BIOspektrum*, 29 (1), Schönberg, P. Y., Ding, L. & Buchholz, F., Genom-Editierung ohne die DNA-Sequenz zu verändern—Geht das?, 46-48, Creative Commons CC BY License, 2023.